Canadian Technical Report of
Hydrography and Ocean Sciences 233

2003

Low-frequency Variability in Lancaster Sound

by

A. van der Baaren*, B. Petrie, and S. Prinsenberg

Ocean Sciences Division
Maritimes Region
Fisheries and Oceans Canada
Bedford Institute of Oceanography
P. O. Box 1006
Dartmouth, Nova Scotia
Canada, B2Y 4A2

* contractor, 8 Toye Lane, Wolfville, Nova Scotia, B4P2C8

Cat. No. Fs 97-18/233E ISSN 0711-6764

Correct Citation for this publication:

van der Baaren, A., B. Petrie, and S. J. Prinsenberg. 2003. Low Frequency Variability in Lancaster Sound. *Can. Tech. Rep. Hydrogr. Ocean Sci. 233*: xii+124 p.

Contents

Figures

Tables

Abstract

van der Baaren, A., B. Petrie, and S. J. Prinsenberg. 2003. Low Frequency Variability in Lancaster Sound. *Can. Tech. Rep. Hydrogr. Ocean Sci. 233*: xii+124 p.

Harmonic analysis of alongshore 2-hourly currents indicates that, on the south shore of Lancaster Sound a depth dependent annual component varies from ~15 cms^{-1} near the surface to ~4 cms^{-1} near the bottom. On the north shore, the annual component with an amplitude of ~8 cms^{-1} exists near the surface, decreases to ~2.7 cms^{-1} at mid-depth, and decreases further to ~0.3 cms^{-1} near the bottom. The annual component is strongest to the east in late October/early November for the south shore and in early February for the north shore.

Along the south shore, phases are constant to within 0.6°. The phase of the current along the north shore is almost constant (within 1.5°) over most of the depth with the exception being near the bottom where the phase leads those at shallower depths. Variance in phase differences for coherence was greatest between shallower and deeper depths for both shores.

Mean flows along the south shore are slightly weaker near the surface and reach their maximum at ~30 m while mean flows along the north shore show a mid-depth minimum. Ice cover results in a reduction in near-surface flow on both shores.

Principal component analysis (PCA) of alongshore current, density, and local wind was performed for three-year oceanographic time series (1998-2001) recorded in Lancaster Sound from 1998 – 2001 and for wind velocity data recorded nearby at Resolute. Analyses were performed on 6-hourly data that had had the major tidal components removed (called "high frequency") and on lowpass filtered data that had been decimated to 14-day intervals (called "low frequency") data. Analyses involving the wind used lowpass filtered meteorological data decimated to 14-day intervals.

PCA results for low frequency data show that, on both shores the first mode accounts for almost all the variance and is the predominant velocity mode, especially in shallow water. The first mode removed (94, 71, 6%) of the variance in the shallow, mid-depth, and deeper water in the north and removed (95, 98, 88%) of the variance in the south. Neither local wind forcing nor internal adjustment influenced the low-frequency variability observed in the flow record. There does not appear to be a local meteorological nor density influence on the low frequency flow at all.

Résumé

van der Baaren, A., B. Petrie, and S. J. Prinsenberg. 2003. Low Frequency Variability in Lancaster Sound. *Can. Tech. Rep. Hydrogr. Ocean Sci. 233*: xii+124 p.

L'analyse harmonique de données horaires sur deux courants littoraux indique que sur la rive sud du détroit de Lancaster une composante annuelle dépendant de la profondeur varie d'environ 15 cms^{-1} près de la surface à environ 4 cms^{-1} près du fond. Sur la rive nord, il existe une composante annuelle d'une amplitude d'environ 8 cms^{-1} près de la surface dont la valeur diminue à environ 2,7 cms^{-1} à mi-profondeur et encore davantage à environ 0,3 cms^{-1} près du fond. La composante annuelle est la plus forte à l'est à la fin octobre et au début novembre dans le cas de la rive sud et au début de février dans le cas de la rive nord.

Le long de la rive sud, les phases sont constantes à 0,6° près. La phase du courant observé le long de la rive nord est presque constante (à 1,5° près) sur la plus grande partie de la profondeur sauf près du fond où la phase devance celles aux moindres profondeurs. La plus grande variance des différences de phase en ce qui a trait à la cohérence a été observée entre les eaux peu profondes et les eaux plus profondes pour les deux rives.

Les écoulements moyens le long de la rive sud sont légèrement plus faibles près de la surface et atteignent un maximum à environ 30 m alors que le long de la rive nord on observe des écoulements moyens minimums à mi-profondeur. La couverture glacielle résulte d'une réduction de l'écoulement près de la surface sur les deux rives.

Une analyse des composantes principales (ACP) du courant littoral, de la densité et des vents locaux a été effectuée avec une série chronologique (1998 à 2001) de données océanographiques enregistrées dans le détroit de Lancaster et des données sur la vitesse du vent enregistrées dans les environs à Resolute. Les analyses ont été effectuées avec des données à intervalles de six heures dont avaient été supprimées les principales composantes tidales (dites «haute fréquence») et des données soumises à un filtre passe-bas et décimées pour l'obtention d'intervalles de 14 jours (dites «basse fréquence»). Les analyses faisant intervenir le vent étaient basées sur des données météorologiques soumises à un filtrage passe-bas et décimées pour l'obtention d'intervalles de 14 jours.

Les résultats de l'APC pour les données de basse fréquence indiquent que, sur les deux rives, le premier mode explique presque la totalité de la variance et est le mode prédominant pour la vitesse, surtout en eau peu profonde. Le premier mode permettait de supprimer 94, 71 et 6 % de la variance respectivement en eau peu profonde, à mi-profondeur et en eau profonde du côté nord et 95, 98 et 88 % de la variance du côté sud. Ni le forçage par les vents locaux ni un ajustement interne n'influencent la variabilité de basse fréquence observée dans les enregistrements de l'écoulement. Il semble n'exister aucune influence de la météorologie locale ou de la densité sur la variabilité de basse fréquence de l'écoulement.

Introduction

Oceanography of the Barrow Strait/Lancaster Sound region has been described in Prinsenberg and Bennett (1987), Prinsenberg (1998), Hamilton et al. (2002, 2003), and in numerous federal government reports from the 1980s. In these studies, fluxes were seen to have strong seasonal and annual variability as did the sea level. To date, conclusions about the low frequency variability in fluxes, etc. have been based solely on year-long records. Now, for the first time, long term oceanographic records are available to more closely examine the phenomena. This data report presents variation analysis of three-year current and moored CTD data recorded in Lancaster Sound. The primary tool is principal component analysis used to extract major, coherent variance patterns and to determine possible causal relations between physical water properties and meteorological forcing at frequencies greater than fourteen days.

Data

ADCP and moored conductivity, temperature, and pressure (CTD) data were recorded at two locations in Lancaster Sound in the Canadian high Arctic from August 1998 to autumn 2001 (Figure 1). Since the moorings were located close to the magnetic north pole, they were equipped with independent compass packages to provide direction information (Hamilton, 2001).

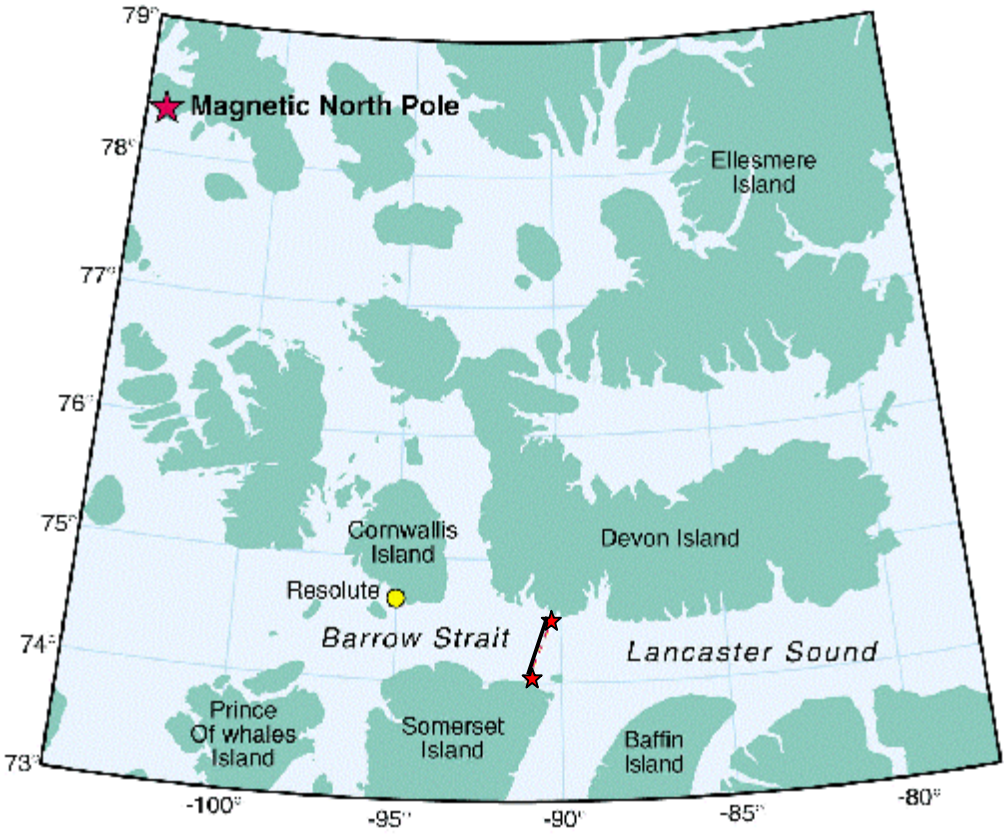

Figure 1 Location of Lancaster Sound and the transect (black line) on which the moorings (small stars) were located

The ADCP data were resolved to alongshore components (eastward to 105°) for the two moorings, one of which was in the north and one of which was in the south side of the Sound. It was not possible to obtain an accompanying cross-channel current since ADCP direction data were missing for a large part of 2000 due to compass failure (Hamilton et al., 2003). Only using alongshore currents was judged adequate because previous studies had observed currents to be mostly parallel to shore (Prinsenberg, 1998) and Hamilton et al. (2002, 2003) showed that the variance of the alongshore current was close to 4 or 5 times that of the cross-strait variance. The alongshore currents were strongest during times of open water and weakest under ice cover (Appendix 1) which is consistent with earlier records. Also, magnitudes lessened with depth. Ice, in the form of mobile or landfast ice, was present in the Sound from Nov. 1 1998 – Jul. 20 1999; Oct. 12 1999 – Jul. 15 2000; and Oct. 18 2000 – Jul. 10 2001. During these periods, landfast ice was present from Feb. 6 1999 – Jul. 14 1999; Dec. 13 1999 – Jul. 2 2000; and Feb. 13 2001 – Jul. 10 2001 (Prinsenberg and Hamilton, 2003). These dates are indicated in time series plots presented in Figure 27 to Figure 31.

The moored CTD (Microcat) data from the same moorings and from moorings adjacent to the ADCP sites also resulted in virtually continuous 3-year records. Only those instruments whose data were used in this analysis are pictured in the mooring diagram (Figure 2).

Hourly meteorological observations were obtained from Environment Canada for the station at Resolute to examine the ocean's response to local wind forcing. Data included air temperature, wind direction and magnitude, and sea level pressure. Data, data products, and analyses results are presented in detail in Appendices 1 to 5.

Data Processing and Analyses

Create a complete 3-year record for Microcat data

The ADCP and Microcat data from northern and southern sites were collected from 3 separate moorings (replaced annually) for 3 years for each shore. Times of recovery and consequent redeployment of the instruments produced gaps (10-14 days) in what would have been continuous 3-year data records. The ADCP data were supplied with these gaps already filled by a tidal prediction based on analysis of the adjacent records (Roger Pettipas, personal communication). For the CTD data, averaging the data for the day prior to and the day following the start and end of each gap and then linearly interpolating between these two average values filled the CTD time series gaps. Since interest was in periods longer than 2 weeks, a more comprehensive approach such as that which was used for the ADCP data was not necessary. The 3-year CTD time series are presented in Appendix 3.

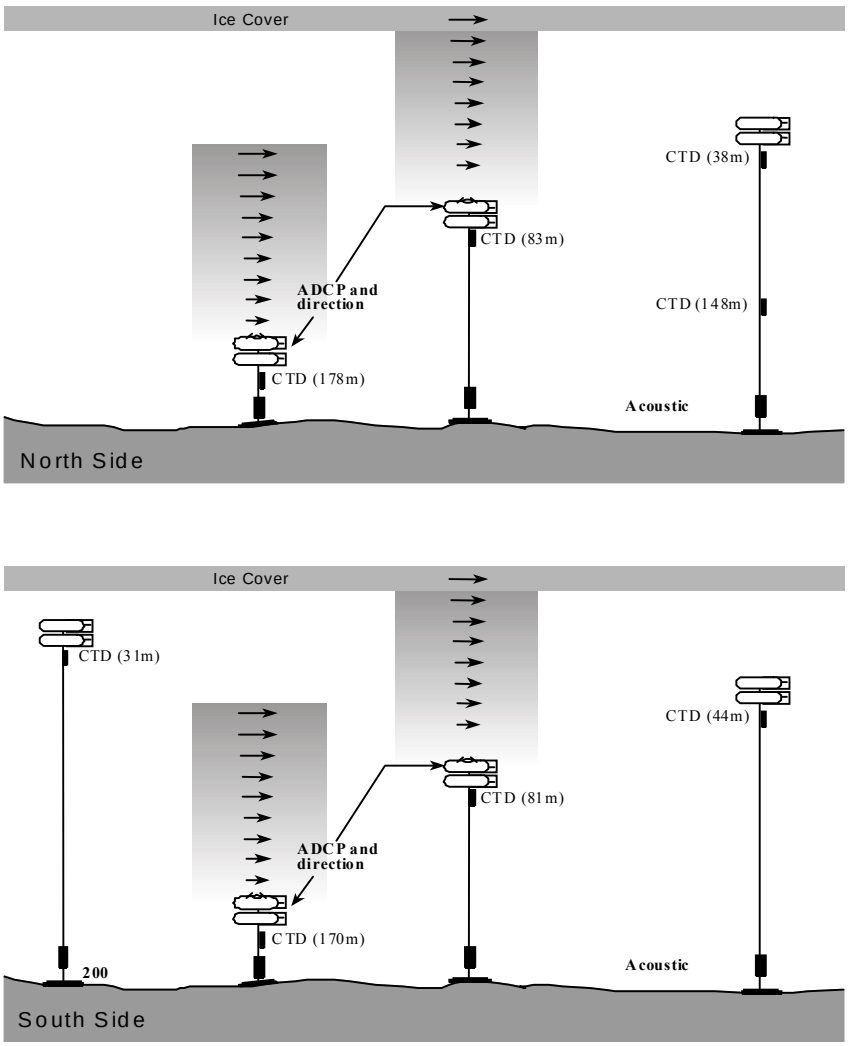

Figure 2 Mooring diagram showing instruments which sampled the data used in this study (amended from Hamilton et al., 2002).

Cross-correlation of ADCP data

The cross-correlation matrix was computed for the original, unfiltered, 2-hourly, 3-year ADCP data for both shores together at 3 representative depths (shallow, mid-depth, and deep) to see if the alongshore flow in the north was related to the southern alongshore flow (Table 1).

Table 1 Cross-correlation matrix for alongshore flows at 3 representative depths. Data were from raw, unfiltered, 2-hourly, 3-year ADCP records.

		38 m	74 m	146 m	29 m	69 m	161 m
north	38 m						
	74 m	0.81					
	146 m	0.63	0.83				
south	29 m	**0.30**	**0.39**	**0.41**			
	69 m	**0.39**	**0.48**	**0.49**	0.89		
	161 m	**0.44**	**0.54**	**0.59**	0.77	0.85	

The alongshore flow correlations of the raw data are all values positive. This means that the Sound reacts and moves in one direction, in general, in response to outside forcing including tidal forcing. The weaker correlations between the north and south alongshore currents (9-35% of variance accounted for) indicate that the two areas act more independently than the water column at each shore. Clearly there is inter-depth dependence over the total water column within each region (40-80% of variance is inter-related).

Nonlinear fit of annual harmonic to ADCP data

The one-year time series presented by Hamilton et al. (2002) showed that the currents and hydrographic properties exhibited a considerable annual cycle. We decided to extract this cycle by fitting an annual mean and single harmonic component with a period of 1 year. The harmonic (mean current) could then be compared to low frequency forcing such as the relative sea level slope between the Arctic Ocean and Baffin Bay. Consider, for example, the frictional barotropic response to the sea level slope: ($-g\frac{\partial \zeta}{\partial x} = c_D \frac{|u|u}{h}$). An estimate for the surface tilt $\partial\zeta$ between the Arctic Ocean and Baffin Bay would be 0.03 m if g = 10 ms^{-2}, C_D = 3 x 10^{-3}, h = 100 m, ∂x = 1000 km (estimated distance between Arctic Ocean and Baffin Bay), and the amplitude of the low frequency harmonic is 10^{-1} ms^{-1}. That is, a 3-cm sea level difference between the Arctic Ocean and Baffin Bay would drive a 10 cms^{-1} flow through an idealized channel.

The nonlinear fit of the annual harmonic, $\hat{y} = \beta_0 + \beta_1 \cos(\omega(t - \beta_2))$ ($\omega = \frac{2\pi}{\lambda}$; λ=*366 days)* was made to the unfiltered 2-hourly ADCP data for selected depths (Appendix 1, Figure 27 to Figure 31). Computed amplitudes and phases (β_2) are listed in Table 2 and are plotted with respect to depth in Figure 3 and Figure 4. The phase gives the time of the peak mean current and is listed as calendar days in Table 2 with respect to a January 1 reference point when t = β_2. Negative amplitude values are made positive by adding a half cycle (π rad = 183 days = 6 mo.) from the computed phase (new phase is in parenthesis).

The 3-year ADCP means in Table 2 show that the outflow from the Arctic Ocean into Baffin Bay (positive values) was found along the southern shore. It occurs at all depths and reaches seasonal maxima in August; earlier but weaker at the bottom than at the top. Along the northern shore a 3-year mean flow is from Baffin Bay but is mainly restricted to the top 100 m. This surface flow reaches its seasonal maximum (negative values) in the middle of September to early October, about a month later than the outflow along the southern shore.

On the north shore, the annual component amplitude is significant, varying almost linearly from ~ 8 cms^{-1} at the shallowest depth to ~ 2.7 cms^{-1} at mid-depth then decreasing to ~0.3 cms^{-1} near the bottom. This indicates that the response at the annual frequency is strongly depth dependent with very weak mean currents below 100 m. The mean current peaks after about 73 days in the near-surface (early March)

and after about 20 days (mid-January) near the bottom. However, at mid-depth, the current peaks from about 100 days to 160 days which is in the spring. The current near the bottom leads the shallow flows, an effect that may be cause by non-linear friction (Proudman, 1953, pp. 310-311).

On the south shore, the annual components are even stronger, varying from ~15 cms^{-1} near the surface to ~4 cms^{-1} near the bottom. The peak is anywhere from 214 days at depth (August) to 245 days near the surface (October) with the phases nearly constant below 70 m.

Ignoring the weaker deeper flows along the northern shore, the listed phases show that the north and south shore are anywhere from 2 weeks to 6 weeks out of step with each other depending on depth; however, they are in opposite directions. If we use a mean amplitude of 0.073 ms^{-1} (weighting the north and south equally, and peak eastward flow in early November) and a depth of 150 m, then the barotropic response would have to be driven by a relative gradient of $\frac{0.003 \times 0.073^2 \times 10^6}{9.8 \times 150} = 0.109$ m.

The mean flows along the north shore show a mid-depth minimum that is consistent from year to year (see Appendix 1, Table 19, Figure 32 to Figure 34). The annual harmonics are also very consistent among years. On the other hand, the strong mean flows along the south shore reduce near the surface and reach their maximum at ~30 m. This is also seen in the analysis for each year treated separately (Appendix 1, Table 20, Figure 35 to Figure 37). Note also, that unlike the north shore, the annual mean flow and the harmonic amplitudes for the south shore are approximately twice as strong in 1999 and 2000 as they were in 1998.

The amplitude decreases with depth on both shores indicating that there is some drag from the bottom or internal mass adjustment. Except for the decrease of the mean flow at 9 m on the south shore (Table 2) there is no obvious effect from ice cover that was present for 5.5 (1999), 6.5 (1999-2000), and 5 (2001) months of the year as landfast ice. Nevertheless, the effects of ice cover on the current are seen most dramatically in Figure 38, Figure 40, Figure 42, Figure 44, Figure 48, and Figure 50 as a profound reduction in the near surface flow during the period when landfast ice was present.

Table 2 Three-year means, amplitudes and phases for nonlinear fit to 3-year ADCP data (2-hourly and unfiltered).

North Depth (m)	Mean (cm/s)	Amplitude (cm/s)	Phase (calendar day)
10	-2.6	7.9	73
30	-1.9	6.5	87
50	-1.1	4.2	106
70	-0.2	2.7	121
90	-0.4	1.6	167
110	-0.7	0.7	160
130	-1.3	0.2	79
146	-1.7	0.3	19

Initial conditions for iterations: [-3 6 40]

South Depth (m)	Mean (cm/s)	Amplitude (cm/s)	Phase (calendar day)
9	10.3	15.3	245
29	13.2	10.9	226
41	13.0	10.1	223
61	12.3	9.0	219
69	11.9	8.4	217
97	11.8	7.6	212
109	11.3	6.9	213
125	10.4	6.2	214
141	9.4	5.5	213
161	8.0	4.3	214

Initial conditions for iterations: [-3 6 40]

From the harmonic analysis results of the 3-year ADCP data, a best fit linear regression (current = constant + slope*depth) of the amplitudes in Figure 3 for the north shore gives a constant of 7.5 cms^{-1} and a slope of -5.8 cms^{-1} per 100 m. For the south shore (Figure 4) the slope is nearly identical, -5.9 cms^{-1} per 100 m but the constant, 13.4 cms^{-1}, is larger. The similarity in the slopes shows that the vertical shear is nearly identical despite the difference in the constants (the constant represents the velocity). Figure 5 shows scatter plots of the amplitudes and phases for both shores with their linear fits. Note that the bottom depths at both sites are within 8 m of each other. If the depths were radically different then the shears would be different to accommodate the annual cycle.

The time series plots of the nonlinear fit to the 3-year unfiltered 2-hourly ADCP records are found in Appendix 1 (Figure 27 to Figure 31) along with fit results to 1-year unfiltered 2-hourly ADCP data records (Figure 38 to Figure 52). It is evident for some of the depth records (see southern mooring at 29, 41, 61 m in Figure 29 in particular) that the annual harmonic varies from year to year. This is confirmed in Table 3 where the surface and mid-depth results for 1-year harmonic fits are tabulated (see also Table 19 and Table 20 in Appendix 1 for complete results). For the mid-depth, the phases differ by 2 months on the north shore in 1998 from the other two years and differ by 40 days on the south shore in 2000 from the previous two years. At the surface the phases appear more stable from year to year with the greatest inter-annual difference being one week and occurring in the north. We note that in almost

all years, in the surface layer, the stronger currents along both shores are in phase but flow in opposite directions to each other: there is an inflow along the north shore that peaks in early September (add 180 days to phases for the north at 10 m) in all years while an outflow peaking in early September is seen along the south shore for all three years.

Table 3 Mean, amplitude, and phase of harmonic fit to 1-year ADCP data records for mid-depths.

	Year	Mean (cm/s)	Amplitude (cm/s)	Phase (calendar day)
North 10 m	1998	-4.9	8.9	68
	1999	-1.7	7.0	69
	2000	-1.7	7.9	77
North 70 m	1998	-0.8	2.8	165
	1999	-0.7	3.3	102
	2000	0.9	3.0	104
South 9 m	1998	7.4	8.9	247
	1999	11.3	19.2	241
	2000	11.4	18.2	246
South 69 m	1998	6.0	5.7	201
	1999	13.9	9.7	200
	2000	15.5	10.4	240

Data collected in 1978 and 1979 by Lemon and Fissel (1982) at the eastern end of Lancaster Sound presents the strongest inflow in early September in the north and the strongest outflow in mid-October in the south. This is consistent with our findings at the western end in the south but out of phase with our findings in the north by a few months. The Lemon and Fissel data in the north at 250 m produce a harmonic amplitude of 5.5 cms^{-1} and a phase of 8 months and at 400 m the data produce an amplitude of 7.4 cms^{-1} with an 8.2 month phase; this leads our deepest record by a few months. Also, it appears that our deepest amplitude values are dampened in the north. In the south the Lemon and Fissel data give amplitudes of 11.4, 13.5, and 5.2 cms^{-1} (35, 250, and 500 m) and phases of 9.4, 9.6, and 9.6 months. The phases lag our data by a month or two but both the lead in the north and lag in the south seem reasonable considering that the Lemon and Fissel stations are further east than our moorings. The shallow and deep amplitudes of the historic southern station data are consistent with our findings. This leads us to propose that Baffin Bay water enters Lancaster Sound in the north, flowing westward and following the topography. Lancaster Sound becomes shallower at its western end as it joins Barrow Strait so we propose that the Baffin Bay water turns around at this point to flow eastward along the southern part of the sound. This is consistent with the pressure difference noted by Prinsenberg and Bennett (1987). The smaller amplitude in the north is due to damping by the surface tilt between the Arctic Ocean and Baffin Bay whereby the forcing is eastward, acting against the flow in the north.

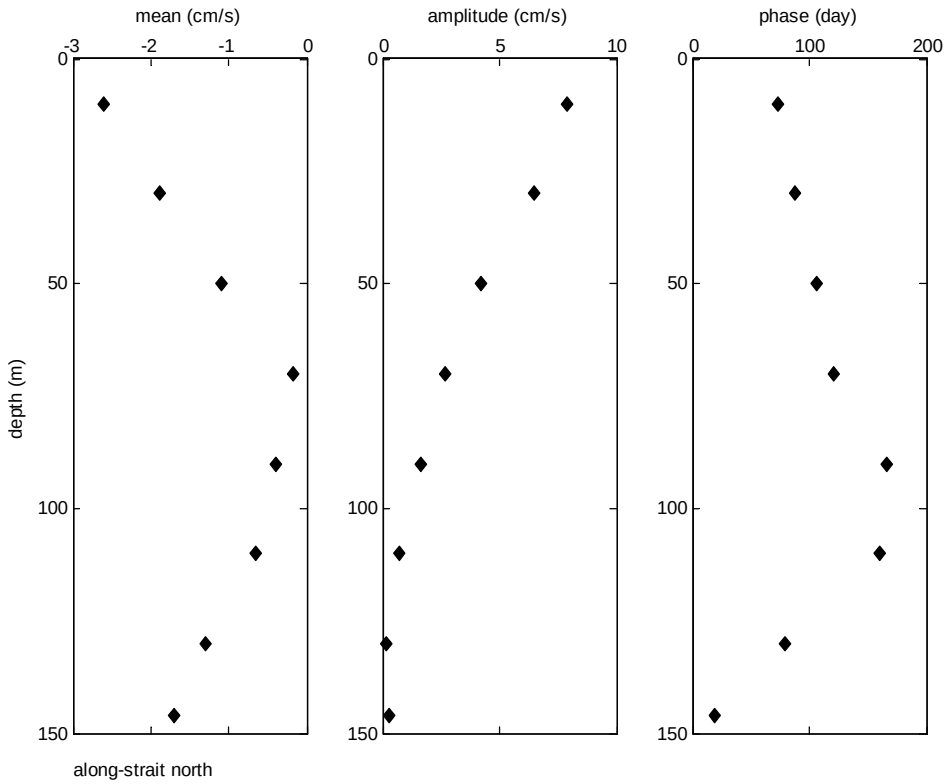

Figure 3 Vertical profile of amplitude and phase information for nonlinear fit of the annual harmonic to the raw 3-year ADCP data (north shore).

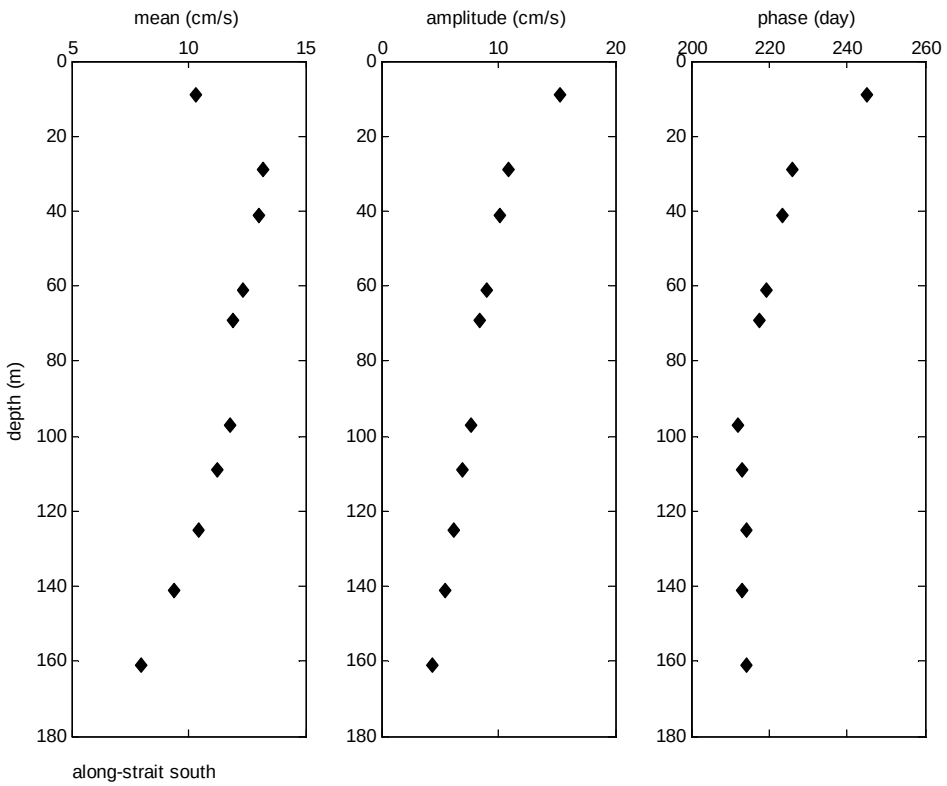

Figure 4 Vertical profile of amplitude and phase information for nonlinear fit of the annual harmonic to the raw 3-year ADCP data (south shore).

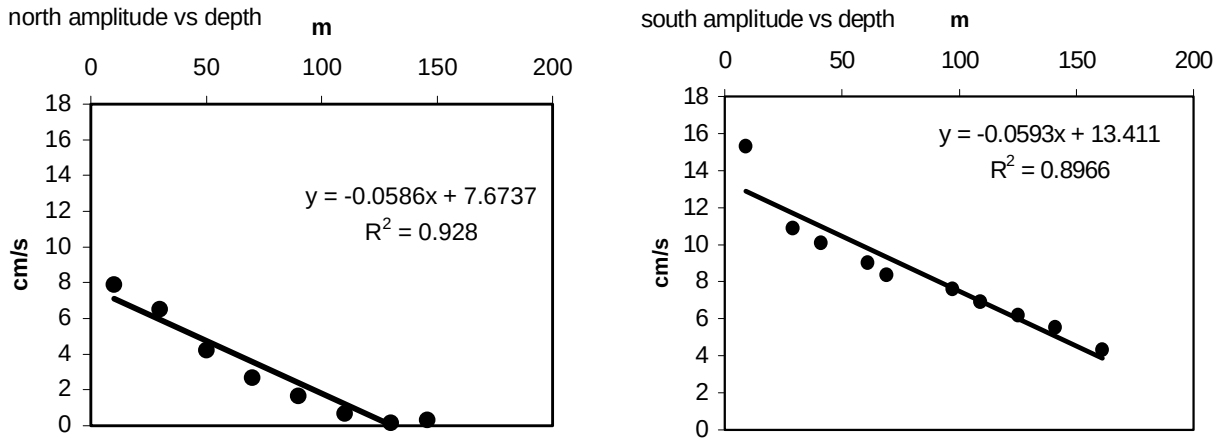

Figure 5 Least squares fit of depth to amplitude for north and south annual harmonic fits to 3-year data.

Spectra

Spectra were calculated on ADCP 3-year records for both shores at the same depths as the annual harmonic fits except at 90 m on the north shore since so much of the original data were missing for the final deployment year (see the first plot in Figure 43). The 3-year linear trends and the 3-year means were removed. The goal was to see if low frequency distributions were concentrated in specific bands: meteorological, seasonal, etc. The window size was 256 points and the number of FFTs was 4096 points (about a year's data for 12 samples per day). Spectra are shown in Appendix 2 in Figure 53 to Figure 56 with data units converted to *SI* measures. The diurnal and semidiurnal tides are obvious in the spectra but there is also a 3 times daily weaker signal in mid-depth and deep. This is the MK_3 tidal constituent that is the nonlinear interaction between the M_2 and K_1 tides with a period of 8.2 hours. The energy in the low frequency, diurnal, and semi-diurnal bands was computed by integrating under the spectrum across each band. The results are given in Table 4 and shown in Figure 6. In the north the diurnal band slightly intensifies towards the bottom and the semi-diurnal band has slightly less energy at 10 m but is otherwise the same. In the south, there is reduced energy at 9 m in the diurnal band but it is very constant below this level with slightly higher peaks at the deepest point. In the south, the semi-diurnal band is reduced at 9 m but is otherwise the same below this point. The low-frequency bands in the north and south show greatest energy in the upper depths with the south side having significantly more energy than the north, a reflection of the seasonal variation seen in Table 2.

Table 4 Integration under the spectra for each depth across the low frequency, diurnal, and semi-diurnal bands. Values are in units of power $(ms^{-1})^2$.

North			
Depth (m)	Low freq. (0 to 0.9e-5 Hz)	Diurnal (2.1e-5 to 2.5e-5 Hz)	Semi-diurnal (1.1e-5 to 1.2e-5 Hz)
10	1.22e-002	2.59e-003	1.82e-003
30	9.84e-003	5.38e-003	3.43e-003
50	7.18e-003	6.14e-003	4.03e-003
70	5.36e-003	5.56e-003	4.92e-003
110	5.78e-003	4.89e-003	6.75e-003
130	4.98e-003	5.01e-003	7.67e-003
146	4.09e-003	5.45e-003	8.62e-003
South			
Depth (m)	Low freq. (0 to 0.9e-5 Hz)	Diurnal (2.1e-5 to 2.5e-5 Hz)	Semi-diurnal (1.1e-5 to 1.2e-5 Hz)
9	2.41e-002	1.51e-003	2.08e-003
29	1.69e-002	3.66e-003	4.45e-003
41	1.58e-002	4.65e-003	4.66e-003
61	1.48e-002	6.11e-003	4.93e-003
69	1.49e-002	5.96e-003	4.99e-003
97	1.58e-002	4.80e-003	4.74e-003
109	1.47e-002	5.27e-003	5.29e-003
125	1.38e-002	5.17e-003	5.54e-003
141	1.21e-002	4.96e-003	6.08e-003
161	8.47e-003	4.27e-003	7.51e-003

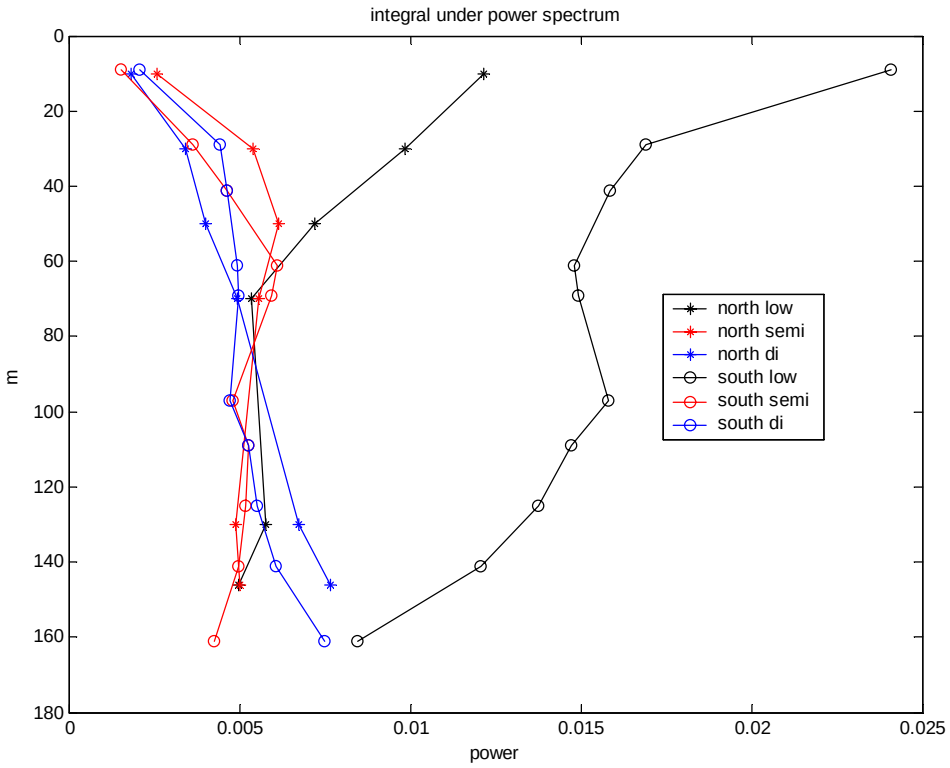

Figure 6 Integration for 3 power spectral bands on the north and south shores.

The annual harmonic fit to the flow showed that the lower frequencies might have been highly coherent for all depths (i. e. consistent phase) so the coherence was computed between shallow and mid-depth water, shallow and deep water, and mid-depth and deep water. The window size and number of FFTs used were the same as for the previous spectral density estimates. The coherence function estimates are displayed as line graphs in Appendix 2 in Figure 57. All plots show the same distributions of coherence with peaks at semidiurnal, diurnal, and at very low frequencies. Table 5 lists the coherence maxima for both shores.

Table 5 Approximate coherence magnitudes of semi-diurnal, diurnal, and low frequency maxima.

	north			south		
	semi-diurnal	diurnal	low	semi-diurnal	diurnal	low
shallow and mid-depth	0.73	0.81	0.48	0.70	0.87	0.65
mid-depth and deep	0.97	0.94	0.52	0.95	0.97	0.85
shallow and deep	0.77	0.73	0.17	0.74	0.83	0.46

The semidiurnal peaks range from ~0.7 – 0.97 with the highest values between mid and deep levels. The diurnal coherences are slightly higher, with greatest values between mid and deep levels. The behaviour is the same for the north and south shores. The low frequency peaks are higher (~0.46 – 0.85) on the south compared to the north shore (~0.17 – 0.52). Again for both sides of the Sound, the mid-depth and deep levels have the highest values with the south showing more coherence than the north. Note also that the coherence has a peak (for mid-depth and deep) that has a period of ~8 h for both shores but there is no corresponding significant energy peak.

The phase differences for the coherence estimates of each of the three depth pairs are shown in Figure 7 and Figure 8. As expected the lowest frequencies showed very little difference in phase for the depth pairings with the one exception being the shallow and deep pairing for the northern mooring. The figures also show that little phase difference exists in the diurnal and semi-diurnal bands.

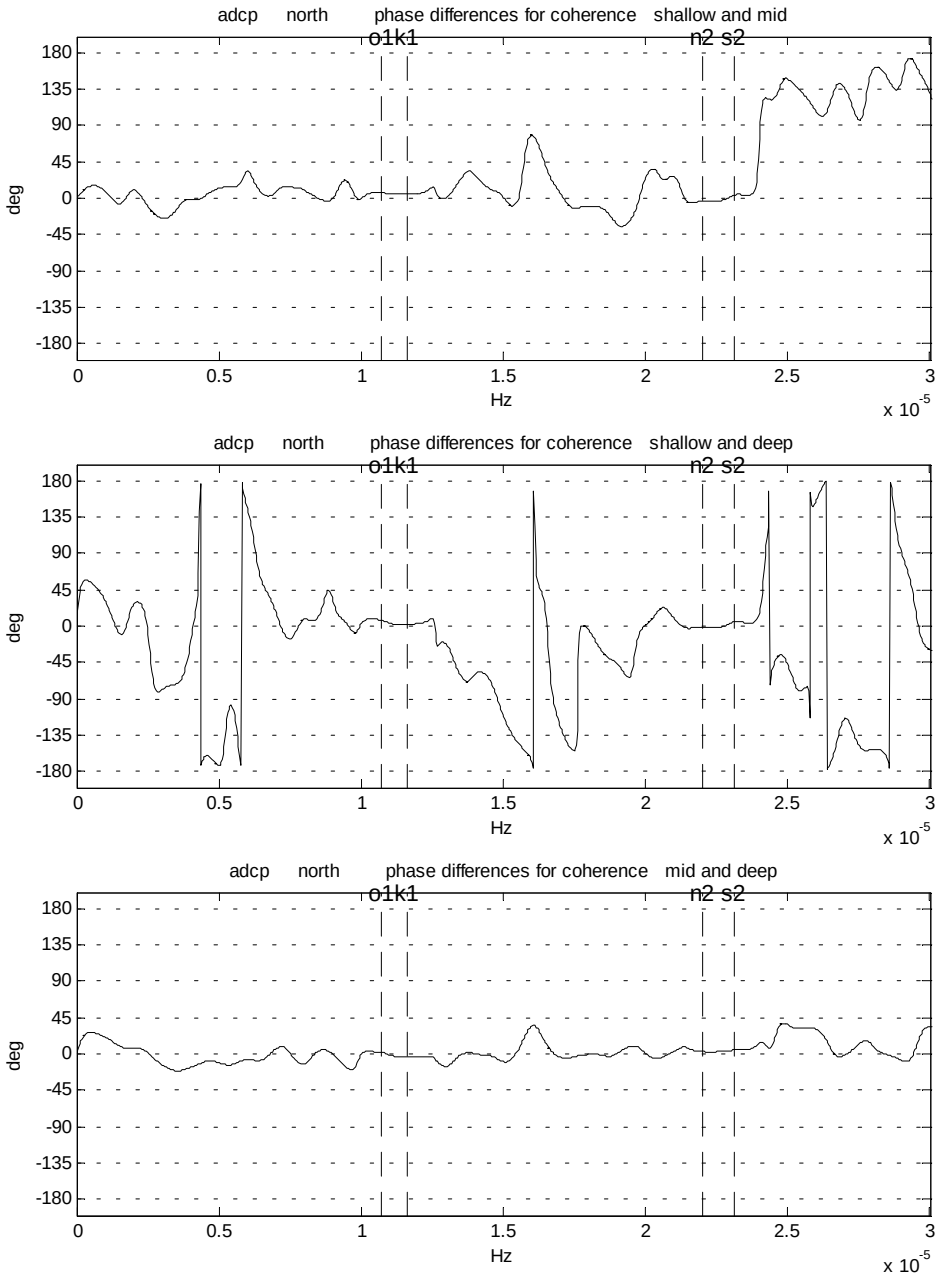

Figure 7 Phase differences for frequencies at 3 depths. Data are from the northern ADCP mooring. Red dashed lines depict frequency of S_2, N_2, K_1, and O_1 tides.

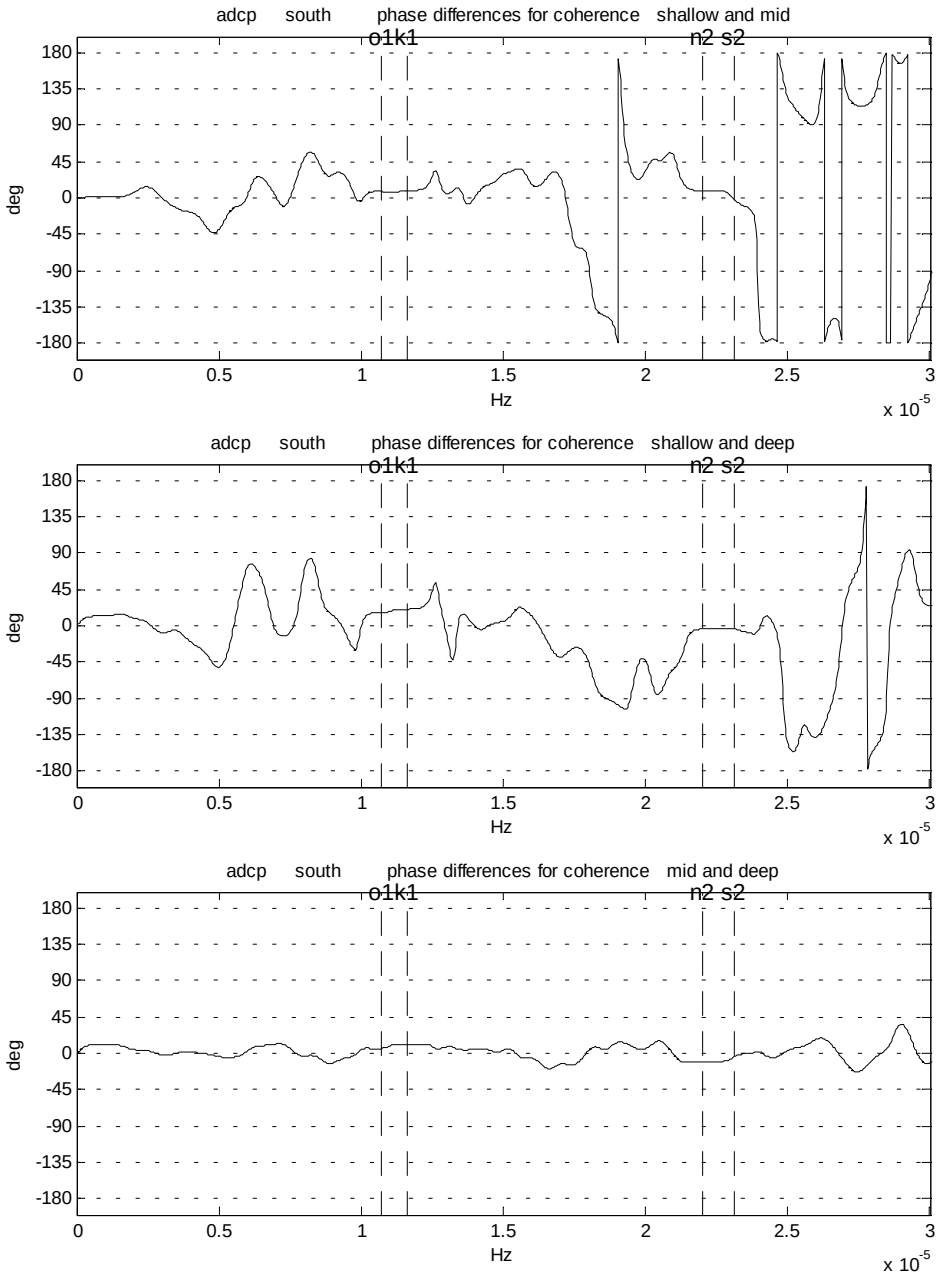

Figure 8 Phase differences for frequencies at 3 depths. Data are from the southern ADCP mooring. Red dashed lines depict frequency of S_2, N_2, K_1, and O_1 tides.

Lowpass filtering

Since our interest was in the low frequency bands it seemed prudent to reduce the size of the dataset by lowpass filtering it. Decimation of the data to 14-day intervals involved applying an eighth order Chebyshev Type I filter with cutoff frequency equal to $0.8\times\left(\frac{1}{7200s\times 2}\right)\times\left(\frac{1}{12samples\times 14days}\right)$. The data were then resampled at

1/168 of the original 2-hourly sampling rate. The filter response curve is shown in Figure 9 and shows that 50% of the power is passed at approximately 0.45 x 10^{-6} Hz. Data were not detrended before decimation. Time series of the filtered data are shown in Figure 10 and Figure 11. A harmonic fit (annual harmonic) to these data underestimates the extreme maxima/minima of the shallow water but fits the data quite well for mid-depth and deeper waters. The deep water shows little variation in the north with a stronger annual cycle at the southern mooring. The shallow water is a little out of phase with the deeper water. On the north shore, the low frequency variance ranges from 4 to 21% of the total; whereas, on the south shore, the range is 18 to 42%. This indicates that low frequency variability is more concentrated on the south shore because of the Coriolis effects and because the width of the Sound is much greater than the local Rossby radius.

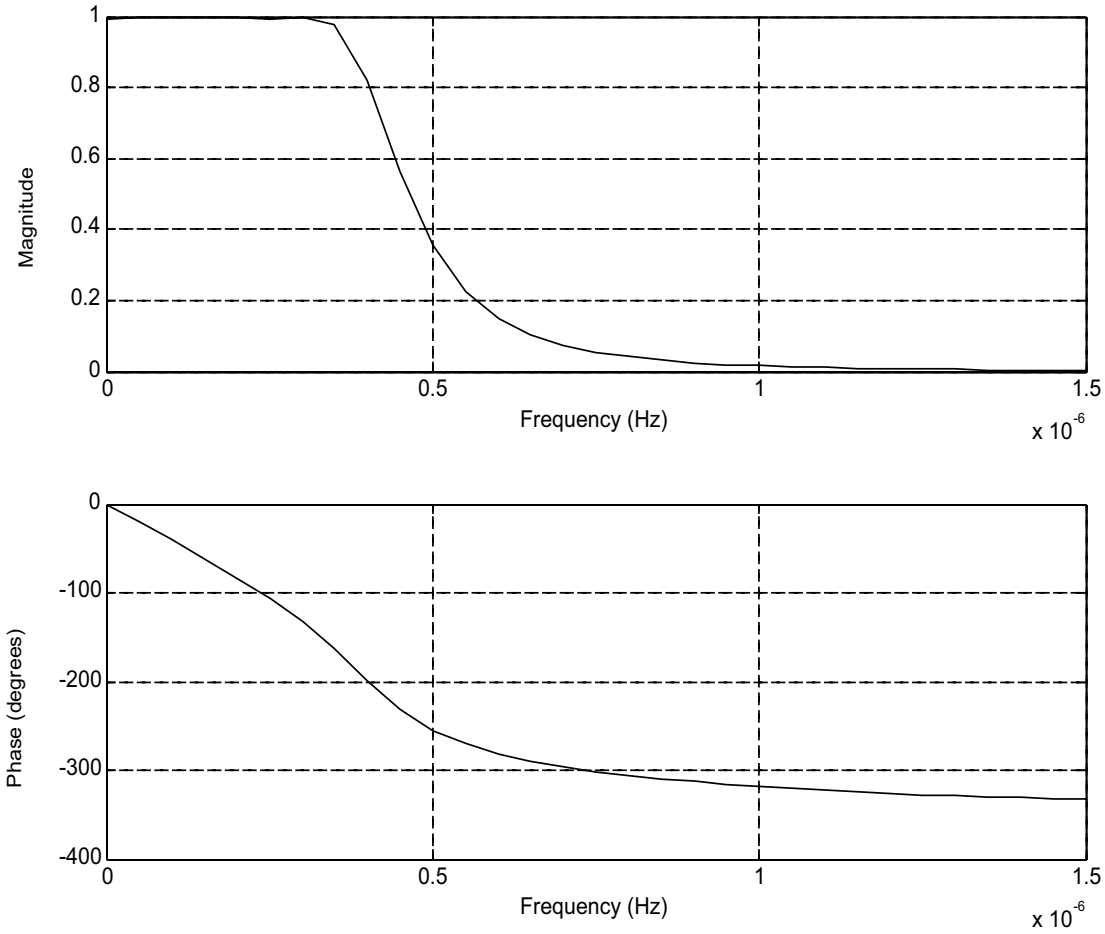

Figure 9 Frequency response curve for lowpass Chebyshev filter.

Table 6 Variances of raw (unfiltered) ADCP data and of lowpass filtered data.

north			south		
depth (m)	raw $(mm/s)^2$	filtered $(mm/s)^2$	depth (m)	raw $(mm/s)^2$	filtered $(mm/s)^2$
38	18628.19	3979.61	29	29770.70	12558.36
74	17949.97	1836.83	69	30883.16	11314.53
146	21294.19	871.62	161	25632.92	4570.56

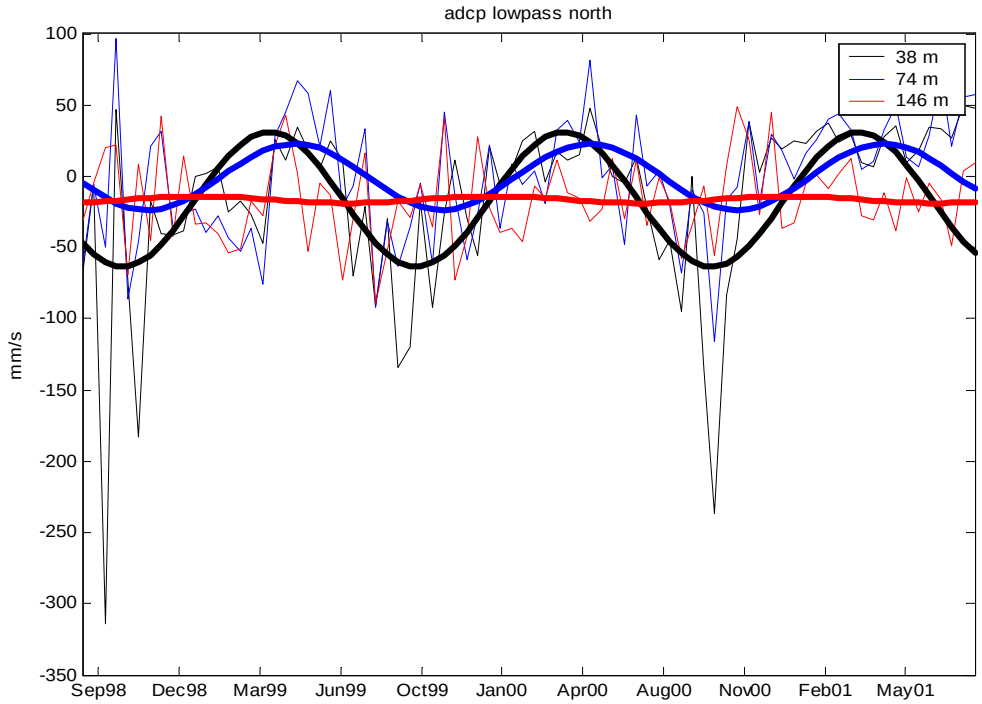

Figure 10 Lowpass filtered ADCP data with annual harmonic superimposed. Three depths: shallow, mid-depth, and deep are shown for the northern mooring.

The 3-year moored CTD data (Figure 58 to Figure 65) were also lowpass filtered and decimated so that analyses involving ADCP and CTD data could be completed. Lowpass filtered CTD data are presented in Appendix 3 (Figure 66 and Figure 67). The lowpass CTD data in the appendix were not detrended before being filtered.

The water mass properties appear to have less of an annual cycle in the sinusoidal sense than the currents, particularly for the north shore (Figure 58 to Figure 65). However, this conclusion is less compelling when the harmonics are superimposed on the filtered records (Figure 66 and Figure 67). For temperature, salinity, and density, we note the large amplitudes at depth and the apparent phase difference in the south, which indicates the influence of a different water mass. The north shore seems more smoothly varying with depth with the amplitude decreasing with depth and the phase becoming progressively later. Vertical CTD profiles (Figure 68 to Figure 73) show variation in the pycnocline from year to year for the August casts yet little difference in deep water density; however, contoured time series (Figure 74 to Figure 76) show periodic occurrences of high density water at depth, especially in the north.

The cross-correlation matrix (Table 7) for low-pass filtered density data (14-day), calculated for each year, shows that the southern shore's deep water is negatively correlated with the water above it. This implies that estuarine dynamics may control the vertical density distribution in this region consistent with what is seen in the

contoured time series in Figure 74 to Figure 76 (heavier, saline water at depth opposing fresher water surface-flow to satisfy continuity conditions). Figure 11 compared to Figure 67 shows that the time of the lowest deep water alongshore velocity in the south (winter) almost corresponds to the time of highest density at that depth.

Table 7 Cross-correlation matrix for yearly low-pass filtered (14-day) density data.

Density data north				
1998	38 m	83 m	148 m	178 m
38 m				
83 m	0.53			
148 m	-0.26	0.20		
178 m	-0.29	0.17	0.90	
1999	38 m	83 m	148 m	178 m
38 m				
83 m	0.65			
148 m	-0.42	0.08		
178 m	-0.54	-0.29	0.82	
2000	38 m	83 m	148 m	178 m
38 m				
83 m	0.69			
148 m	0.55	0.71		
178 m	0.57	0.47	0.85	
Density data south				
1998	31 m	44 m	81 m	170 m
31 m				
44 m	0.90			
81 m	0.51	0.46		
170 m	-0.65	-0.65	-0.05	
1999	31 m	44 m	81 m	170 m
31 m				
44 m	0.77			
81 m	-0.05	0.28		
170 m	-0.38	-0.44	-0.07	
2000	31 m	44 m	81 m	170 m
31 m				
44 m	0.74			
81 m	0.25	0.72		
170 m	-0.06	-0.14	-0.14	

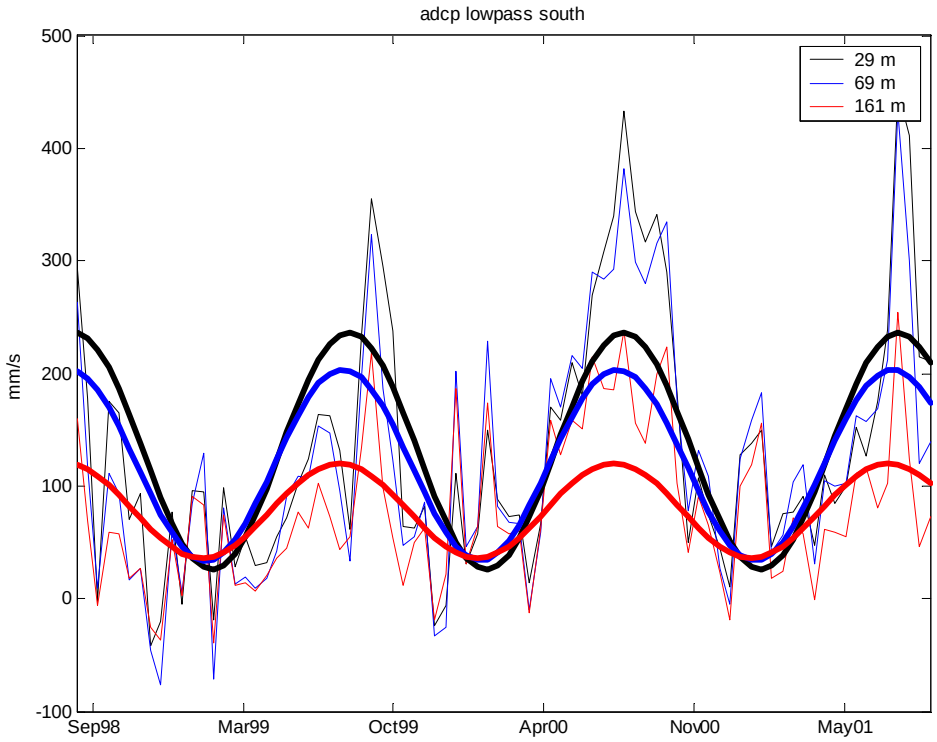

Figure 11 Lowpass filtered ADCP data with annual harmonic superimposed. Three depths: shallow, mid-depth, and deep are shown for the southern mooring.

Principal Components Analysis

To explore the relationship among the observed low frequency variations, principal component analyses (PCA) were performed on the data records. The analysis is an attempt to reduce the number of parameters needed to describe the variance of the physical system observed in Lancaster Sound. Lorenz (1956) used this statistical analysis technique in a meteorological application with respect to weather prediction. Emery and Thomson (1997) describe the application of the analysis with respect to oceanography in the book, Data Analysis Methods in Physical Oceanography.

In our analysis, the principal components were at first computed for the ADCP records (shallow, mid-depth, and deep) and the temperature, salinity, and σ_t records (4 depths) separately. Objectives of the initial analyses were to look at the:

1. distribution of variance by mode
2. amplitude structure
3. modal variability
4. time series of individual modes with significant variance

The initial analysis was carried out on time series filtered to remove the diurnal and semi-diurnal tides. We used a Cartwright filter with 50% power passed at 28 h. These filtered records were decimated to 6-hour intervals. We call these filtered series the "high-frequency" series.

Cross-correlation matrices were computed for the high-frequency (6-hourly) ADCP and CTD data to look for superficial relationships between depths and water properties. These matrices are presented in Table 21 and Table 23 in Appendix 4. It is no surprise that the southern ADCP data shows better correlation among its three data depths than the northern data did. Nor are the correlation values a great surprise considering the cross-correlation of the raw data shown in Table 1. Nevertheless, comparing Table 1 with Table 21 we note that removing the major tidal currents and higher frequency currents reduced the vertical correlation along the north shore but increased it along the south shore. The relationship between depths is not as clearly defined in the CTD data but we note the water property data in the south are better correlated in the shallower section of the water column than the deeper water below 44 m. In the south, mid-depth data is not well correlated with shallower or deeper water reflecting the earlier ADCP coherence results. In the north, water that is below 140 m is highly correlated but not well correlated with shallower water. Density (salinity) at mid-depth (83 m) is better correlated with the shallower water than the temperature.

Using the high frequency data (6-hourly), eigenvectors and eigenvalues for the PCA were computed for the *covariance* matrix where, at first, each time series was centered by removing its mean. The eigenvectors for the computations and plots of the modal behaviour of significant modes are tabulated and presented in Appendix 4 (Figure 77 to Figure 80; Table 22 and Table 24). Even though the records had variance for periods as short as approximately one day, the initial analysis reflected the high coherence at low frequencies within the alongshore currents and physical properties of the water. The first mode accounted for (72, 78, 77, 79%) and (93, 61, 65, 66%) of the (alongshore current, T, S, ρ) variance for the north and south shores. The north and south shore currents, south shore T, and north shore S and ρ eigenvectors have the same sign throughout the water column for Mode 1.

PCA was performed on the lowpass-filtered data (decimated to 14-day intervals) for each measured parameter using the covariance matrix on centred data. These lowpass-filtered data records will be referred to as the *low frequency* data in contrast to the earlier 6-hourly data referred to as high frequency. Results for the ADCP analyses are tabulated in this section in Table 8 with accompanying plots and analysis results for CTD data in Appendix 4 (Table 25, Figure 81 to Figure 86). The first mode accounted for (76, 80, 81, 83%) and (95, 66, 73, 73%) of the (U, T, S, ρ) variance for the lowpass-filtered data from the north and south shores. These values are slightly higher than those from the analysis that retained more of the high frequency variability. Thus the low frequency current variability is more coherent vertically at each site and horizontally across the entire sound than the high frequency current variability. The time series plots for the low frequency analysis (Figure 12 to Figure 14) includes a "synthetic data" series constructed using first and second modes for all depths and the "residual" computed from the difference between the original data and its synthesis. Individual PCA results for the lowpass CTD parameters at 4 depths are tabulated and presented in Appendix 4 (Table 25; Figure 81 to Figure 86).

The synthetic series was computed by adding the mean of the original lowpass data to the product of the eigenvectors with the modal series (also known as "z-scores").

The PCA analysis of the ADCP data by itself reveal that the first two modes represent more than 90% of the variance of the original system (Table 9). The minimum variance accounted for by the first two modes of the three uncorrelated time series is 82.3%. The eigenvectors in Table 8 show that the first mode carries most of the variance for the shallow water in the north and it represents little of the variance in the deep water. This is not surprising since little variation was seen in the deep water as was stated before (Figure 8). In order to "pick up" the deep water in the north, the eigenvectors show that at least the first 2 modes need to be used to "reconstruct" the original data (Figure 13). The data from the southern mooring show that the first mode can account for most of the variance in the system. This is very evident from Figure 14. The flow at all depths also seems to be uni-directional for the first mode which can be seen from the sign of the eigenvectors (either all positive or all negative).

Table 8 Results of principal component analysis (PCA) of low frequency (14-day) ADCP data for comparison of 3 depths (shallow, mid-depth, and deep).

ADCP ALONGSHORE FLOW						
North						
Eigenvectors					Eigen-values	% variance
	Mode 1	Mode 2	Mode 3			
Shallow	0.8561	0.4118	0.3122	Mode 1	5093.4442	76.16
Mid	0.5067	-0.5505	-0.6635	Mode 2	1260.4103	18.85
Deep	0.1014	-0.7262	0.6799	Mode 3	334.2049	5.00
South						
Eigenvectors					Eigen-values	% variance
	Mode 1	Mode 2	Mode 3			
Shallow	-0.6647	0.6903	0.2858	Mode 1	27115.0237	95.33
Mid	-0.6404	-0.3293	-0.6939	Mode 2	1179.0245	4.19
Deep	-0.3849	-0.6442	0.6610	Mode 3	111.4040	0.48

Table 9 Variance of ADCP series from PCA results (14-day data) using the first mode only and then the first 2 modes. Units are mm/s^2.

Variance: north shore	Mode 1			Modes 1 and 2	
	Original	Residual	% Removed	Residual	% Removed
Shallow	3979.6117	246.3105	93.8107	32.5712	99.1815
Mid	1836.8287	529.0409	71.1981	147.1286	91.9901
Deep	871.6190	819.2638	6.0067	154.5051	82.2738
Variance: south shore	Mode 1			Modes 1 and 2	
	Original	Residual	% Removed	Residual	% Removed
Shallow	12558.3552	579.5813	95.3849	11.0607	99.9119
Mid	11314.5334	194.5731	98.2803	65.1898	99.4238
Deep	4570.5637	554.2741	87.8730	59.1535	98.7058

Table 9 shows that the first mode alone removed (94, 71, 6%) of the variance from the ADCP records for the north shore and (95, 98, 88%) from the records for the south shore. The first mode in the north seems to be a shallow mode. Regardless of

the coherence then, the first mode accounts for almost all the variance on both shores and is the predominant velocity mode, especially in the shallow water.

It is noted that the PCA was also performed on data that had had their linear trend removed prior to lowpass filtering whereby the accounted for variance changed only by 1% in the shallow water and negligibly, if at all, for the other depths. This was also the case for the CTD data. Four time series of T, S, and ρ were analysed for both the north and south shores (Table 25). The first mode removed (80, 81, 83%) and (66, 73, 73%) of the (T, S, ρ) variance for the north and south shores, respectively.

Flow variance was compared with density variance by performing the PCA on the lowpass ADCP and σ_t data. The results are given in Table 10. This time the analysis was performed on data that had been normalized by their standard deviations to make their variances of the same order numerically. Centring and scaling the normalized data means that the PCA was essentially performed using a cross-correlation matrix since the covariance matrix and cross-correlation matrix would be equivalent under the circumstances. The difference made by detrending the data manifested itself in the modes of lesser significance (5 and 6) where the eigenvectors changed sign and the variance accounted for by the first mode changed by a few percent only. The analysis results that are presented are for data that were not detrended. Time series of original data, synthetic series, and residuals are presented in this section (Figure 15 to Figure 16) along with a table of variances for the three series at all depths (Table 12).

Table 10 shows that the first modes account for about 50% of the variance on both shores with slightly more being accounted for in the south shore than in the north. On the north shore, the components of the first eigenvector have the same sign; on the south shore, only the 170-m density component differed in sign. Strong shearing between the upper two levels and the bottom level in Mode 1 for the north shore is manifested by the difference in magnitudes of the flow eigenvectors as well as the vast difference in variance between those layers accounted for by that mode (Table 12). The density eigenvectors in the south show a reversal at the deepest level for Mode 1 that is also the mode that accounts for the least amount of density variance at the uppermost density level. These facts prompt investigation of a possible coupling between the alongshore flow and density response.

Table 10 Results of PCA of low frequency (14-day) ADCP data and density. The depths in metres are in the first column with instrument type.

ADCP AND CTD
ALONGSHORE FLOW (3 depths) AND DENSITY (4 depths)

North

Eigenvectors								Mde	Eig. vals	% var
	1	2	3	4	5	6	7			
Adcp 38	0.42	-0.24	0.48	-0.27	0.22	-0.60	0.23	1	3.58	51.18
Adcp 74	0.41	0.24	0.38	-0.42	-0.44	0.49	-0.07	2	1.65	23.51
Adcp 146	0.15	0.60	0.35	0.68	-0.07	-0.18	-0.00	3	0.86	12.34
Ctd 38	0.33	-0.52	0.22	0.41	0.31	0.38	-0.40	4	0.47	6.75
Ctd 83	0.39	-0.35	-0.34	0.32	-0.57	-0.06	0.43	5	0.29	4.17
Ctd 148	0.44	0.19	-0.47	-0.12	-0.05	-0.34	-0.64	6	0.08	1.15
Ctd 178	0.42	0.31	-0.34	-0.04	0.58	0.30	0.44	7	0.06	0.90

South

Eigenvectors								Mde	Eig. vals	% var
	1	2	3	4	5	6	7			
Adcp 29	-0.43	0.35	-0.06	0.15	-0.32	0.64	0.39	1	3.83	54.76
Adcp 69	-0.47	0.29	0.04	0.15	-0.00	-0.01	-0.82	2	1.71	24.43
Adcp 161	-0.46	0.24	0.01	0.30	0.26	-0.63	0.41	3	0.88	12.58
Ctd 31	-0.21	-0.64	0.17	0.50	0.41	0.31	-0.00	4	0.30	4.28
Ctd 44	-0.33	-0.53	-0.03	-0.04	-0.72	-0.28	-0.00	5	0.15	2.08
Ctd 81	-0.27	-0.18	-0.84	-0.32	0.28	0.07	-0.02	6	0.12	1.74
Ctd 170	0.40	0.10	-0.50	0.71	-0.25	-0.08	-0.08	7	0.01	0.13

The magnitude of the eigenvectors for the first mode on the north shore is equally high for the ADCP shallow and mid-depth water and for the density of the deeper water while the first mode eigenvectors for the deep flow and surface density are somewhat smaller. Note also that the eigenvectors are of the same sign for the first mode: all positive so that the response of both density and velocity are in phase. This means that increased velocity westward (negative velocity) in the north will be accompanied by an expected decreased density with depth (negative density response) due to the internal mass adjustment. Geostrophically balanced westward flow raises the sea level on the north shore and generates an offshore flowing bottom Ekman layer. This, in turn, causes the pycnocline to adjust downwards giving a density decrease at a fixed depth.

In the south, as flow increases eastward, one expects a similar response in density; i.e. the internal adjustment would be that density decreases (negative) with depth as the flow increases (positive). The expectation is not unreasonable considering cross-sections of density presented in Hamilton et al. (2002). However, looking at the first mode eigenvectors in Table 10, our hopes are dashed: the eigenvectors all have the same sign save for that which is associated with the deep water density. Eastward flow gives rise to increased density except at the bottom. Another possible explanation could be internal adjustment to the along-strait sea level gradient, but this would also lead to opposite signs between the velocity and ρ components. In fact, Mode 2, accounting for 24% of the variance, looks more like the response to internal mass adjustment than Mode 1. The cross-correlation matrix (Table 11) shows that the first mode on the south shore is dominantly a velocity mode with very strong

correlations between pairs of velocity data records for the three depths. The density is not as well correlated to the current as it is for north shore case. In fact there is notable negative correlation only in the deep water as in the eigenvectors. So at the southern mooring, when flow increased, density decreased only in the deepest water.

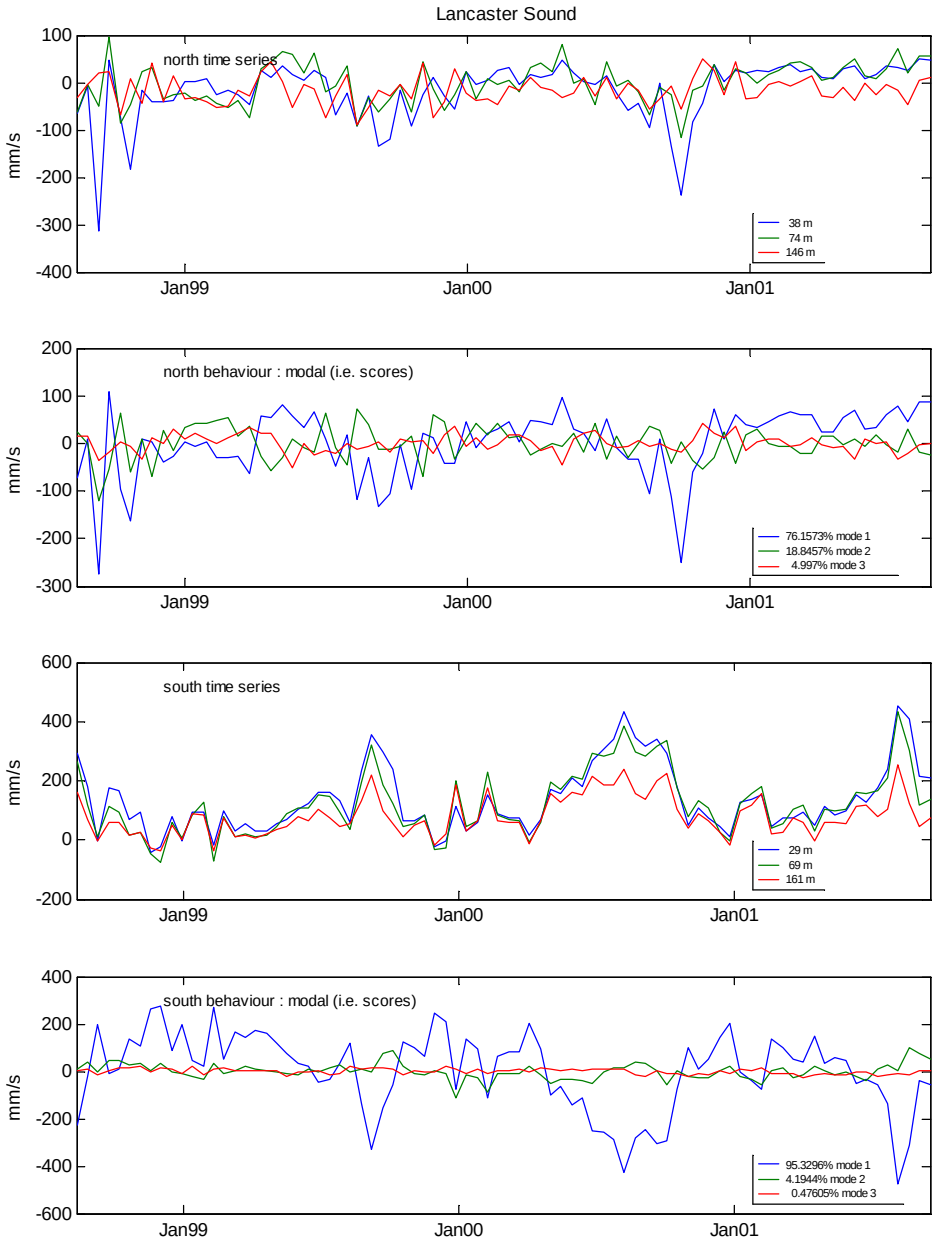

Figure 12 Time series of north and south low-pass filtered ADCP data (14-day) and first 3 principal components modal behaviour for shallow, mid-depth, and deep water.

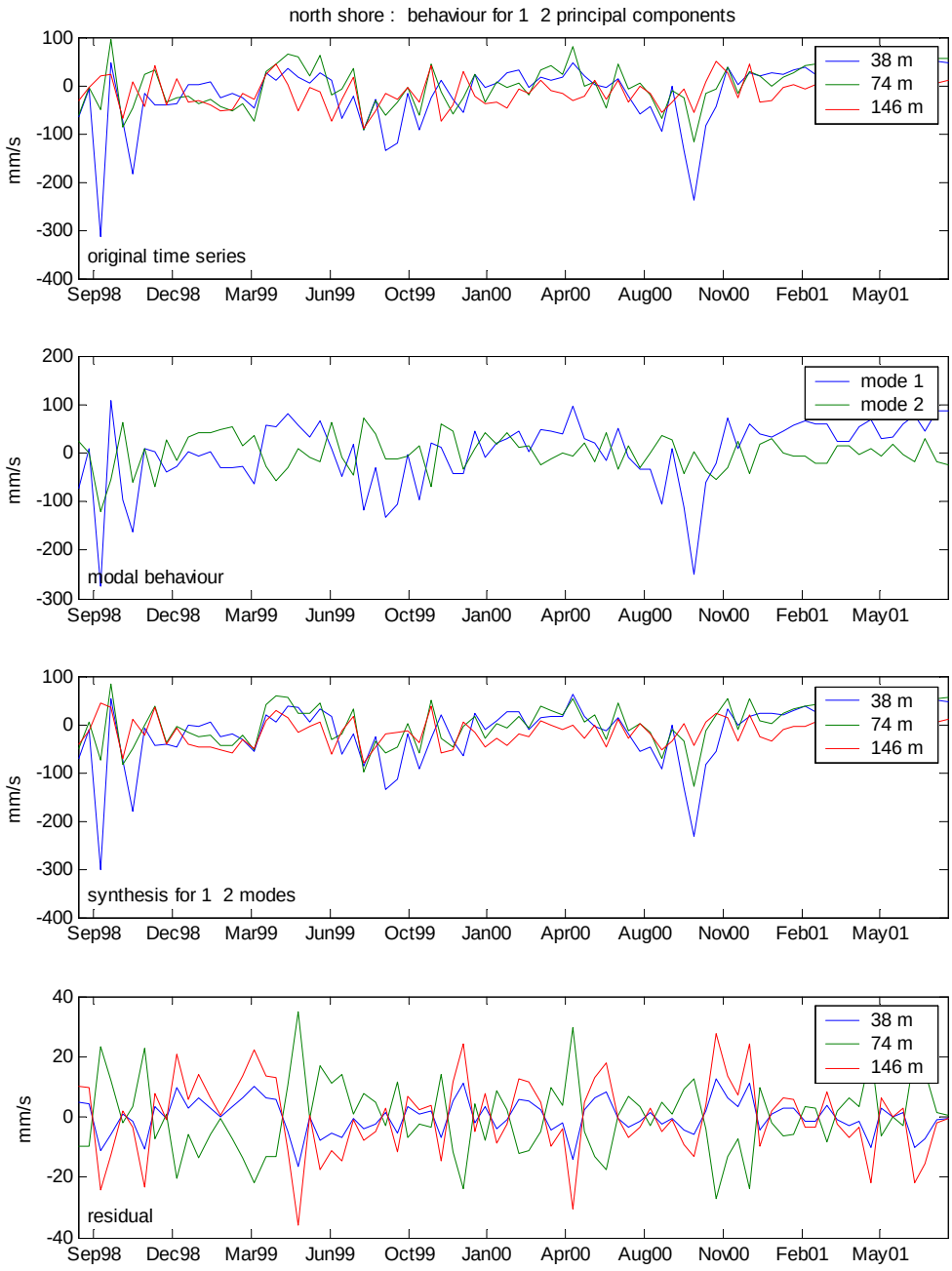

Figure 13 Principal component analysis (PCA) results for north shore ADCP data (14-day).

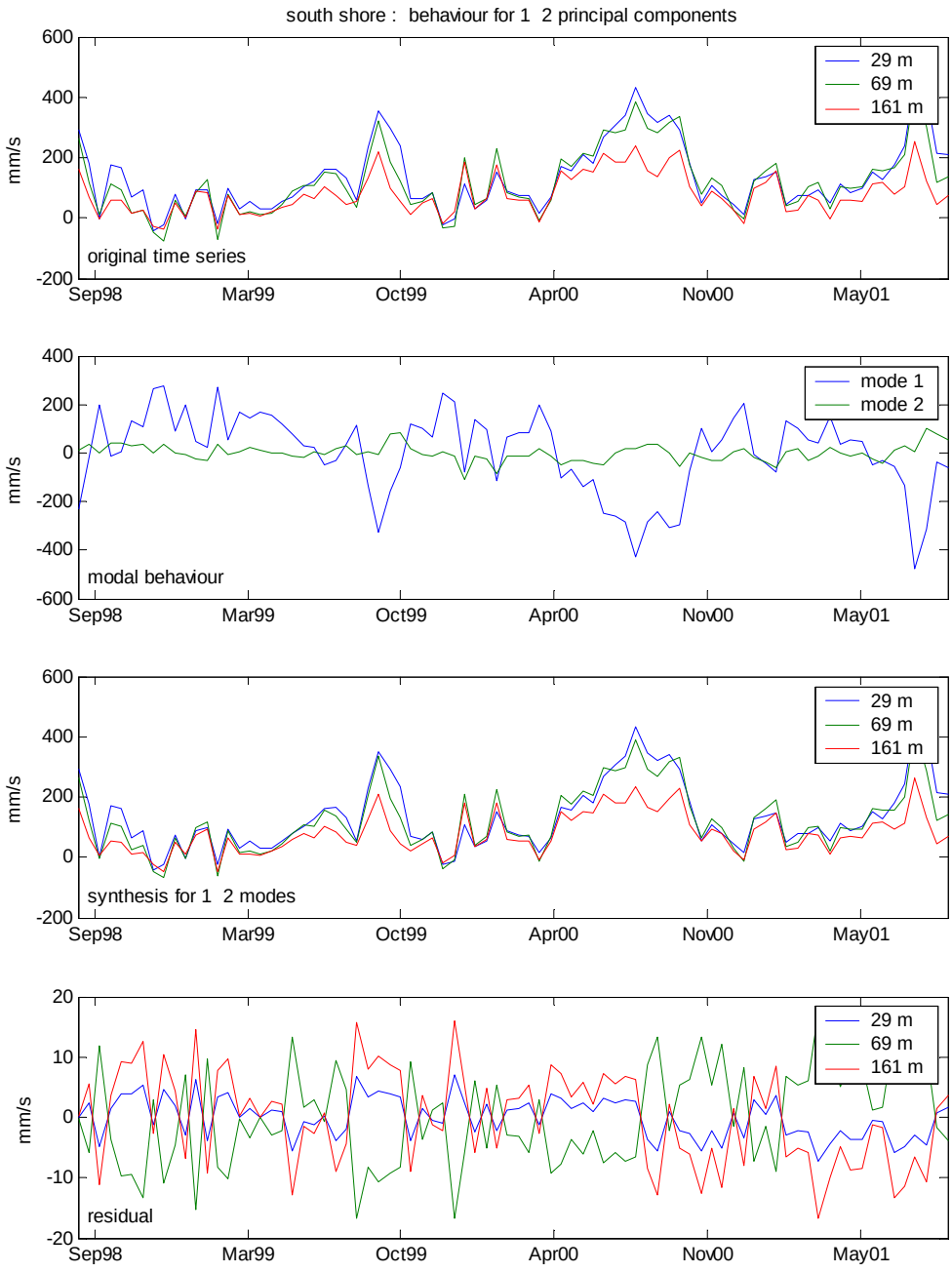

Figure 14 PCA results for south shore ADCP data (14-day).

Table 11 Cross-correlation matrix for ADCP and density data (14-day).

North							
	ADCP 38	ADCP 74	ADCP 146	CTD 38	CTD 83	CTD 148	CTD 178
ADCP 38							
ADCP 74	0.68						
ADCP 146	0.06	0.45					
CTD 38	**0.73**	**0.24**	**-0.15**				
CTD 83	**0.51**	**0.33**	**-0.12**	0.69			
CTD 148	**0.42**	**0.60**	**0.25**	0.24	0.62		
CTD 178	**0.40**	**0.58**	**0.39**	0.20	0.42	0.87	
South							
	ADCP 29	ADCP 69	ADCP 161	CTD 31	CTD 44	CTD 81	CTD 170
ADCP 29							
ADCP 69	0.95						
ADCP 161	0.86	0.96					
CTD 31	**-0.01**	**0.09**	**0.14**				
CTD 44	**0.24**	**0.33**	**0.36**	0.79			
CTD 81	**0.36**	**0.34**	**0.37**	0.25	0.50		
CTD 170	**-0.53**	**-0.65**	**-0.60**	-0.42	-0.57	-0.14	

Constructing a synthetic series from the first two modes, in this case, involved not only the multiplication of the eigenvectors with the modal time series but also "unstandardizing" and "uncentring" the series by multiplying that product by the standard deviations of the original series and then adding the means of the original series. Figure 15 and Figure 16 show that the residuals of the density data are close to 0 while those of the flow data show a bit of variation.

Table 12 gives the actual variance figures for the original data series and the residual series. The percentage of variance removed from the system is represented by the difference in variance between the original series and residual as a fraction of the variance of the original series (multiplied by 100 to get the percentage). These computations were for synthetic series constructed from the first mode only and from the first two modes.

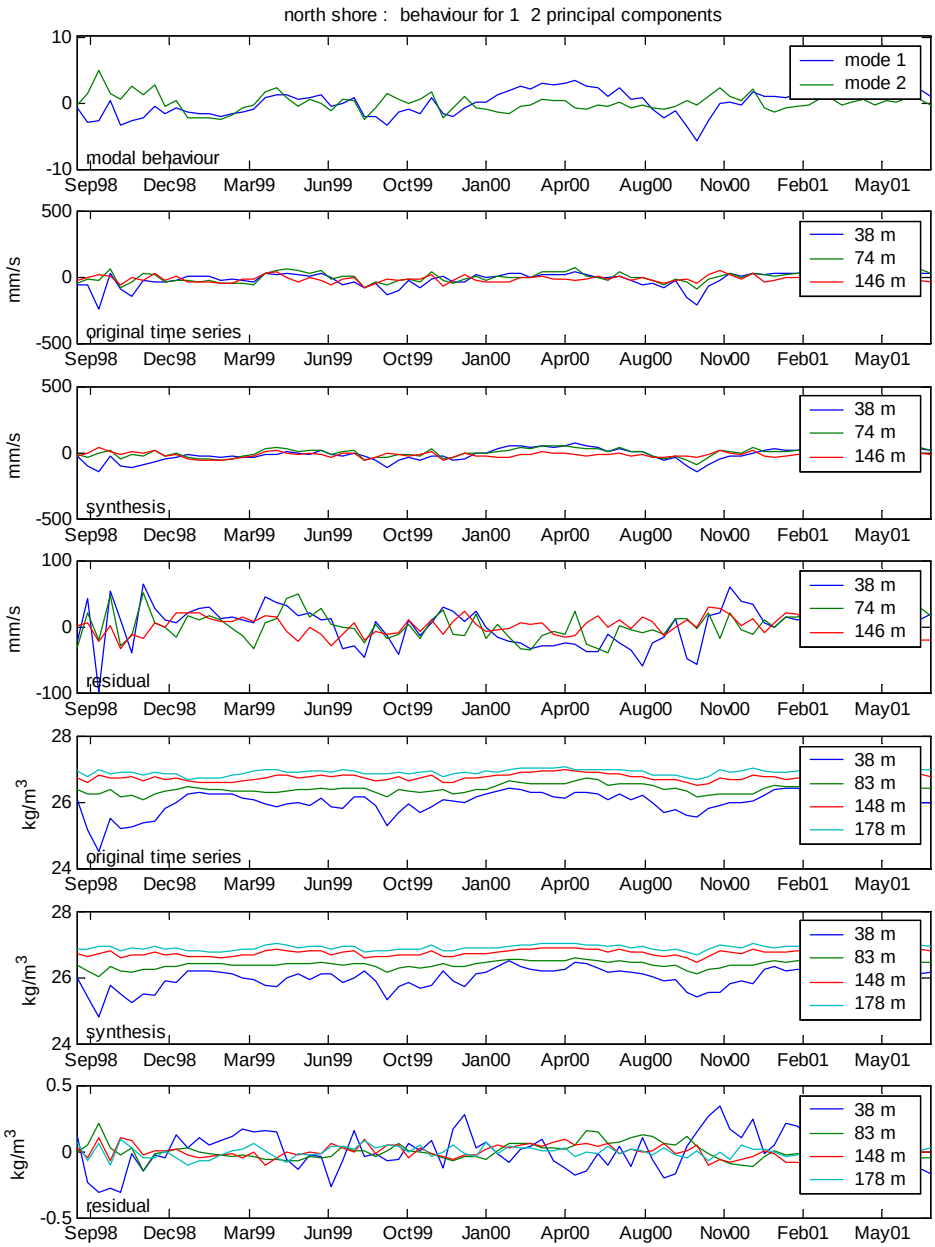

Figure 15 Results from PCA for northern ADCP data and σ_t data. Shown are the modal series of the first 2 modes, the original time series at all evaluated depths, the series constructed from the first 2 modes ("synthetic"), and the residual series (difference between the original and the constructed series).

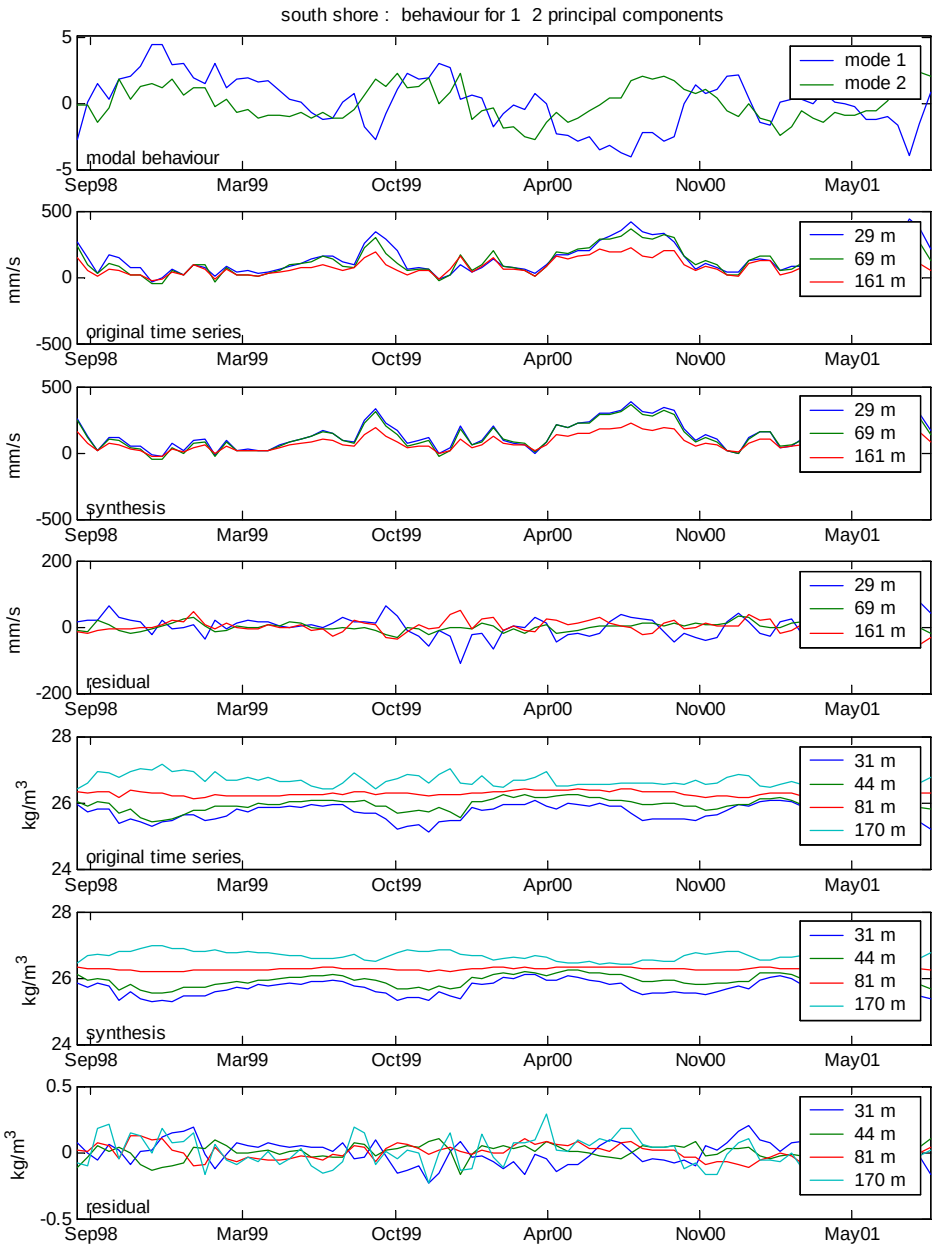

Figure 16 Results from PCA for southern ADCP data and σ_t data. Shown are the modal series of the first 2 modes, the original time series at all evaluated depths, the series constructed from the first 2 modes ("synthetic"), and the residual series (difference between the original and the constructed series).

Table 12 Variance of ADCP and density series and residual from PCA results using the first mode only and then the first 2 modes.

Variance : north shore		Mode 1		Modes 1 and 2	
	Original	Residual	% Removed	Residual	% Removed
ADCP 38 $(mm/s)^2$	3101.4867	1156.7319	62.70	871.9644	71.89
ADCP 74 $(mm/s)^2$	1363.4338	524.4796	61.53	391.5363	71.28
ADCP 146 $(mm/s)^2$	584.5771	537.1106	8.12	190.7474	67.37
CTD 38 $(kg/m^3)^2$	0.1130	0.0701	37.96	0.0194	82.84
CTD 83 $(kg/m^3)^2$	0.0156	0.0071	54.44	0.0040	74.46
CTD 148 $(kg/m^3)^2$	0.0109	0.0032	70.49	0.0025	76.82
CTD 178 $(kg/m^3)^2$	0.0080	0.0030	63.00	0.0017	78.31
Variance : south shore		Mode 1		Modes 1 and 2	
	Original	Residual	% Removed	Residual	% Removed
ADCP 29 $(mm/s)^2$	11578.3328	3331.2586	71.23	881.6760	92.39
ADCP 69 $(mm/s)^2$	10143.6534	1622.4442	84.01	154.4805	98.48
ADCP 161 $(mm/s)^2$	3905.7229	736.8871	81.13	340.1185	91.29
CTD 31 $(kg/m^3)^2$	0.0566	0.0469	17.04	0.0078	86.19
CTD 44 $(kg/m^3)^2$	0.0329	0.0189	42.50	0.0028	91.57
CTD 81 $(kg/m^3)^2$	0.0048	0.0035	27.45	0.0032	32.96
CTD 170 $(kg/m^3)^2$	0.0293	0.0117	59.96	0.0112	61.70

It is seen that for the north shore, the first mode is a coupled velocity and density mode in that it removes quite a bit of variance at all depths except for the deep velocity and shallow density points. Adding the second mode increases the amount of variance removed for the latter two points substantially. For the south shore, it is as suspected previously from looking at the eigenvectors: the first mode is indeed dominated by velocity. Adding the second mode substantially increases the amount of variance removed for all points although Mode 2 predominantly removes variance from the density at 31 and 44 m. Figure 18 illustrates the effect of the first mode for the south shore. This first mode removes from 71% to 84% of the variance from the velocity but only removes from 17% to 60% of the variance from the density (Table 12). Figure 16 shows the effect of the first two modes. Hamilton et al. (2002, 2003) moored CTD time series show clear distinction in water properties between 83 and 148 m in the north and between 81 and 170 m in the south. Profiles from individual CTD casts (Figure 68 to Figure 73) performed in August 1998, 1999, and 2000 show the pycnocline at above 30 m on both shores at this time of year so the moored CTDs were deployed at or below the surface layer for the most part. Nevertheless, Figure 74 to Figure 76 show that during their deployment the instruments recorded an increase in density at the uppermost level as winter set in, pack ice formed, and salt rejection occurred. The deepest instruments managed to capture intrusions of denser water at depth in fall and early winter.

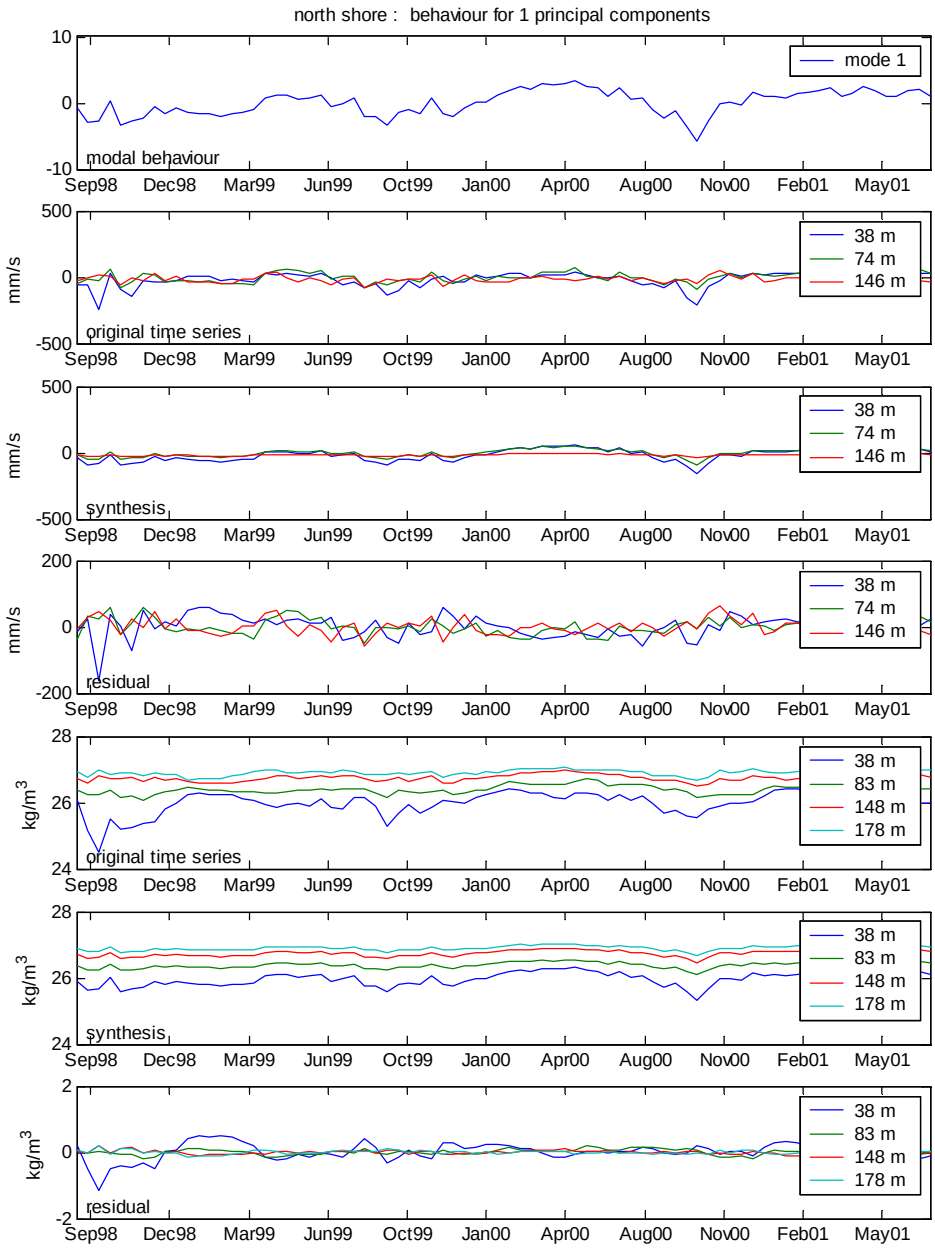

Figure 17 Results from PCA for northern ADCP data and σ_t data. Shown are the modal series of the first mode, the original time series at all evaluated depths, the series constructed from the first mode ("synthetic"), and the residual series (difference between the original and the constructed series).

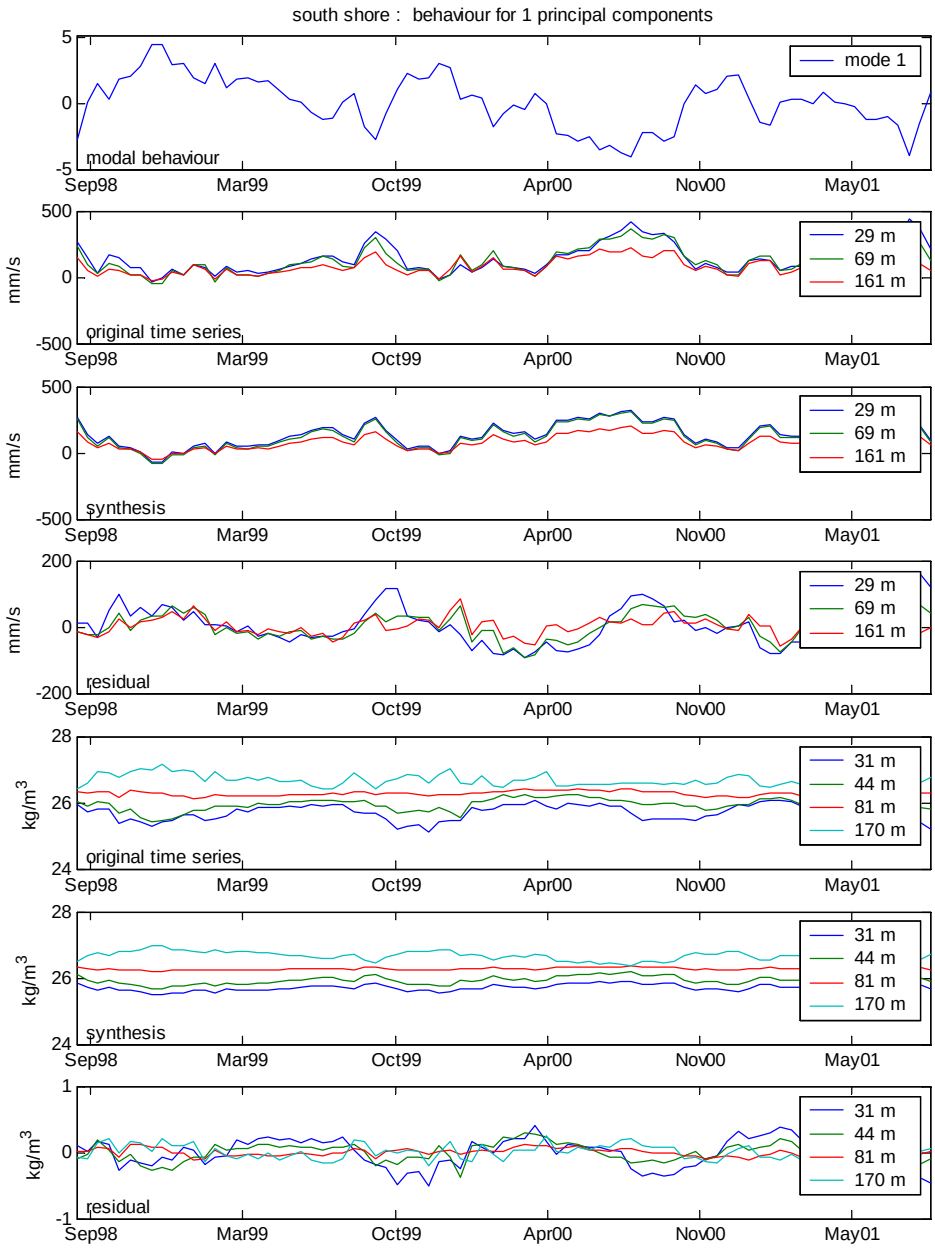

Figure 18 Results from PCA for southern ADCP data and σ_t data. Shown are the modal series of the first mode, the original time series at all evaluated depths, the series constructed from the first mode ("synthetic"), and the residual series (difference between the original and the constructed series).

Using the meteorological data

Time series plots of the hourly meteorological observations obtained from Environment Canada for the station at Resolute are presented in Appendix 5, Figure 87 to Figure 92. The wind tower at Resolute is 10 m high and the station itself is at 40-m elevation. The geographic position is 74°43' N and 94°59' W. Data consisted of air temperature, wind direction and magnitude, and surface layer pressure. To include the wind data in the principal component analysis, it first was decomposed into U and V components and rotated to have the major axis aligned with the channel. A progressive vector diagram was drawn to see if there was a preferred wind direction. While the mean wind had a preferred direction and changes in direction followed a strong seasonal signal, overall changes in direction seemed evenly distributed so it was concluded that a decomposition could be east-west (along-strait = u) and north-south (cross-strait = v) with impunity. The virtually equivalent variances of each component support this claim: u_{var} = 2.14 m/s and v_{var} = 2.16 m/s; the variance is almost circular with the major and minor axes having a ratio of close to 1.

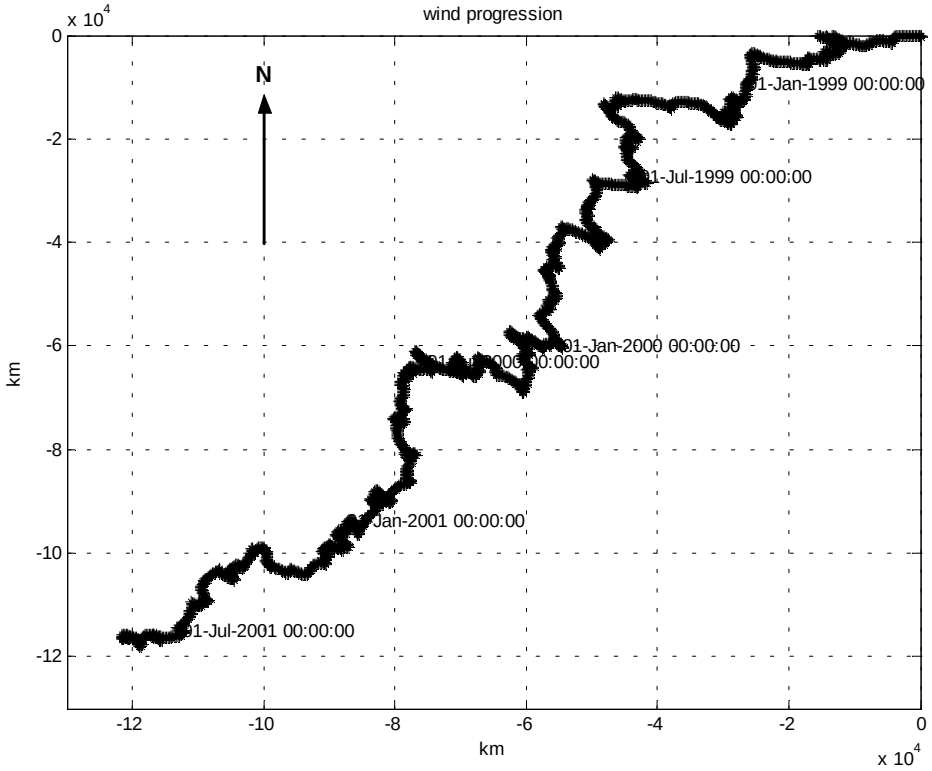

Figure 19 Progressive vector diagram of the wind velocity from 1998 to 2001

The lowpass filtered meteorological data, decimated to 14 days (Figure 20), show the strong seasonal signal hinted at in the previous diagram but note there is not a strong annual signal similar to that seen in the current data. This makes one doubt the existence of a local connection between wind and current with respect to low-frequency signals.

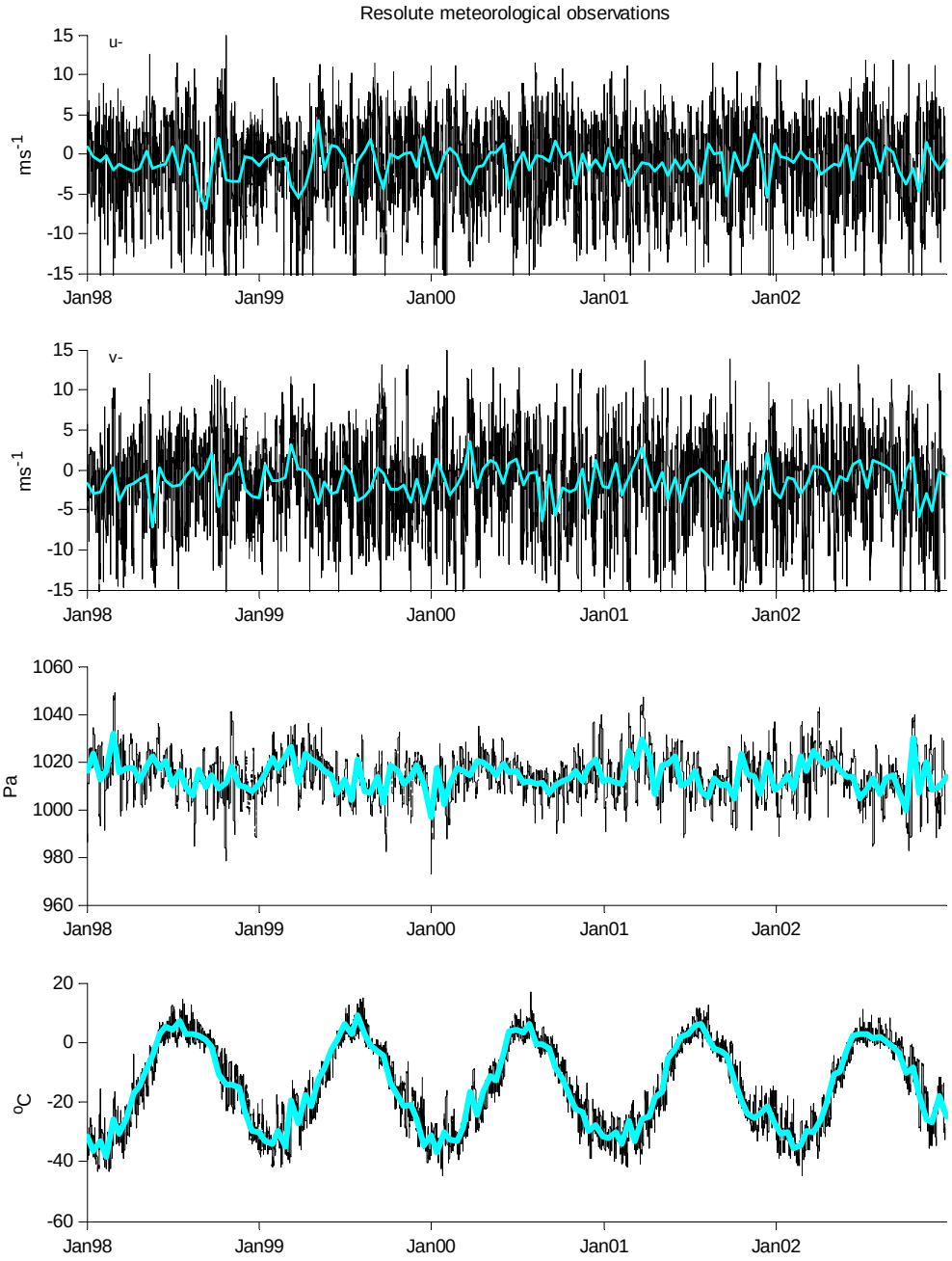

Figure 20 Lowpass filtered meteorological data for Resolute from 1998 to 2003

The cross-correlation matrix for the meteorological data is given in Table 13. There seems to be no strong connection between any pair of parameters.

Table 13 Cross-correlation matrix for Resolute meteorolgical data.

wind	u	v	slp	air
u				
v	-0.36			
Surface layer pressure	-0.09	0.17		
Air temperature	-0.04	0.09	-0.22	

The alongshore component of the wind velocity was combined into a system with the ADCP and density data for the principal component analysis. The eigenvectors, eigenvalues, and percent of variance removed by each mode are in Table 14.

Table 14 Results from PCA for current, density, and wind, 3-year data records.

ALONGSHORE FLOW (3 depths), DENSITY (4 depths), AND ALONGSHORE WIND

North

	Eigenvectors								Eigen-		% var
	M 1	M 2	M 3	M 4	M 5	M 6	M 7	M 8	values		
U1	0.42	-0.22	0.32	-0.38	0.27	0.19	-0.62	0.17	M 1	3.58	44.79
U2	0.41	0.19	0.41	-0.05	0.42	-0.44	0.50	-0.04	M 2	1.89	23.58
U3	0.15	0.52	0.47	0.04	-0.68	-0.05	-0.18	-0.00	M 3	0.91	11.43
σ1	0.33	-0.46	0.03	-0.34	-0.41	0.29	0.42	-0.37	M 4	0.73	9.08
σ2	0.39	-0.29	-0.37	0.09	-0.33	-0.59	-0.10	0.39	M 5	0.47	5.91
σ3	0.44	0.18	-0.32	0.38	0.12	0.01	-0.29	-0.65	M 6	0.28	3.51
σ4	0.42	0.31	-0.26	0.16	0.05	0.57	0.27	0.49	M 7	0.08	1.00
Uw	0.02	-0.46	0.45	0.75	-0.01	0.14	0.02	0.10	M 8	0.06	0.70

South

	Eigenvectors								Eigen-		% var
	M 1	M 2	M 3	M 4	M 5	M 6	M 7	M 8	values		
U1	-0.43	0.29	-0.15	0.17	-0.20	0.42	0.55	-0.39	M 1	3.87	48.34
U2	-0.47	0.24	-0.03	0.15	-0.17	0.01	-0.04	0.82	M 2	1.87	23.38
U3	-0.46	0.21	-0.01	0.02	-0.27	-0.36	-0.60	-0.42	M 3	0.90	11.20
σ1	-0.20	-0.60	0.26	-0.13	-0.52	-0.35	0.36	0.01	M 4	0.82	10.19
σ2	-0.32	-0.50	0.09	-0.23	0.09	0.66	-0.37	-0.00	M 5	0.29	3.63
σ3	-0.26	-0.20	-0.76	-0.35	0.31	-0.27	0.13	0.02	M 6	0.14	1.80
σ4	0.39	0.13	-0.41	-0.32	-0.69	0.24	-0.15	0.08	M 7	0.11	1.34
Uw	-0.11	0.39	0.39	-0.81	0.11	-0.03	0.14	0.01	M 8	0.01	0.12

Key:	North	South
U1	U_{38} $(m/s)^2$	U_{29} $(m/s)^2$
U2	U_{74} $(m/s)^2$	U_{69} $(m/s)^2$
U3	U_{146} $(m/s)^2$	U_{161} $(m/s)^2$
σ1	σ_{38} $(kg/m^3)^2$	σ_{31} $(kg/m^3)^2$
σ2	σ_{83} $(kg/m^3)^2$	σ_{44} $(kg/m^3)^2$
σ3	σ_{148} $(kg/m^3)^2$	σ_{81} $(kg/m^3)^2$
σ4	σ_{178} $(kg/m^3)^2$	σ_{170} $(kg/m^3)^2$
Uw	U_w (m/s)	U_w (m/s)

To explain more than 90% of the variance in the system the first four modes need to be included into any representative model. It is nice to see that the current's eigenvectors for the first mode and those of the wind agree in sign meaning that the wind and current are heading in the same direction for this mode although the coupling is weak. The cross-correlation matrix confirms this whereby this matrix is the same as Table 11 with the extra row for correlations with wind presented in Table 15. There really is no difference from the previous analysis (without wind) in the results for either shore; that is, Mode 1

here is essentially the same as the mode 1 for currents alone (Table 12). This indicates that local wind coupling is marginal. Figure 21 and Figure 22 show time series of the results including synthetic series constructed from the first three modes. The original current and density data are well represented by the synthetic series. The series constructed using the first two modes are presented in Appendix 5 (Figure 93 and Figure 94).

Table 15 Correlation matrix for alongshore current and density with alongshore wind speed

North							
	U_{38}	U_{74}	U_{146}	σ_{38}	σ_{83}	σ_{148}	σ_{178}
Uw	0.15	-0.02	-0.23	0.27	0.16	-0.05	-0.24
South							
	U_{29}	U_{69}	U_{161}	σ_{31}	σ_{44}	σ_{81}	σ_{17}
Uw	0.23	0.26	0.32	-0.18	-0.05	-0.06	-0.03

Table 16 contains the variances corresponding to the time series in Figure 21 and Figure 22 and those figures in Appendix 5 showing the PCA results. Again, there is a marked increase in variance removed from the system as a mode is added. In the south, neither the first mode alone nor the first two modes together adequately picks up the density signal. This is shown to great effect in the time series plots in Appendix 5. Basically, these are the same results as in the analysis of current and density coupling alone; that is, the local wind really did not effect the long-term variability in the system, it behaves as if it is uncorrelated with the other time series.

Perhaps the unexpected weak correlation of the wind with the current was a consequence of ice cover for much of the year. Any effect the wind would have on what goes on underneath the ice would either be weak or at the least lagged so analysis results would not be representative. Also, the ice can act as a dampening agent of internal adjustments and the water will be more vertically quiescent and homogeneous. To check this possibility, data were split into times of ice cover (Nov 30 – Jun 30) and times of open water (otherwise).

The difference in the two scenarios can be seen from the cross-correlation matrix in Table 17 and the results of the PCA in Table 18. For the north all the absolute correlation coefficients (|r|) in the bottom row (wind with other variables) are greater for the open water scenario than for under ice cover. Nevertheless, the maximum is only 0.5 (only 25% variance). For the south, |r| for open water is greater than any for under ice cover for all but one pair in the row of wind versus other variables. This time the maximum is coefficient is 0.41 (only 16% variance). Under ice cover, the water in the north appears well mixed. Especially in the south, the first mode is dominated by the strong correlation in the surface and mid-depth currents. There is still no change in sign in the eigenvector membership for the first mode in the south like one would expect if the current and density were connected ("increase current eastward, decrease density down") and the eigenvector members for that mode are more equal in magnitude under ice cover showing increase in homogeneity.

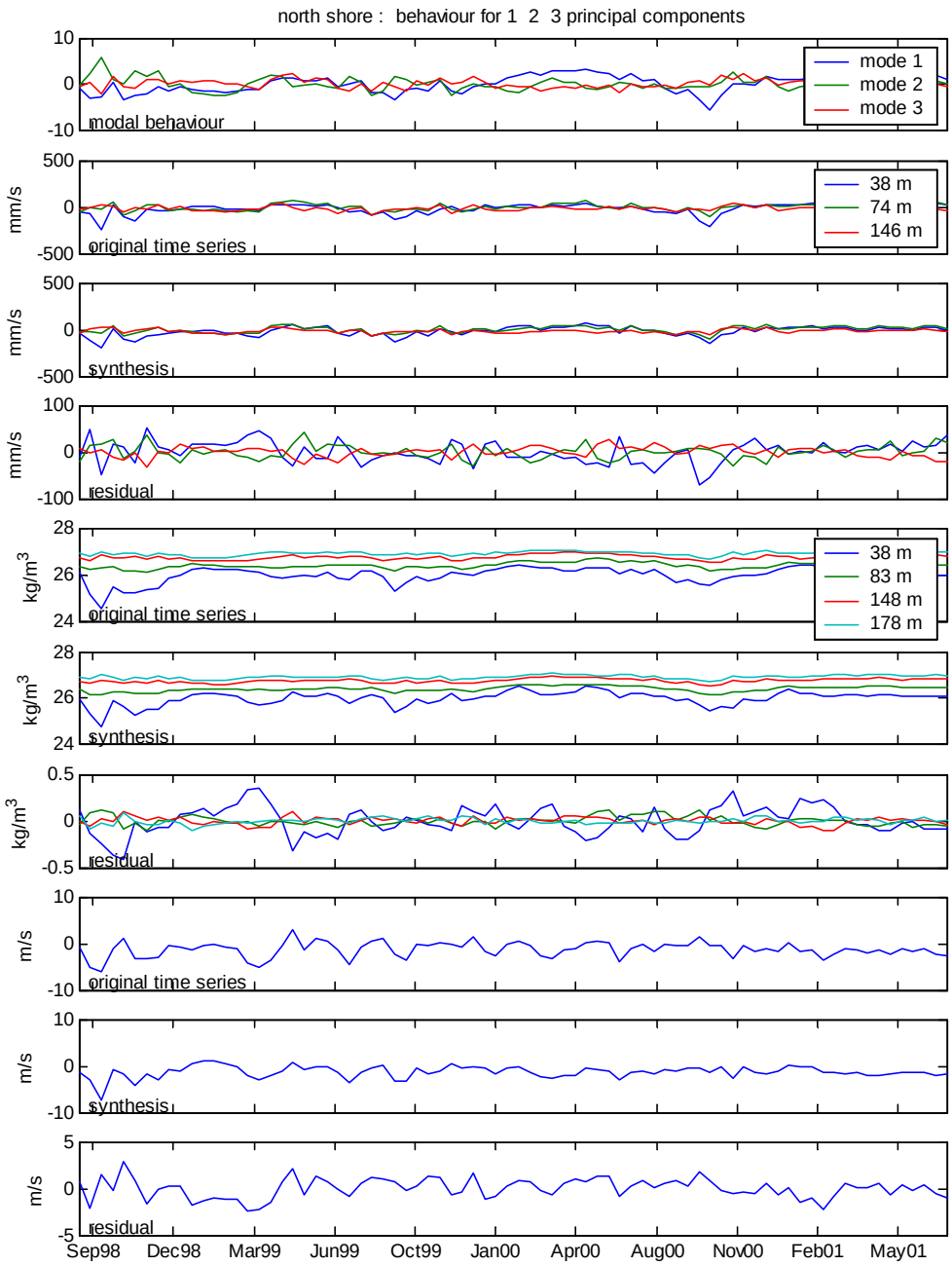

Figure 21 Time series of PCA results for the first three modes for alongshore current, density, and alongshore wind for the northern moorings using lowpass-filtered data.

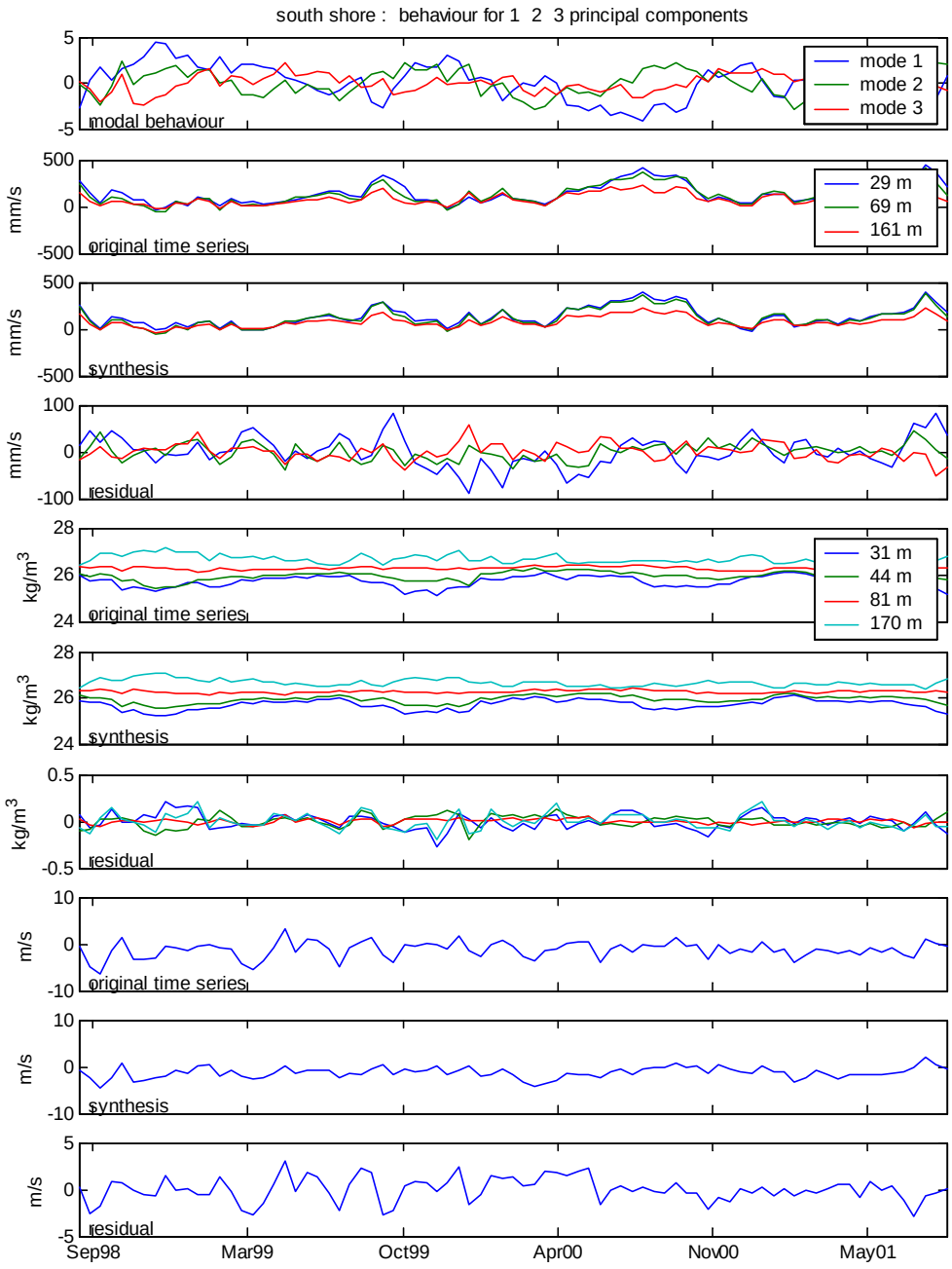

Figure 22 Time series of PCA results for the first three modes for alongshore current, density, and alongshore wind for the southern moorings using lowpass-filtered data.

Table 16 Variances from PCA results using the first mode only, the first 2 modes, and the first 3 modes to construct a synthetic data series. The residual variance is the variance of the difference between the original series and the synthetic series. Also listed is the amount of variance removed when using the first mode, first 2 modes, or the first 3 modes. See key for Table 14.

North							
	original series	mode 1 residual	% remv	modes 1 2 residual	% remv	modes 1 2 3 residual	% remv
U1	3101.4867	1144.4975	63.10	866.0385	72.08	568.4853	81.67
U2	1363.4338	527.3621	61.32	430.5206	68.42	218.1951	84.00
U3	584.5771	538.7280	7.84	246.0833	57.90	129.3761	77.87
σ1	0.1130	0.0694	38.55	0.0234	79.26	0.0234	79.34
σ2	0.0156	0.0070	54.85	0.0045	71.06	0.0025	83.87
σ3	0.0109	0.0032	70.19	0.0026	76.44	0.0016	85.55
σ4	0.0080	0.0030	62.33	0.0015	80.92	0.0010	87.10
Uw	2.7903	2.7862	0.15	1.6496	40.88	1.1428	59.04
South							
	original series	mode 1 residual	% remv	modes 1 2 residual	% remv	modes 1 2 3 residual	% remv
U1	11578.3328	3142.2524	72.86	1339.8196	88.43	1099.9905	90.50
U2	10143.6534	1438.9661	85.81	336.9297	96.68	329.9132	96.75
U3	3905.7229	649.1406	83.37	312.2082	92.01	311.8835	92.01
σ1	0.0566	0.0481	15.03	0.0104	81.57	0.0069	87.72
σ2	0.0329	0.0197	40.14	0.0043	86.83	0.0041	87.53
σ3	0.0048	0.0035	26.16	0.0032	33.87	0.0007	86.02
σ4	0.0293	0.0121	58.61	0.0112	61.71	0.0068	76.68
Uw	3.0593	2.9176	4.63	2.0594	32.68	1.6467	46.17

Summary

Weak correlation between north and south non-tidal alongshore currents allowed the two areas to be treated as two independent systems with inter-depth dependence in each region.

Harmonic analysis of 2-hourly, unfiltered, data showed that, on the north shore, the annual component amplitude is significant, varying from ~ 8 cms^{-1} at the shallowest depth to ~ 2.7 cms^{-1} at mid-depth and decreasing to ~ 0.3 cms^{-1} near the bottom. Response at the annual frequency is strongly depth dependent. Phase increases over the upper 110-m with a range of almost 3 months. The current near the bottom leads the shallower flows at the surface by about 2 months and at mid-depth by about 4 months. On the south shore, the annual components vary from ~15 cms^{-1} near the surface to ~ 4 cms^{-1} near the bottom. Phases are constant to within a range of about one month. The mean flows along the north shore show a mid-depth minimum that is consistent from year to year. The mean flows along the south shore are slightly weaker near the surface and reach their maximum at ~30 m.

The phase differences for coherence estimates for each of three depth pairs showed that the lowest frequencies have very little difference in phase except between the shallow

and deep pairing for the northern mooring. In the 0 to 1 x 10^{-5} Hz range, the phase differences between the shallow and deep pairings had the greatest variances for both shores.

Analysis results showed that strong shearing between the upper two levels and the bottom level in the first mode is observed. PCA of the ADCP low frequency (14-day) data by itself reveals that the first two modes represent more than 90% of the variance of the original system. The first mode carries most of the variance for the shallow water in the north removing (94, 71, 6%) of the variance in the shallow, mid-depth, and deeper water. In the south the first mode accounts for 95% of the variance whereby (95, 98, 88%) of the variance is removed by this mode for shallow, mid-depth, and deeper water. On both shores, then, the first mode is the predominant velocity mode, especially in the shallow water.

Analysis of the variance of low frequency (14-day) northern ADCP data and density data showed that the magnitude of the eigenvectors for the first mode is equally high for the ADCP shallow and mid-depth water and for the density of the deeper water. In the south, as flow increased eastward, the density increased except in the deeper water. The second mode, accounted for 24% of the variance and looked more like the response to internal mass adjustment than the first mode whereby the first mode is likely a velocity mode governed by the variance in the flow. Density eigenvectors for the south shore showed a reversal at the deepest level for the first mode which is also the mode that accounted for the least amount of density variance at the uppermost level. The first mode appeared to be a coupled velocity and density mode in that it removed a great deal of variance at all depths except for the deep velocity and shallow density points. Adding the second mode increased the amount of variance removed for the latter two points substantially. For the south shore the first mode was dominated by velocity. Adding the second mode substantially increased the amount of variance removed for all points although the second mode predominantly removed variance from the density at 31 and 44 m. Adding meteorological data to the analysis showed that, as with density, there seems to be no strong local influence on the current flowing through Lancaster Sound with respect to low-frequency variability.

In conclusion, if one wishes to describe the forcing of the system, it would perhaps be best to look at a larger picture; one that included the Arctic Ocean and Baffin Bay.

Table 17 Cross-correlation matrices for times of ice-cover and of open water for current, density, and wind.

NORTH								
ICE-COVERED								
	U1	U2	U3	σ1	σ2	σ3	σ4	Uw
U1								
U2	0.83							
U3	0.14	0.36						
σ1	0.05	-0.20	-0.17					
σ2	0.37	0.14	-0.06	0.68				
σ3	0.57	0.51	0.21	0.14	0.70			
σ4	0.58	0.51	0.46	0.06	0.46	0.79		
Uw	0.20	0.32	0.02	-0.06	0.14	0.21	-0.14	
OPEN WATER								
	U1	U2	U3	σ1	σ2	σ3	σ4	Uw
U1								
U2	0.65							
U3	0.04	0.54						
σ1	0.72	0.20	-0.20					
σ2	0.43	0.24	-0.21	0.67				
σ3	0.16	0.53	0.35	-0.01	0.32			
σ4	0.17	0.49	0.41	-0.00	0.13	0.89		
Uw	0.20	-0.30	-0.40	0.47	0.23	-0.34	-0.36	
SOUTH								
ICE-COVERED								
	U1	U2	U3	σ1	σ2	σ3	σ4	Uw
U1								
U2	0.96							
U3	0.90	0.96						
σ1	0.29	0.19	0.02					
σ2	0.41	0.30	0.22	0.79				
σ3	0.54	0.50	0.51	0.39	0.71			
σ4	-0.62	-0.64	-0.50	-0.47	-0.36	-0.18		
Uw	0.19	0.23	0.28	-0.19	-0.01	0.06	0.02	
OPEN WATER								
	U1	U2	U3	σ1	σ2	σ3	σ4	Uw
U1								
U2	0.96							
U3	0.90	0.97						
σ1	0.17	0.25	0.33					
σ2	0.50	0.57	0.59	0.71				
σ3	0.45	0.36	0.33	0.10	0.31			
σ4	-0.65	-0.74	-0.70	-0.35	-0.64	-0.07		
Uw	0.27	0.29	0.34	-0.21	-0.05	-0.14	-0.07	

Key:	North	South
U1	U_{38} $(m/s)^2$	U_{29} $(m/s)^2$
U2	U_{74} $(m/s)^2$	U_{69} $(m/s)^2$
U3	U_{146} $(m/s)^2$	U_{161} $(m/s)^2$
σ1	σ_{38} $(kg/m^3)^2$	σ_{31} $(kg/m^3)^2$
σ2	σ_{83} $(kg/m^3)^2$	σ_{44} $(kg/m^3)^2$
σ3	σ_{148} $(kg/m^3)^2$	σ_{81} $(kg/m^3)^2$
σ4	σ_{178} $(kg/m^3)^2$	σ_{170} $(kg/m^3)^2$
Uw	U_w (m/s)	U_w (m/s)

Table 18 PCA results for times when there was ice cover and for when there was open water. See key for Table 14.

ICE-COVERED

ALONGSHORE FLOW (3 depths), DENSITY (4 depths), AND ALONGSHORE WIND

North

	Eigenvectors								Eigen-values		% var
	M 1	M 2	M 3	M 4	M 5	M 6	M 7	M 8			
U1	0.45	0.12	-0.18	0.43	-0.35	0.27	0.52	0.31	M 1	3.40	42.50
U2	**0.41**	0.35	-0.21	0.20	-0.32	-0.44	-0.50	-0.28	M 2	1.79	22.34
U3	0.20	0.36	0.41	-0.69	-0.32	-0.12	0.20	0.16	M 3	1.21	15.08
σ1	0.10	-0.65	0.01	-0.16	-0.55	0.23	-0.39	0.17	M 4	0.77	9.59
σ2	0.35	-0.53	-0.05	-0.13	0.09	-0.45	0.45	-0.40	M 5	0.55	6.89
σ3	0.48	-0.11	0.02	-0.05	0.53	-0.17	-0.26	0.61	M 6	0.13	1.67
σ4	0.46	0.04	0.41	0.03	0.23	0.58	-0.14	-0.47	M 7	0.10	1.27
Uw	0.13	0.11	-0.77	-0.50	0.12	0.32	-0.01	-0.11	M 8	0.05	0.65

South

	Eigenvectors								Eigen-values		% var
	M 1	M 2	M 3	M 4	M 5	M 6	M 7	M 8			
U1	0.46	-0.18	0.09	-0.08	0.35	-0.15	0.74	0.23	M 1	4.11	51.33
U2	0.45	-0.27	0.13	-0.08	0.16	0.10	-0.18	-0.80	M 2	1.78	22.28
U3	0.42	-0.36	0.02	-0.20	0.10	-0.08	-0.60	0.52	M 3	0.99	12.43
σ1	0.25	0.58	0.07	0.32	0.48	-0.48	-0.15	0.12	M 4	0.73	9.15
σ2	0.32	0.49	-0.30	0.09	-0.05	-0.73	-0.12	-0.12	M 5	0.21	2.66
σ3	0.35	0.20	-0.48	-0.44	-0.45	0.44	0.14	0.03	M 6	0.10	1.31
σ4	-0.35	-0.05	-0.54	-0.42	0.63	-0.04	-0.05	-0.09	M 7	0.06	0.72
Uw	0.09	-0.38	-0.60	0.69	-0.03	0.10	0.03	0.01	M 8	0.01	0.11

OPEN WATER

ALONGSHORE FLOW (3 depths), DENSITY (4 depths), AND ALONGSHORE WIND

North

Eigenvectors									Eigen-values		% var
	M 1	M 2	M 3	M 4	M 5	M 6	M 7	M 8			
U1	0.32	-0.41	0.38	-0.06	0.44	-0.05	-0.57	0.25	M 1	3.04	37.99
U2	0.49	-0.02	0.39	-0.14	0.10	0.51	0.55	-0.14	M 2	2.53	31.58
U3	0.31	0.31	0.45	0.33	-0.64	-0.17	-0.22	0.08	M 3	1.00	12.51
σ1	0.16	-0.56	0.05	0.03	-0.13	-0.61	0.29	-0.43	M 4	0.57	7.14
σ2	0.23	-0.43	-0.39	-0.36	-0.55	0.23	-0.06	0.36	M 5	0.45	5.59
σ3	0.48	0.13	-0.46	0.15	0.06	0.19	-0.38	-0.58	M 6	0.29	3.59
σ4	0.46	0.17	-0.36	0.32	0.26	-0.32	0.31	0.50	M 7	0.07	0.84
Uw	-0.20	-0.44	-0.03	0.78	-0.04	0.38	0.05	0.05	M 8	0.06	0.75

South

	Eigenvectors								Eigen-values		% var
	M 1	M 2	M 3	M 4	M 5	M 6	M 7	M 8			
U1	-0.44	0.22	-0.18	0.13	-0.26	-0.17	0.69	-0.38	M 1	4.29	53.67
U2	-0.46	0.18	-0.04	0.13	-0.24	-0.12	-0.06	0.81	M 2	1.52	18.98
U3	-0.46	0.17	0.02	-0.02	-0.30	-0.03	-0.70	-0.44	M 3	1.05	13.16
σ1	-0.22	-0.58	0.29	-0.43	-0.41	0.39	0.16	0.04	M 4	0.61	7.69
σ2	-0.37	-0.40	0.14	-0.22	0.50	-0.62	-0.02	-0.03	M 5	0.29	3.63
σ3	-0.20	-0.10	-0.83	-0.29	0.27	0.32	-0.06	0.04	M 6	0.15	1.82
σ4	0.39	0.06	-0.28	-0.50	-0.48	-0.53	-0.04	0.05	M 7	0.08	0.95
Uw	-0.10	0.62	0.32	-0.63	0.27	0.17	0.10	0.03	M 8	0.01	0.10

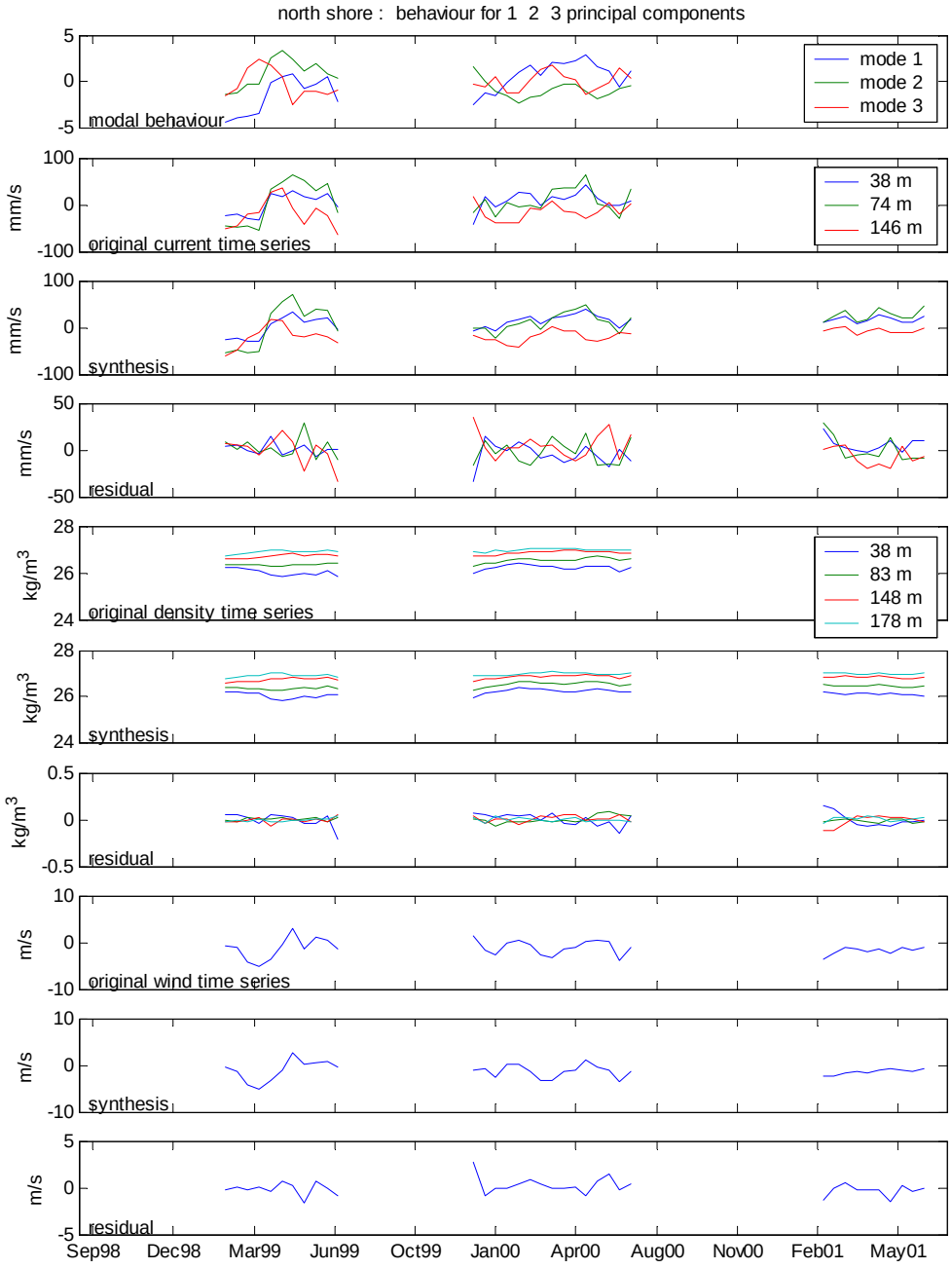

Figure 23 North shore PCA results for times of ice cover.

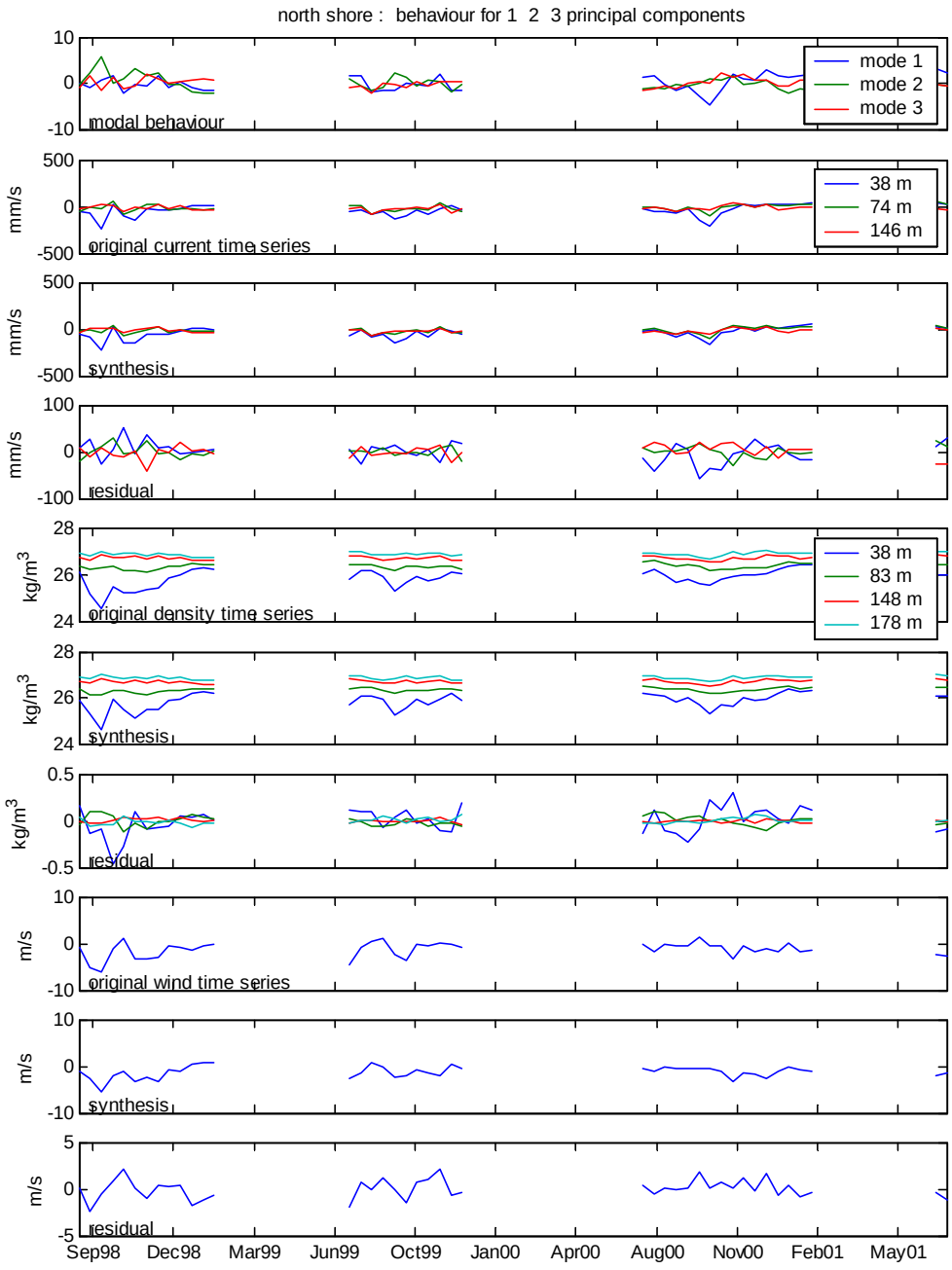

Figure 24 North shore PCA results for times of open water.

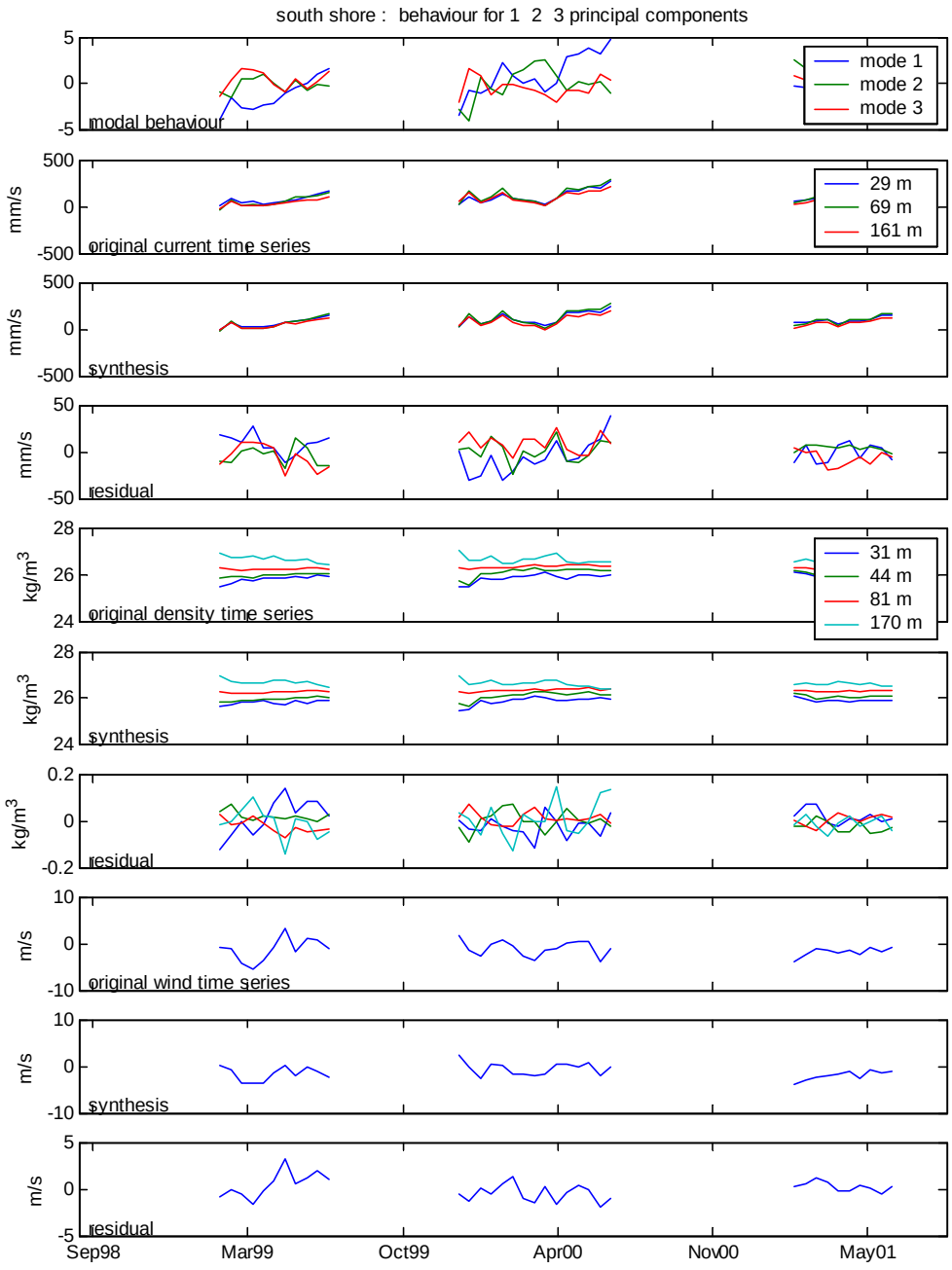

Figure 25 South shore PCA results for times of ice cover.

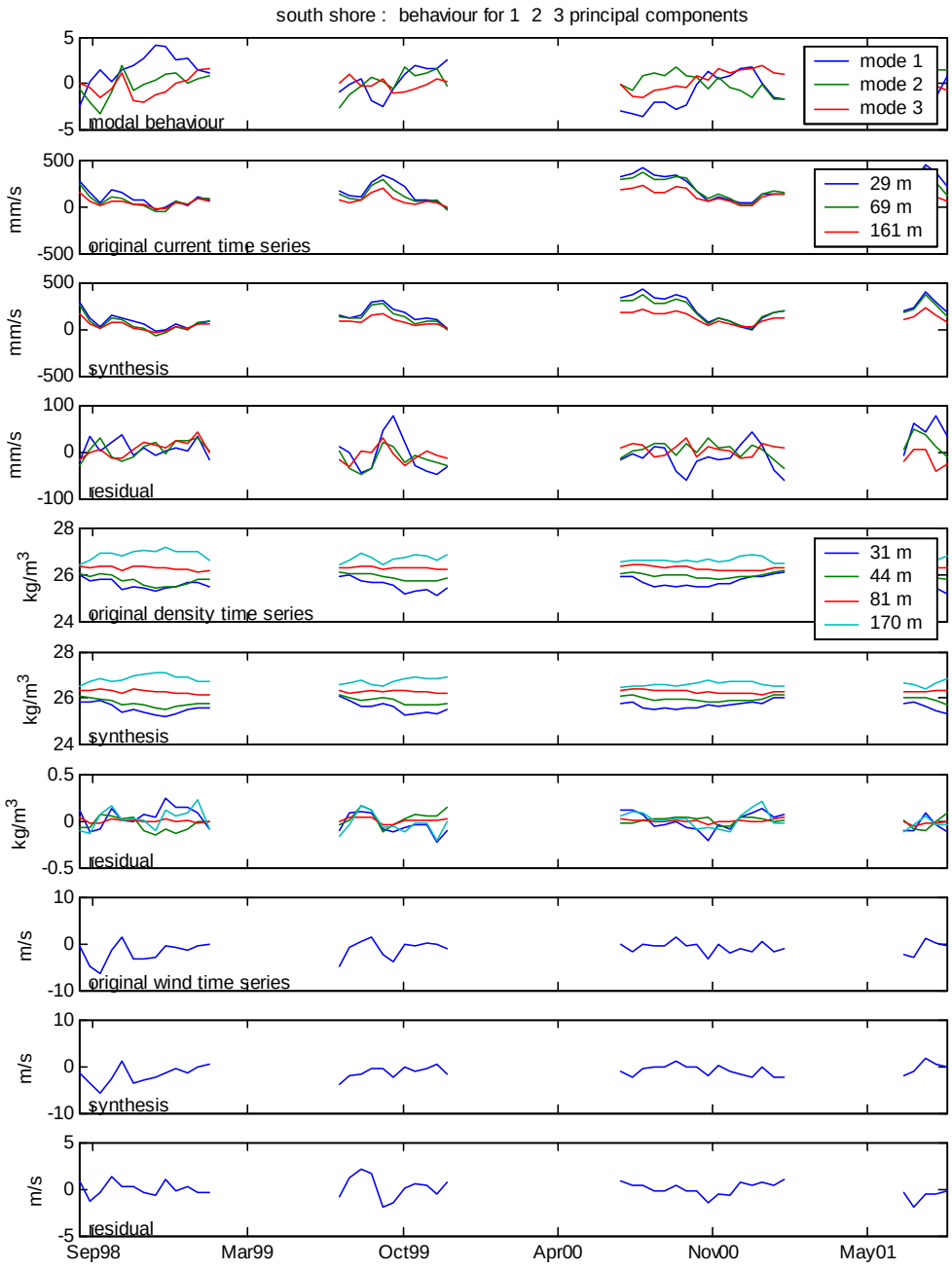

Figure 26 South shore PCA results for times of open water.

References

Emery, W. J. and R. E. Thomson, 1997. Data Analysis Methods in Physical Oceanography. Elsevier, New York, xvi+634 pp.

Lemon, D. D. and D. B. Fissel, 1982. "Seasonal variations in currents and water properties in Northwestern Baffin Bay, 1978 – 1979", *Arctic*, Vol. 35, No. 1, pp. 211–218.

Lorenz, E. N., 1956. Empirical Orthogonal Functions and Statistical Weather Prediction, Sci. Rep. No. 1, Massachusetts Institute of Technology, Dep. Of Meteorology, Cambridge, MA: ii+49 pp.

Hamilton, J., 2001. "Accurate ocean current direction measurements near the magnetic poles", Proc. 11th Int. Offshore Polar Eng. Conf., Stavanger Norway 2001, pp. 656-660.

Hamilton, J., S. Prinsenberg, and L. Malloch, 2002. Moored current meter and CTD observations from Barrow Strait, 1998-1999. Can. Data Rep. Hydrogr. Ocean Sci. 157: v+65 pp.

Hamilton, J., S. Prinsenberg, and L. Malloch, 2003. Moored current meter and CTD observations from Barrow Strait, 1999-2000. Can. Data Rep. Hydrogr. Ocean Sci. 161: v+60 pp.

Prinsenberg, S. J. and J. Hamilton, 2003. "Monitoring the volume, freshwater, and heat fluxes passing through Lancaster Sound of the Canadian Arctic Archipelago", *in press*.

Prinsenberg, S. J., 1998. Volume, heat and freshwater fluxes through the Canadian Arctic Archipelago: Present understanding and future research plans, pp. 200-202.

Prinsenberg, S. J. and E. B. Bennett, 1987. "Mixing and transports in Barrow Strait, the central part of the Northwest Passage". *Continental Shelf Research*, Vol. 7, No. 8, pp. 913-935.

Proudman, J., 1953. Dynamical Oceanography. Methuen, London, 409 pp.

Acknowledgements

The authors are grateful to J. Hamilton for providing the Microcat CTD data and R. Pettipas for providing the ADCP data as a 3-year record. Funding for this project was provided by the Program of Energy Research and Development, the Climate Change Action Fund, and Fisheries and Oceans Canada Science Strategic Fund.

Appendix 1 Harmonic Fit of ADCP Data

3-year data record

Time series plots show original raw traces from selected bins, the 30-day mean, and the annual harmonic superimposed. Landfast ice cover occurred during the time depicted by the shaded area shown on the first trace on each page.

North shore

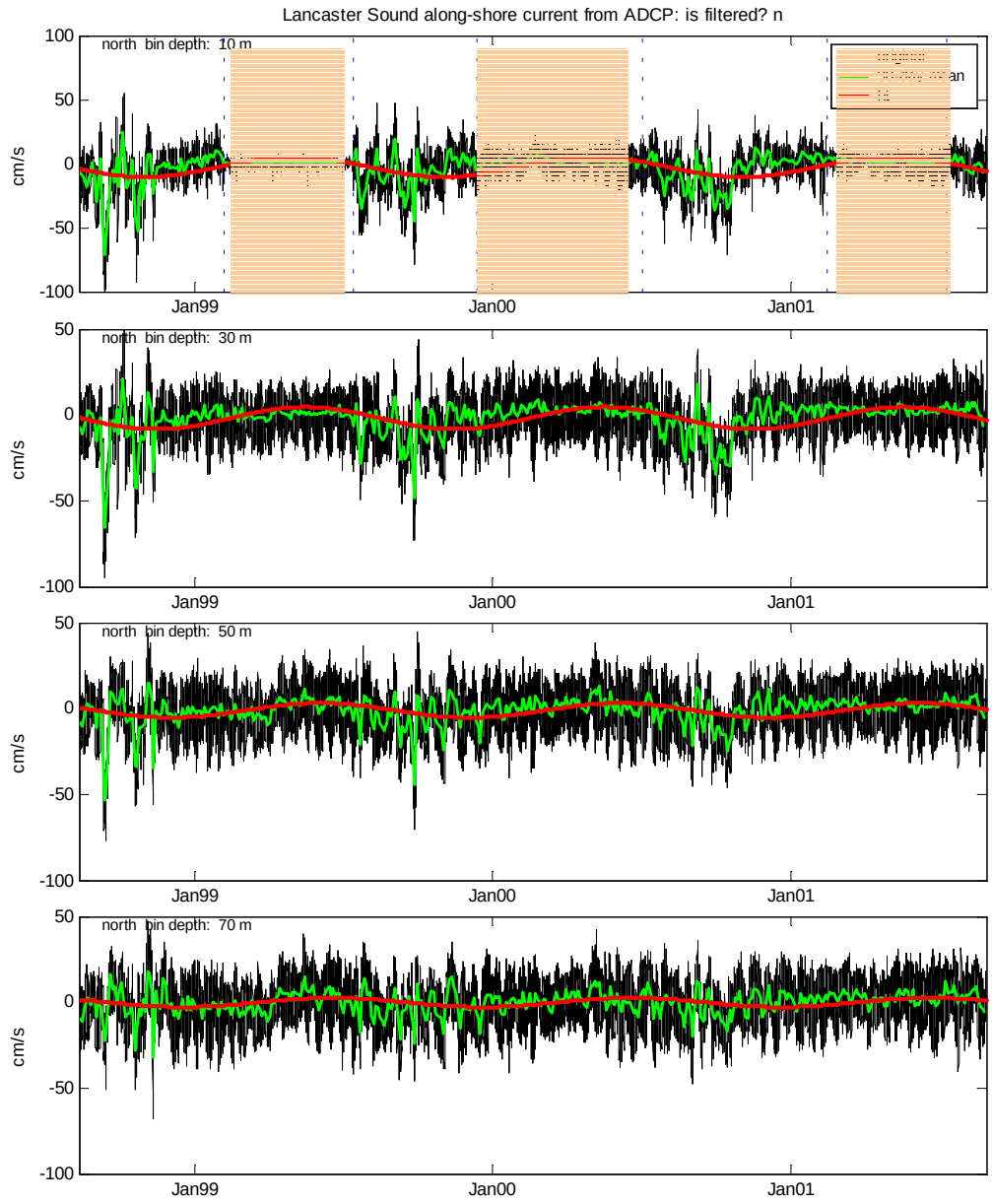

Figure 27 Harmonic fit of ADCP data from northern mooring measured at 10, 30, 50, and 70 m. The vertical blue lines and the shaded area between the lines in the first plot indicate the start and end of landfast ice cover.

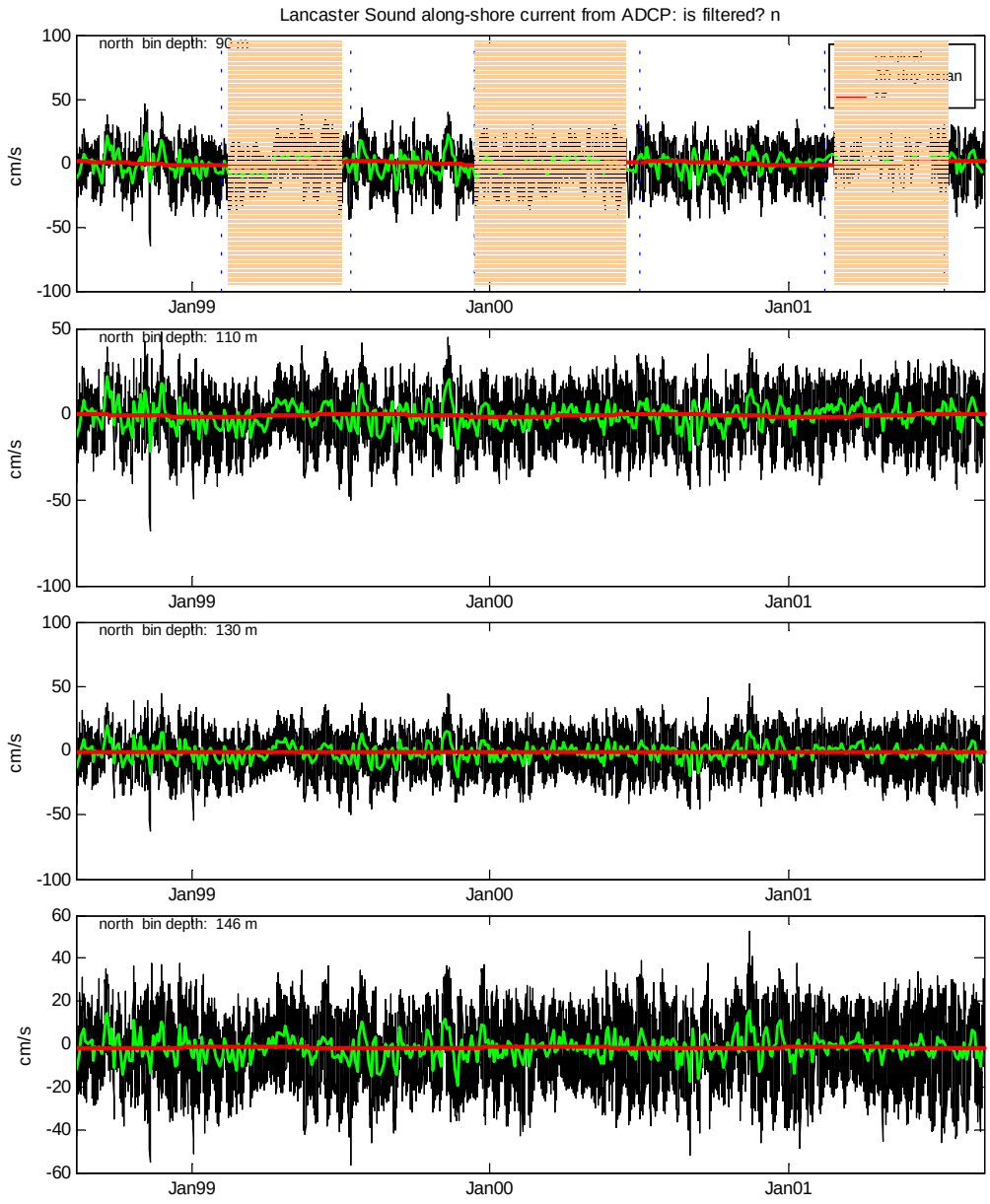

Figure 28 Harmonic fit of ADCP data from northern mooring measured at 90, 110, 130, and 146 m. The vertical blue lines and the shaded area between the lines in the first plot indicate the start and end of landfast ice cover.

South shore

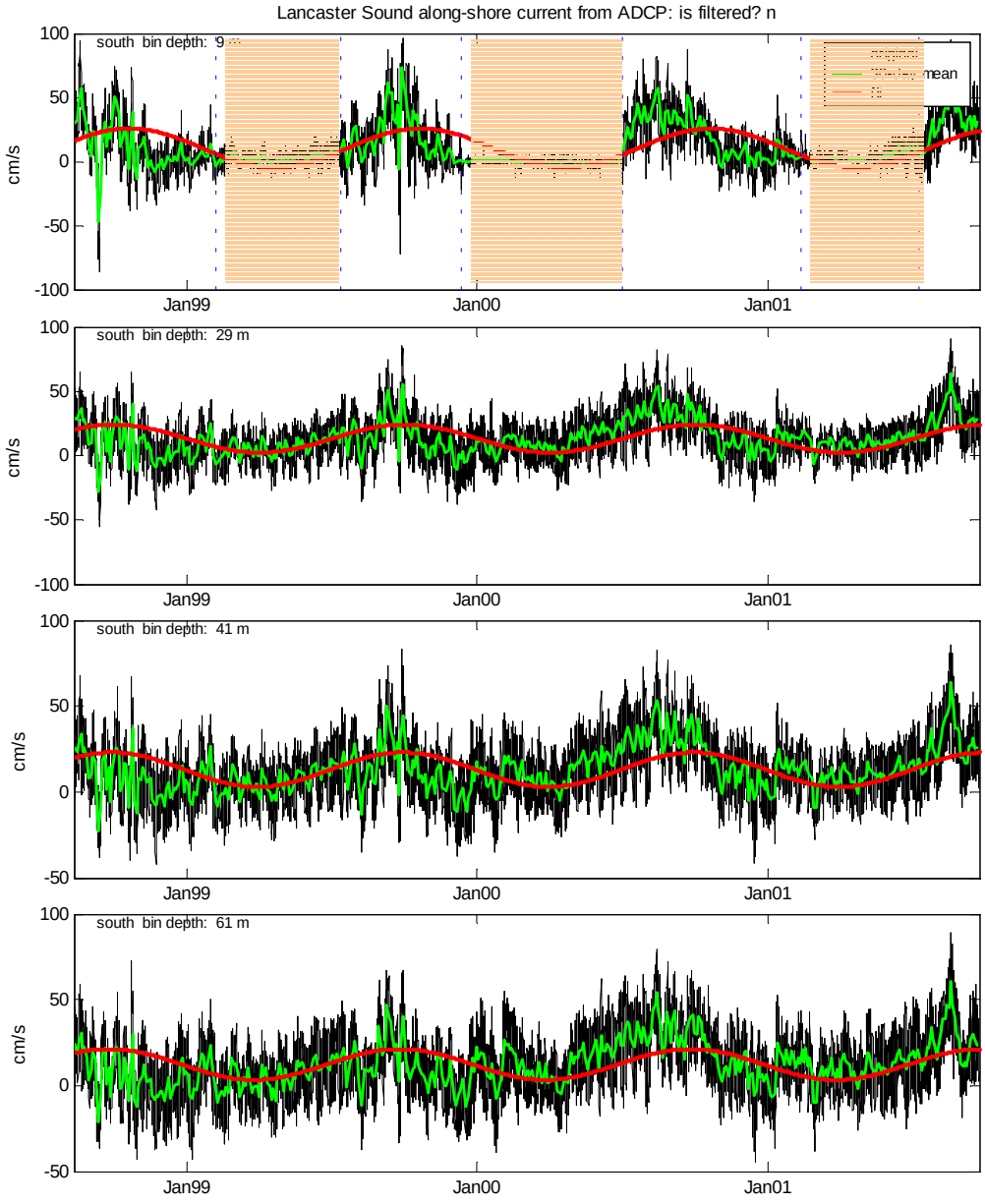

Figure 29 Harmonic fit of ADCP data from southern mooring measured at 9, 29, 41, and 61 m. The vertical blue lines and the shaded area between the lines in the first plot indicate the start and end of landfast ice cover.

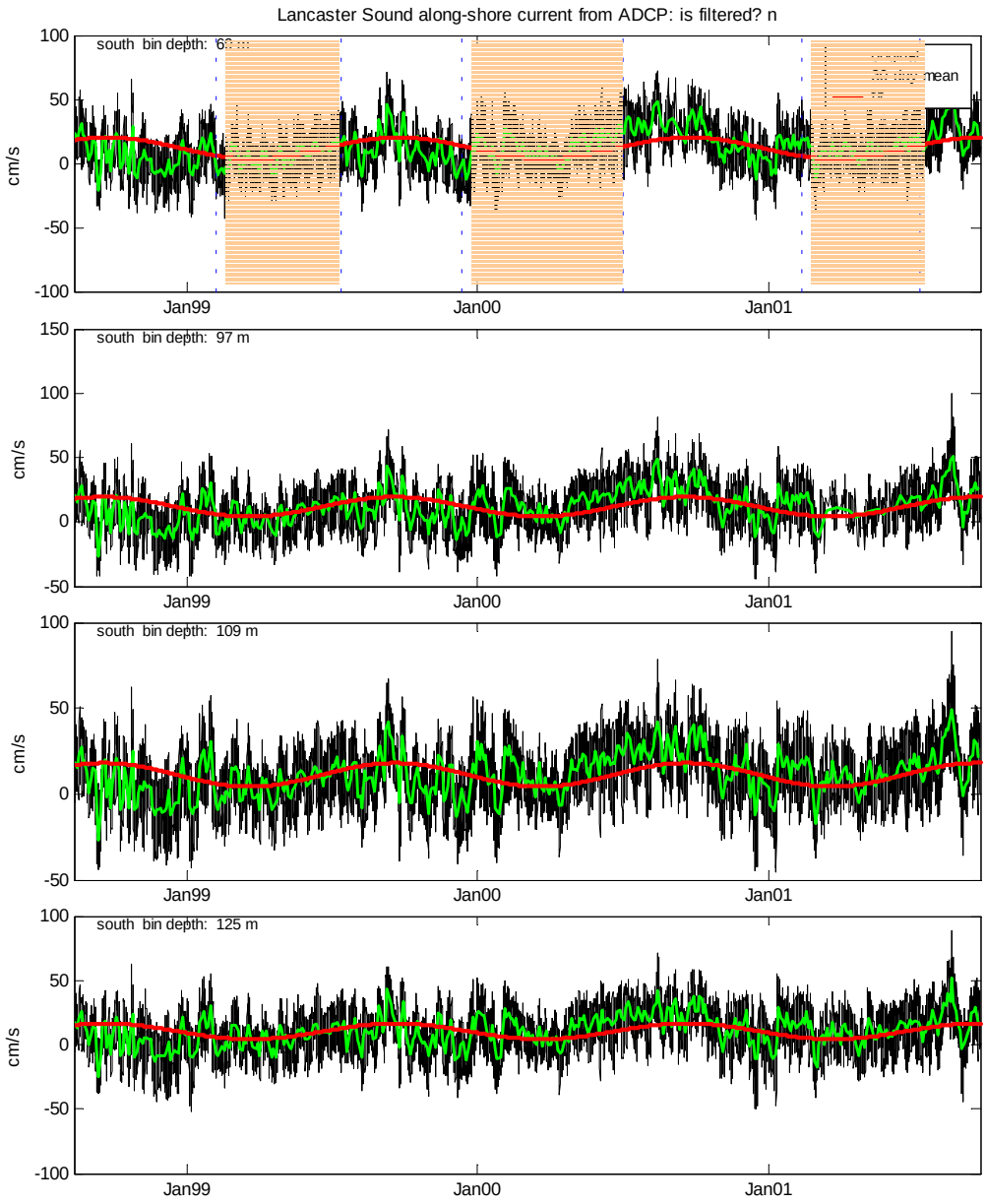

Figure 30 Harmonic fit of ADCP data from southern mooring measured at 69, 97, 109, and 125 m. The vertical blue lines and the shaded area between the lines in the first plot indicate the start and end of landfast ice cover.

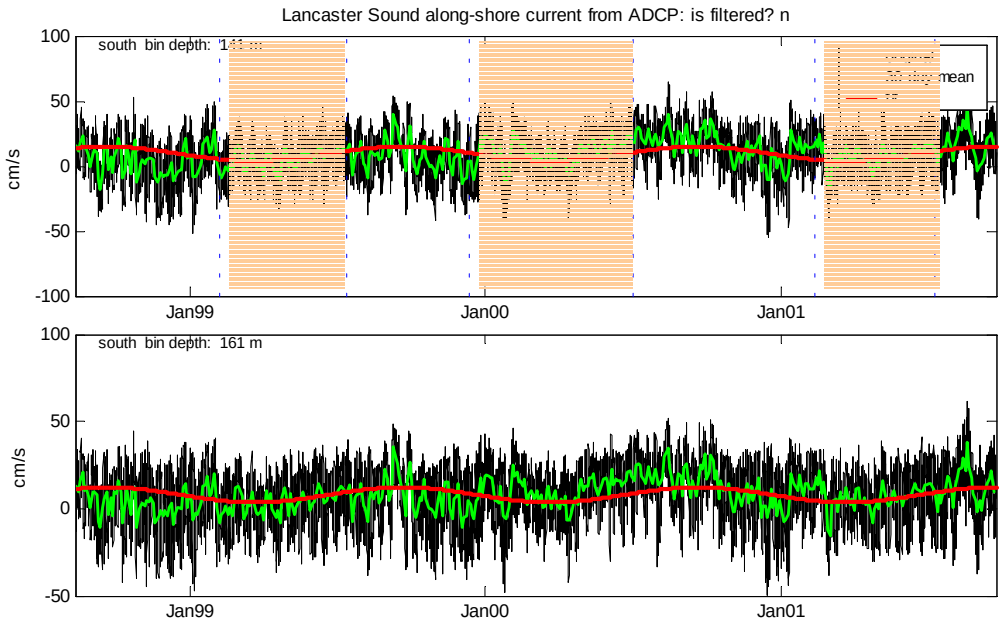

Figure 31 Harmonic fit of ADCP data from southern mooring measured at 141 and 161 m. The vertical blue lines and the shaded area between the lines in the first plot indicate the start and end of landfast ice cover.

Harmonic fit to yearly data

Table 19 Mean, amplitude, and phase of harmonic fit to 1-year ADCP data from northern mooring.

North Depth (m)	Mean (cm/s)	Amplitude (cm/s)	Phase (calendar day)
1998	Initial conditions for iterations: [-3 6 40]		
10	-4.9	8.9	68
30	-3.4	6.0	89
50	-2.1	3.9	124
70	-0.8	2.8	165
90	-0.2	3.2	204
110	-0.7	2.4	218
130	-1.5	1.2	221
146	-1.7	0.5	233
1999	Initial conditions for iterations: [-3 6 40]		
10	-1.7	7.0	69
30	-1.6	7.2	83
50	-1.2	5.2	96
70	-0.7	3.3	102
90	-1.0	1.3	152
110	-1.3	0.7	172
130	-1.7	0.4	148
146	-2.0	0.6	114
2000	Initial conditions for iterations: [-3 6 40]		
10	-1.7	7.9	77
30	-0.7	6.5	90
50	-0.0	4.0	100
70	0.9	3.0	104
90	1.0	3.5	107
110	0.1	2.1	70
130	-0.6	1.7	34
146	-1.3	1.4	6

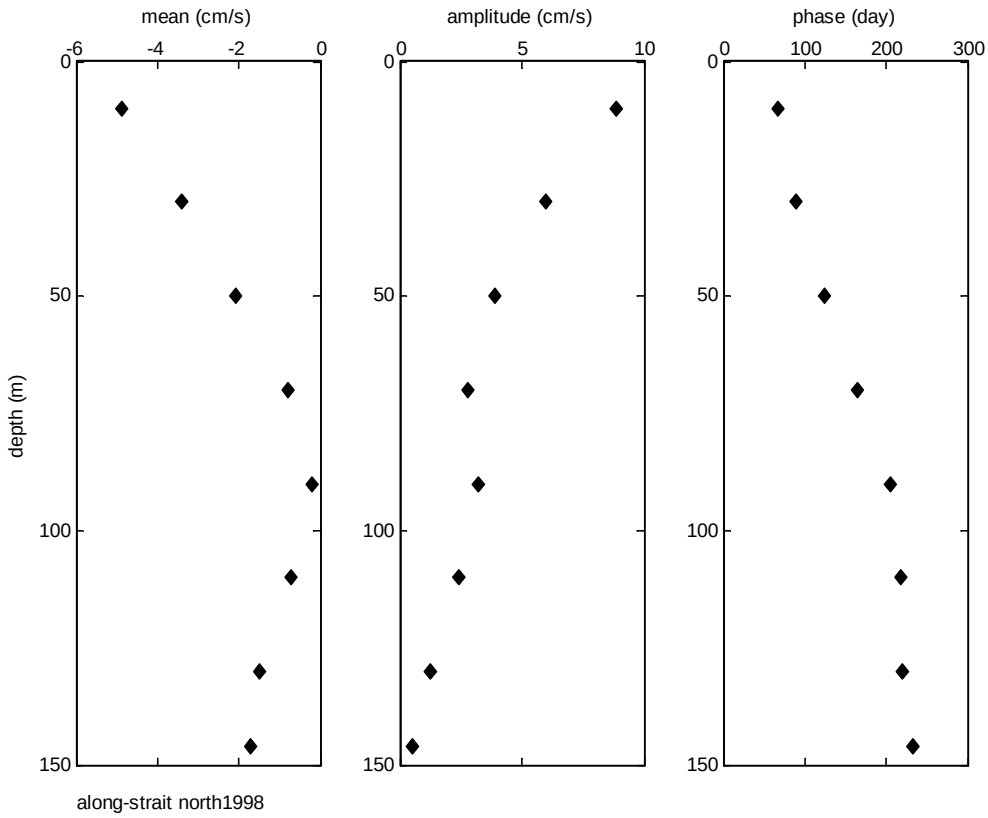

Figure 32 Profile of mean, amplitude, and phase of 1998 current data from northern ADCP mooring.

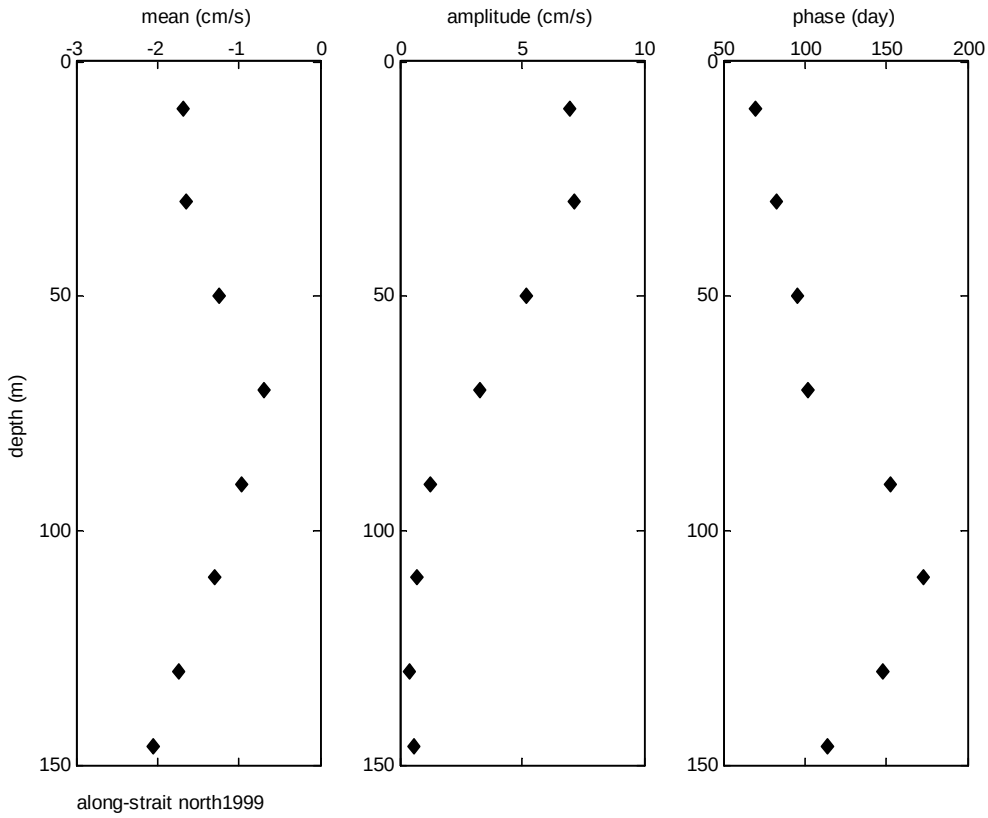

Figure 33 Profile of mean, amplitude, and phase of 1999 current data from northern ADCP mooring.

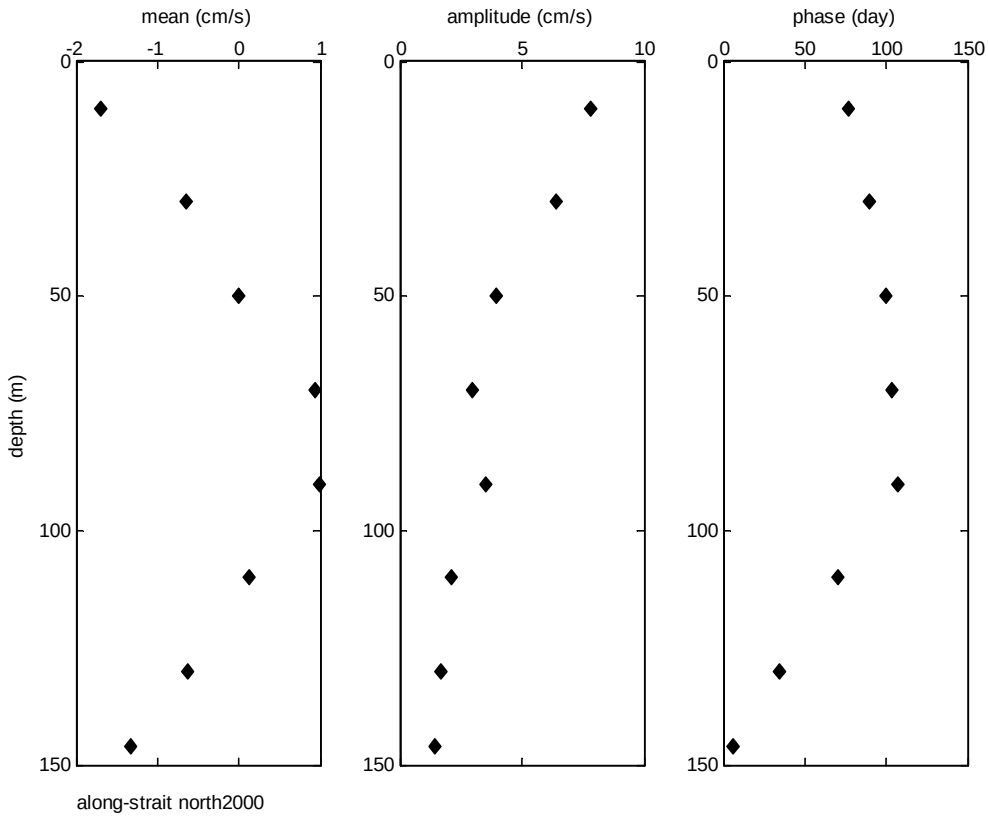

Figure 34 Profile of mean, amplitude, and phase of 2000 current data from northern ADCP mooring.

Table 20 Mean, amplitude, and phase of harmonic fit to 1-year current data record from southern mooring.

South Depth (m)	Mean (cm/s)	Amplitude (cm/s)	Phase (calendar day)
1998	Initial conditions for iterations: [-3 6 40]		
9	7.4	8.9	247
29	8.4	6.4	218
41	7.6	5.8	213
61	6.2	5.7	204
69	6.0	5.7	201
97	5.6	5.3	187
109	5.4	4.8	184
125	5.1	4.2	182
141	4.7	3.6	184
161	4.0	2.6	195
1999	Initial conditions for iterations: [-3 6 40]		
9	11.3	19.2	241
29	14.7	12.3	213
41	14.5	11.4	207
61	14.0	10.1	201
69	13.9	9.7	200
97	13.3	8.7	196
109	12.8	8.0	195
125	12.2	7.5	195
141	11.3	6.9	193
161	10.2	5.9	190
2000	Initial conditions for iterations: [-3 6 240]		
9	11.4	18.2	246
29	15.8	13.5	239
41	16.2	12.7	240
61	15.9	11.3	240
69	15.5	10.4	240
97	15.7	9.3	236
109	14.7	8.7	241
125	13.3	7.9	245
141	11.6	7.0	244
161	9.3	5.4	246

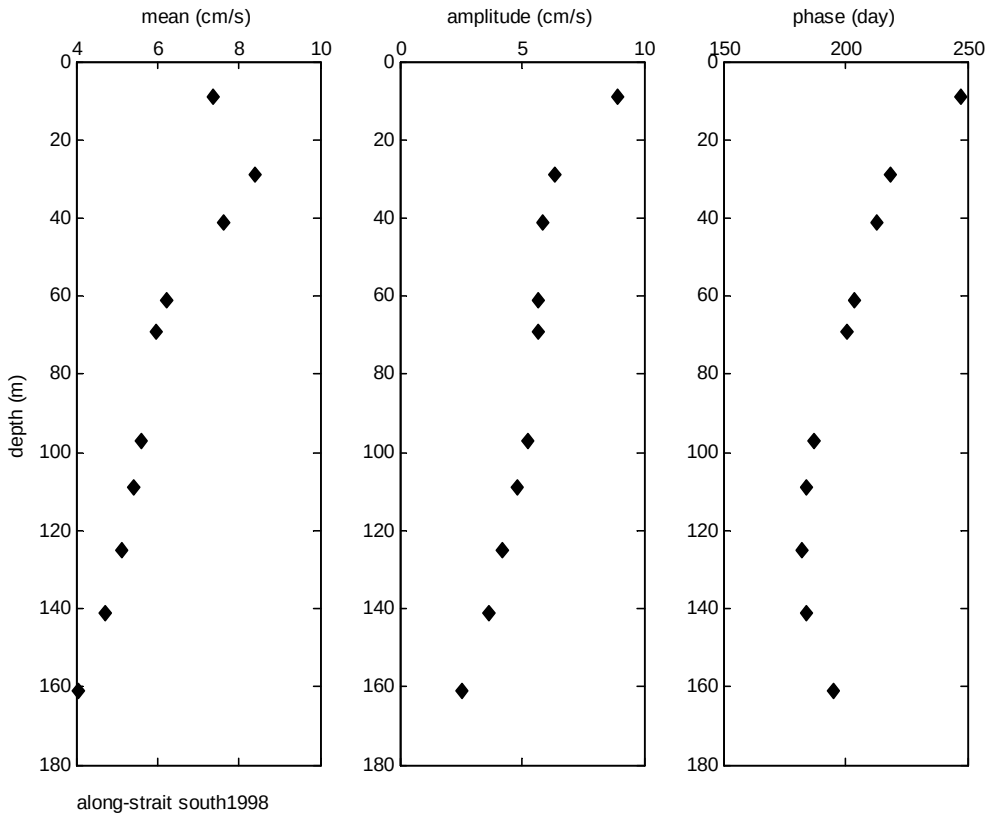

Figure 35 Profile of mean, amplitude, and phase of 1998 current data from southern ADCP mooring.

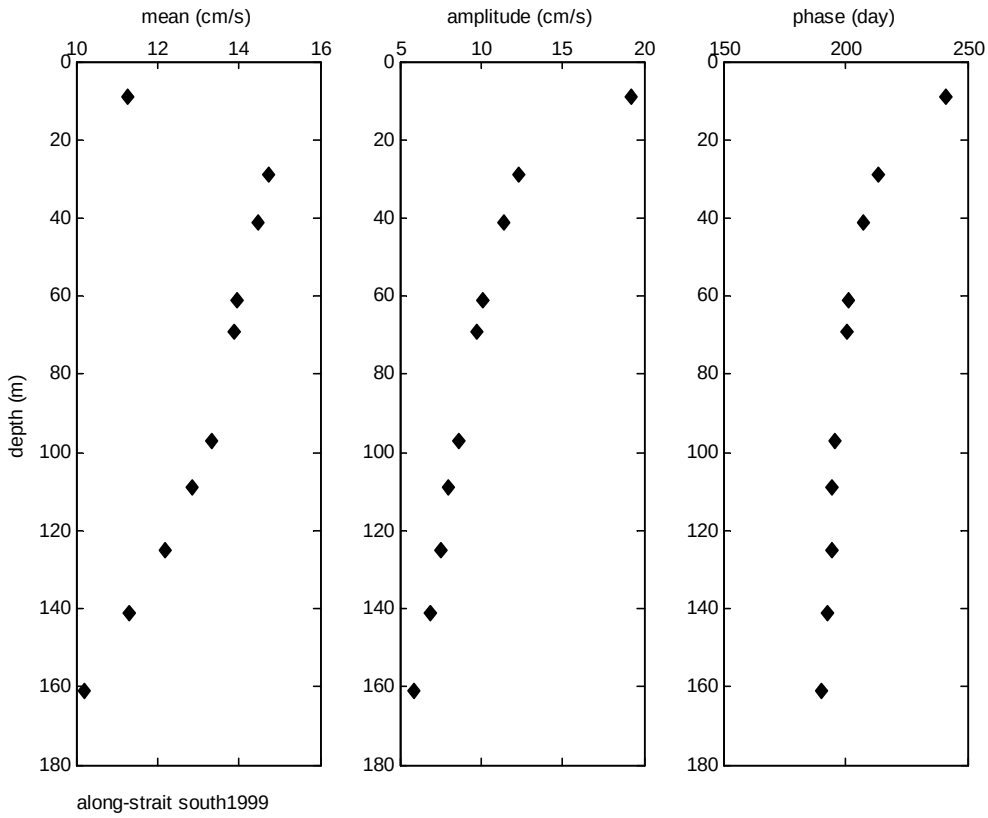

Figure 36 Profile of mean, amplitude, and phase of 1999 current data from southern ADCP mooring.

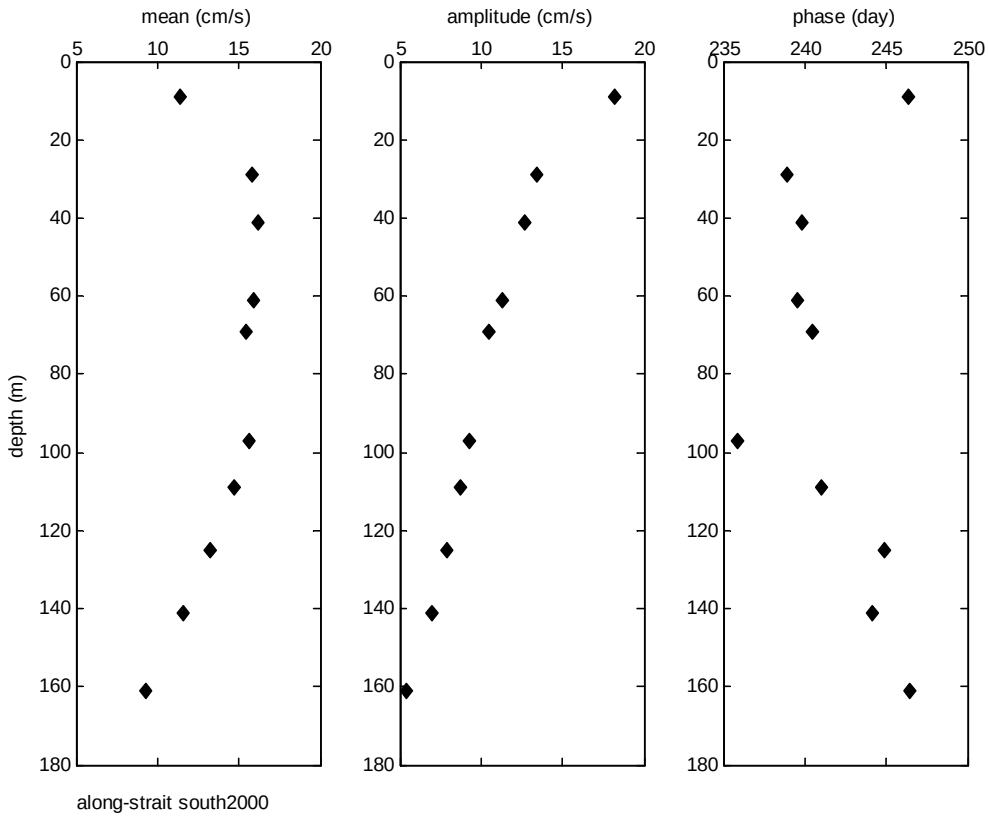

Figure 37 Profile of mean, amplitude, and phase of 2000 current data from southern ADCP mooring.

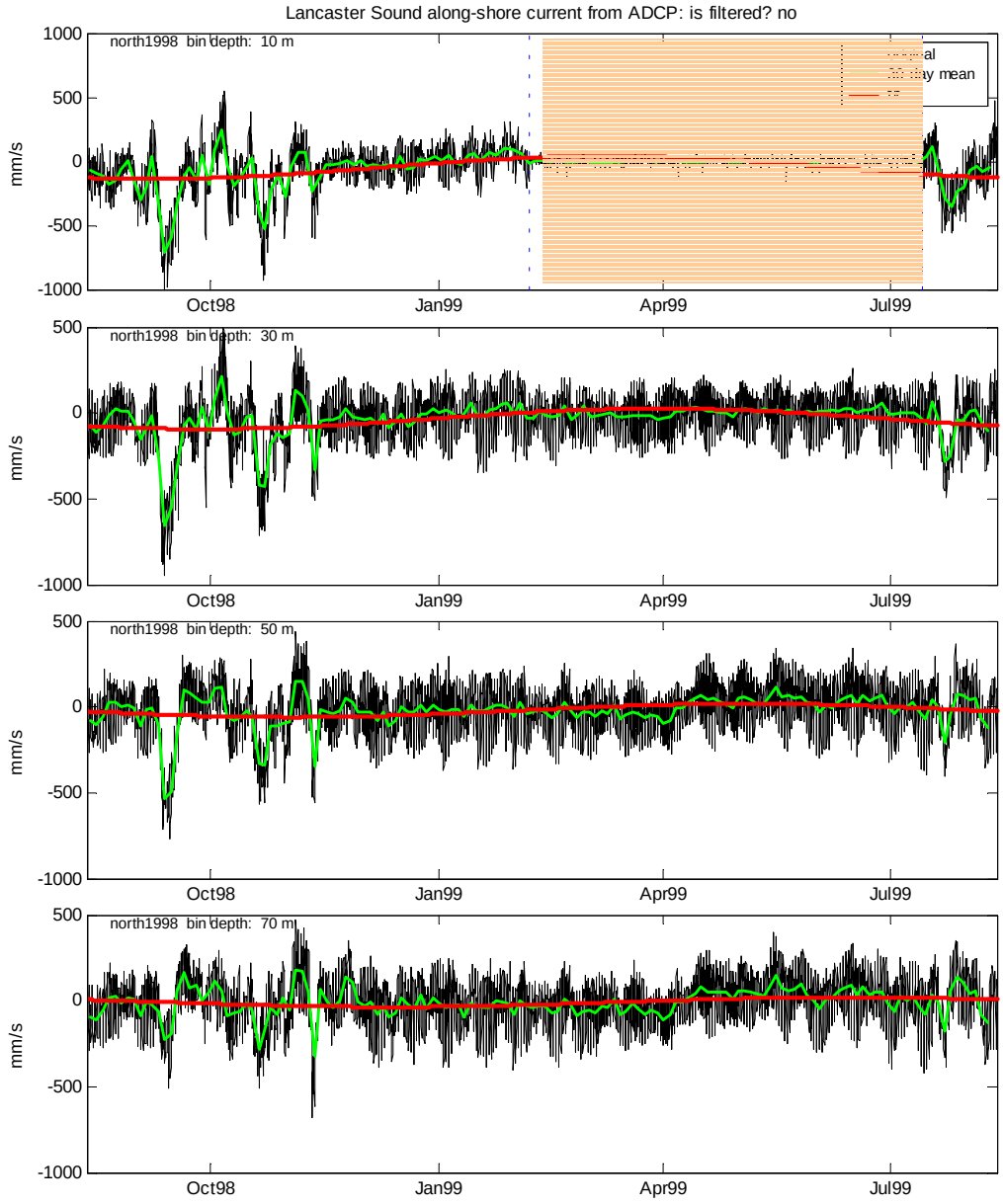

Figure 38 Harmonic fit of 1998 ADCP data from northern mooring measured at 10, 30, 50, and 70 m. The vertical blue lines and the shaded area between the lines in the first plot indicate the start and end of landfast ice cover.

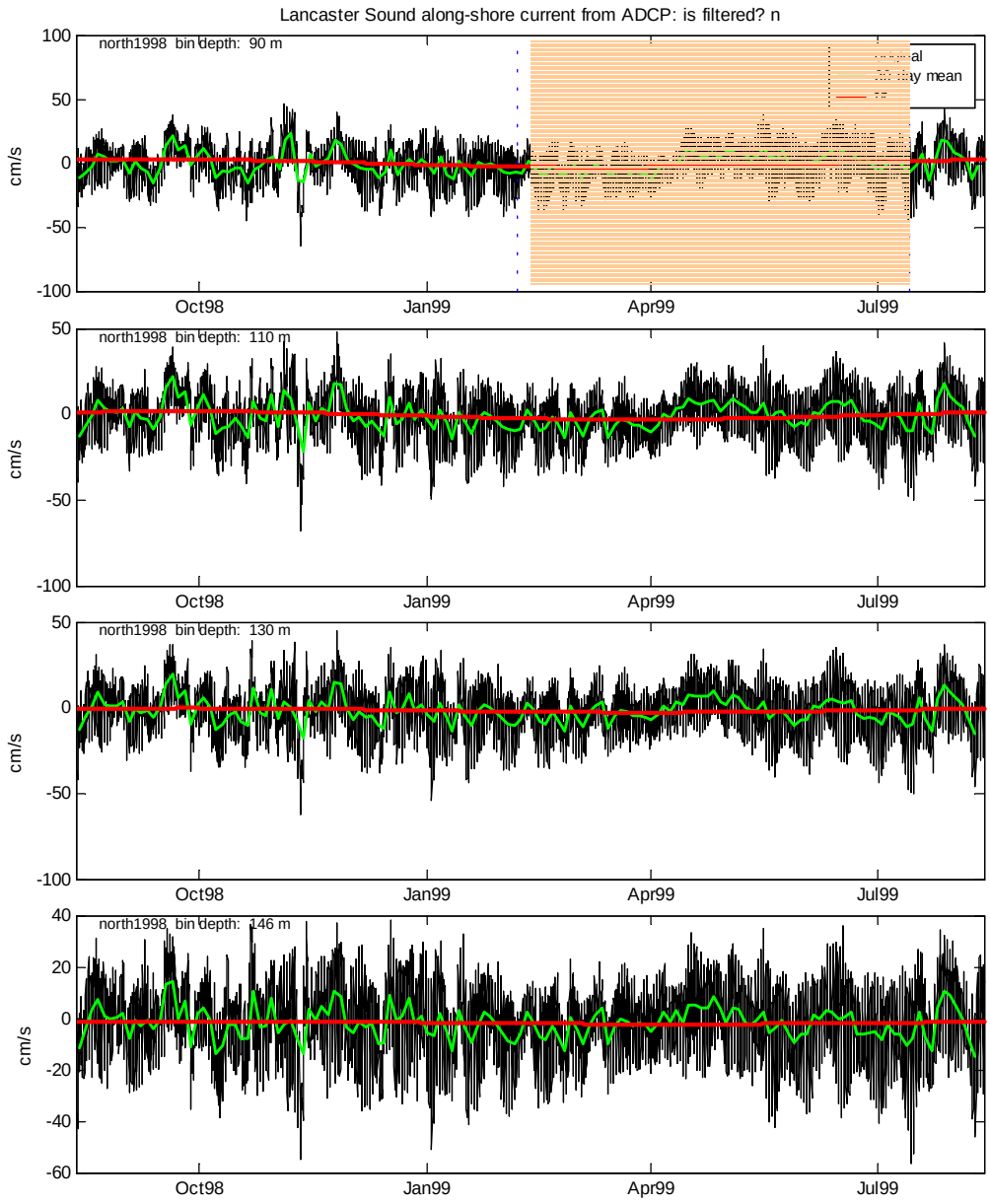

Figure 39 Harmonic fit of 1998 ADCP data from northern mooring measured at 90, 110, 130, and 146 m. The vertical blue lines and the shaded area between the lines in the first plot indicate the start and end of landfast ice cover.

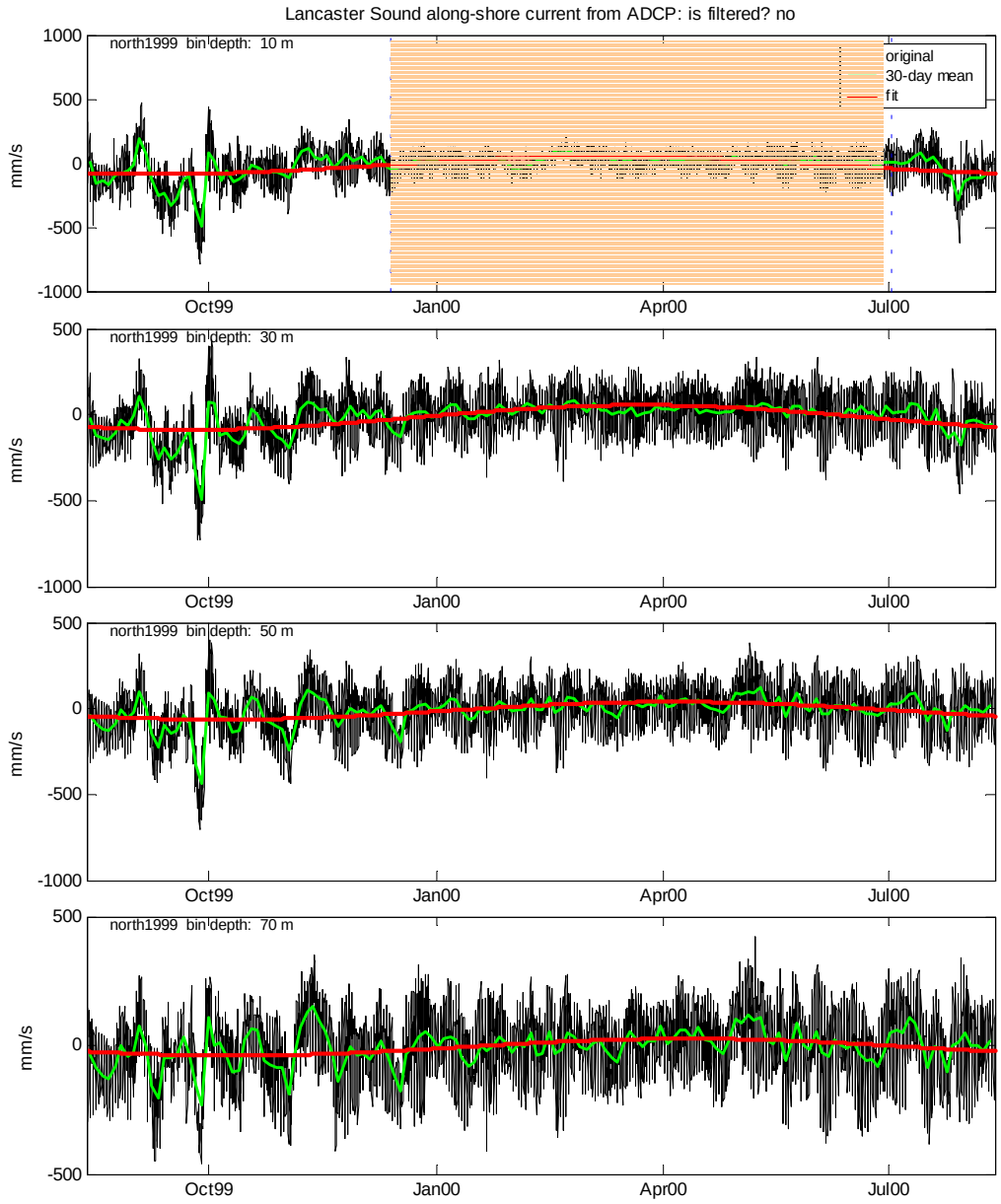

Figure 40 Harmonic fit of 1999 ADCP data from northern mooring measured at 10, 30, 50, and 70 m. The vertical blue lines and the shaded area between the lines in the first plot indicate the start and end of landfast ice cover.

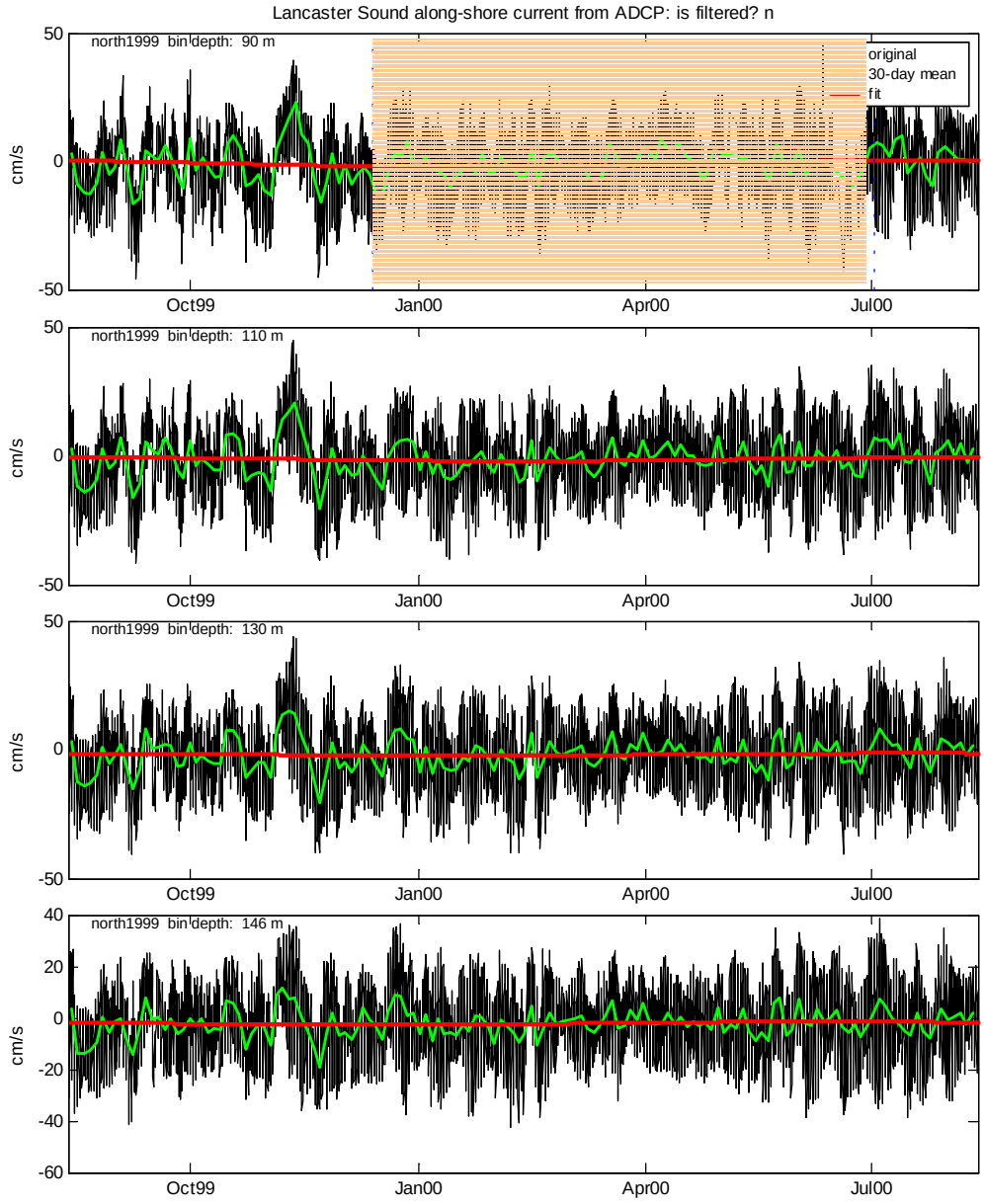

Figure 41 Harmonic fit of 1999 ADCP data from northern mooring measured at 90, 110, 130, and 146 m. The vertical blue lines and the shaded area between the lines in the first plot indicate the start and end of landfast ice cover.

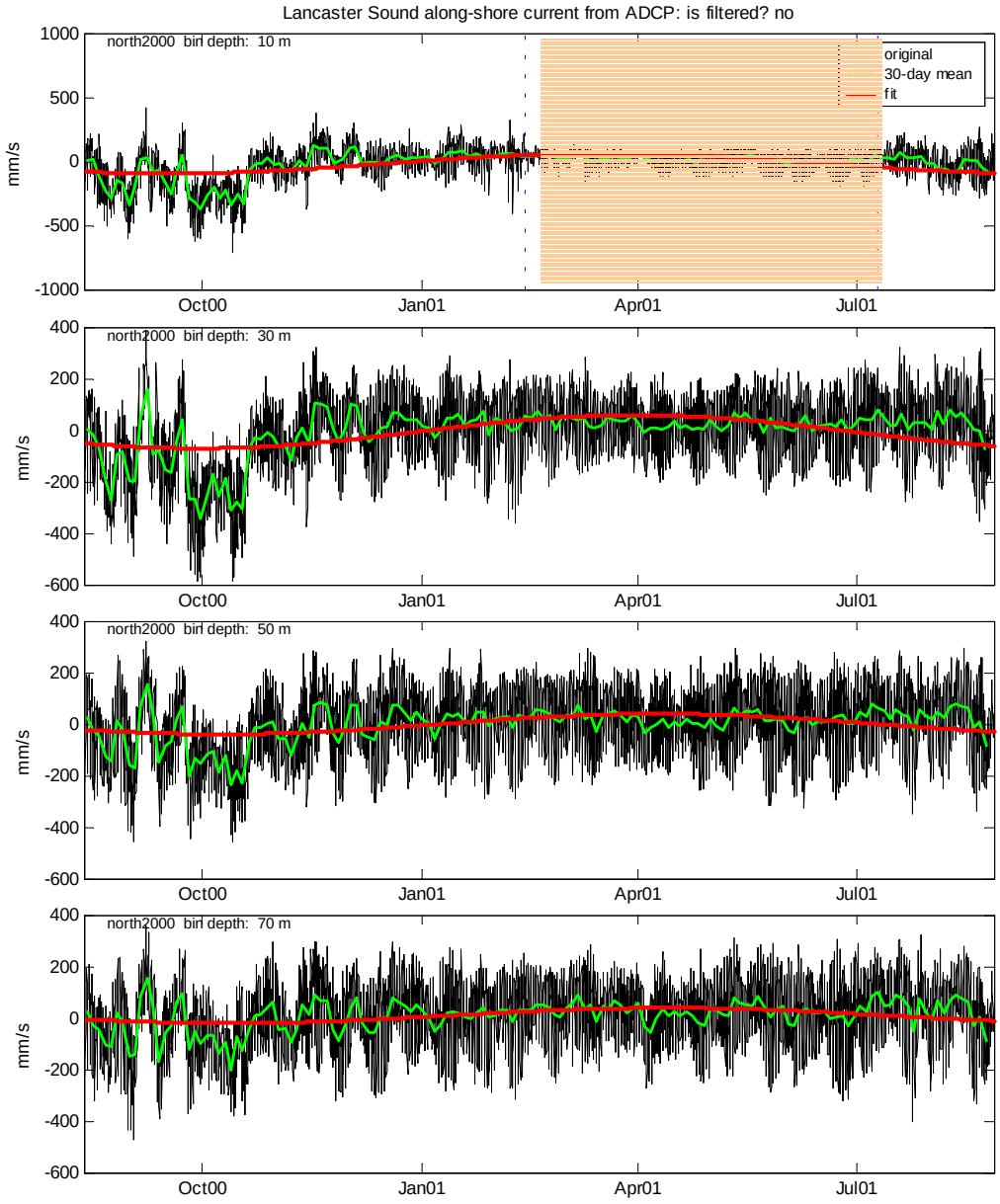

Figure 42 Harmonic fit of 2000 ADCP data from northern mooring measured at 10, 30, 50, and 70 m. The vertical blue lines and the shaded area between the lines in the first plot indicate the start and end of landfast ice cover.

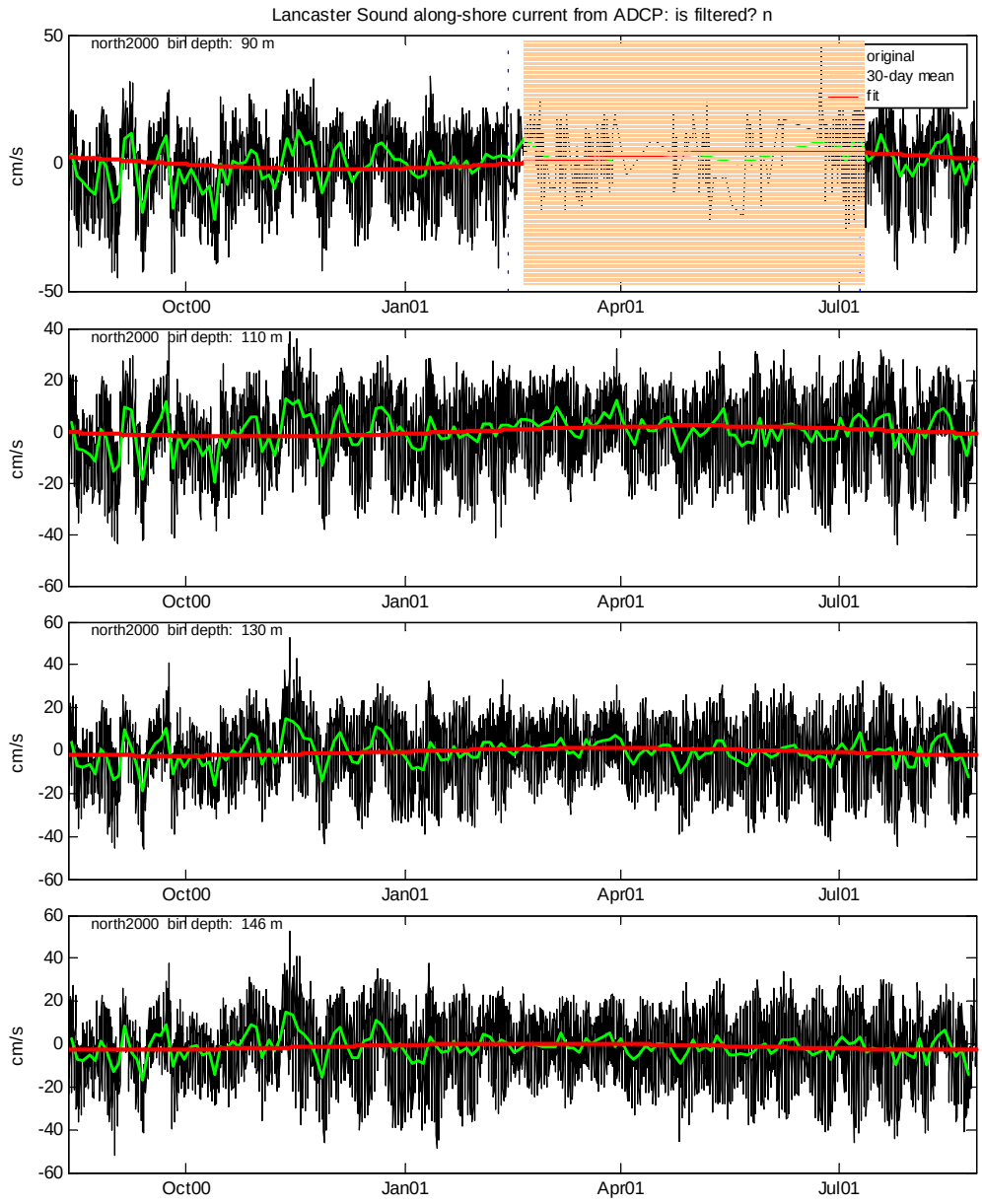

Figure 43 Harmonic fit of 2000 ADCP data from northern mooring measured at 90, 110, 130, and 146 m. The vertical blue lines and the shaded area between the lines in the first plot indicate the start and end of landfast ice cover.

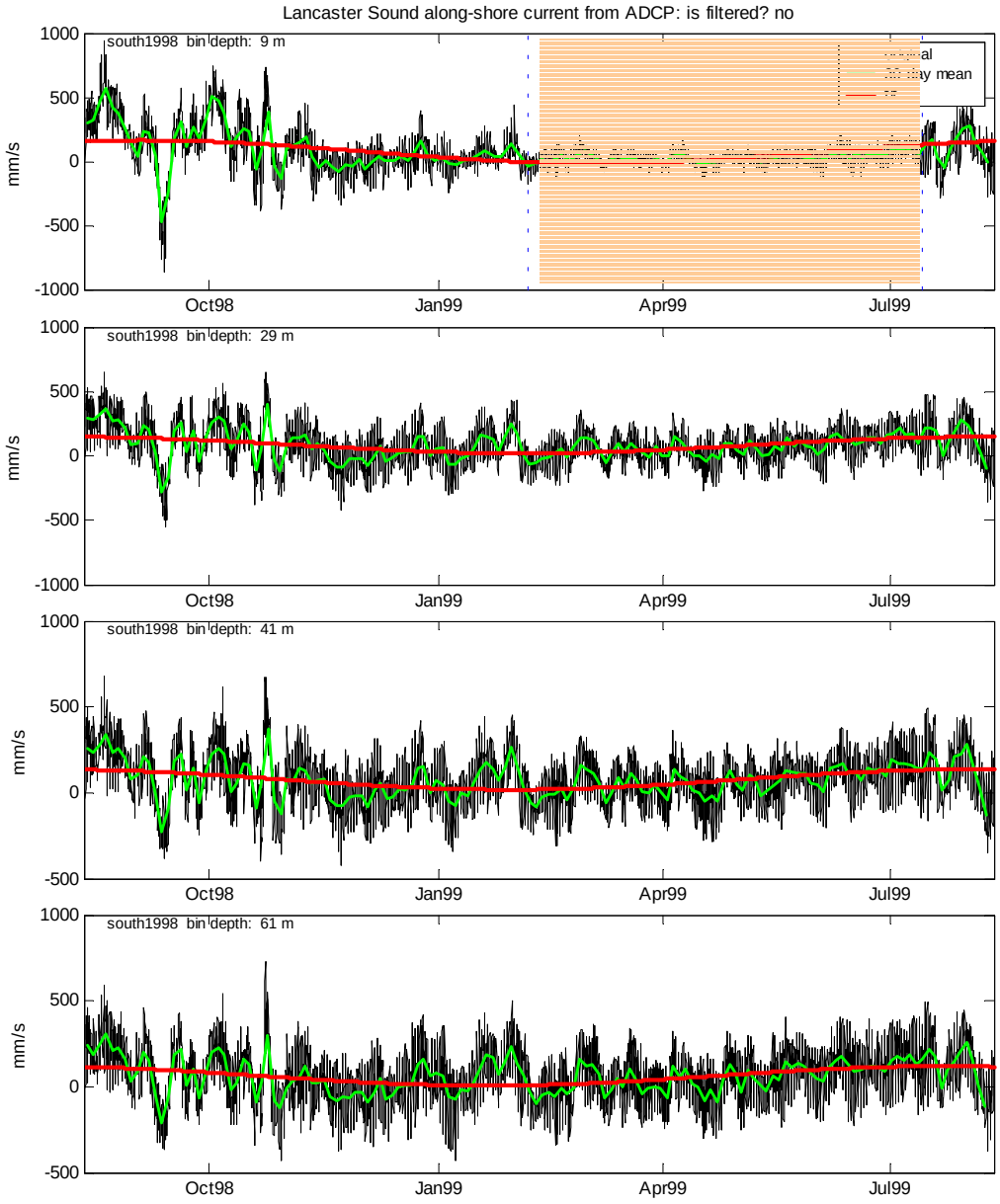

Figure 44 Harmonic fit of 1998 ADCP data from southern mooring measured at 9, 29, 41, and 61 m. The vertical blue lines and the shaded area between the lines in the first plot indicate the start and end of landfast ice cover.

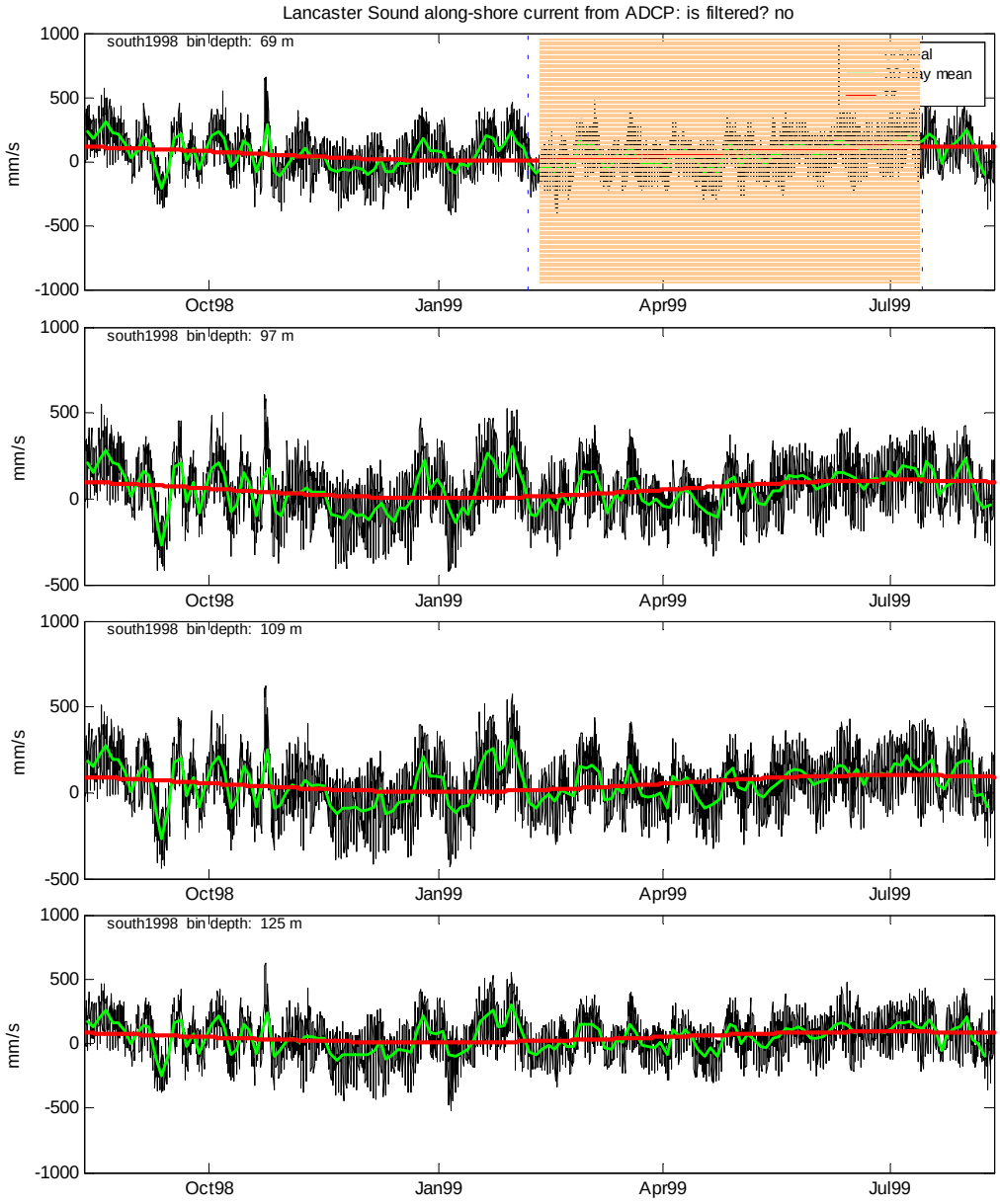

Figure 45 Harmonic fit of 1998 ADCP data from southern mooring measured at 69, 97, 109, and 125 m. The vertical blue lines and the shaded area between the lines in the first plot indicate the start and end of landfast ice cover.

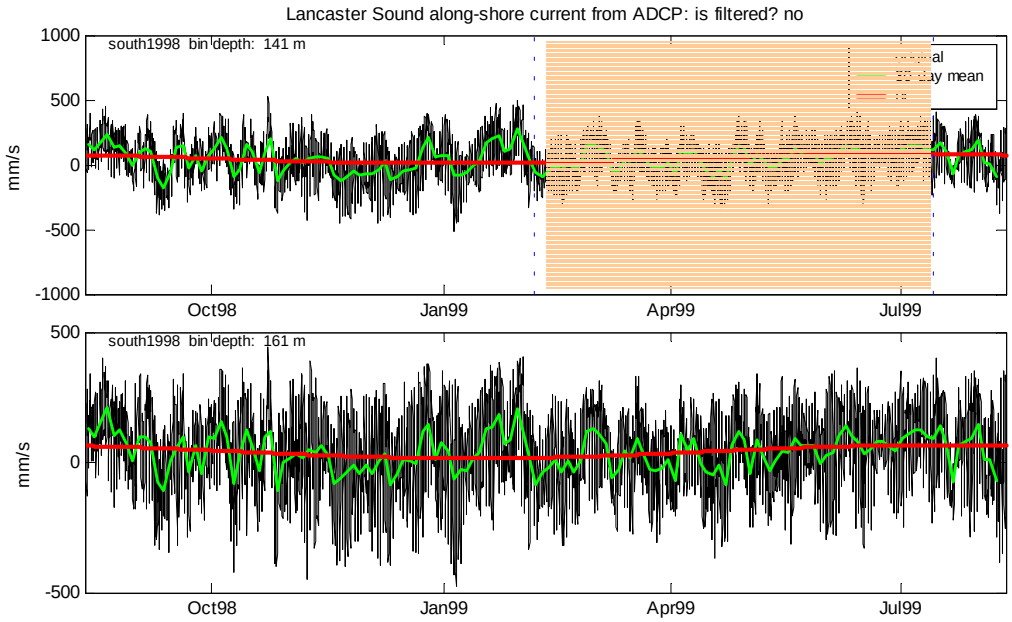

Figure 46 Harmonic fit of 1998 ADCP data from southern mooring measured at 141 and 161 m. The vertical blue lines and the shaded area between the lines in the first plot indicate the start and end of landfast ice cover.

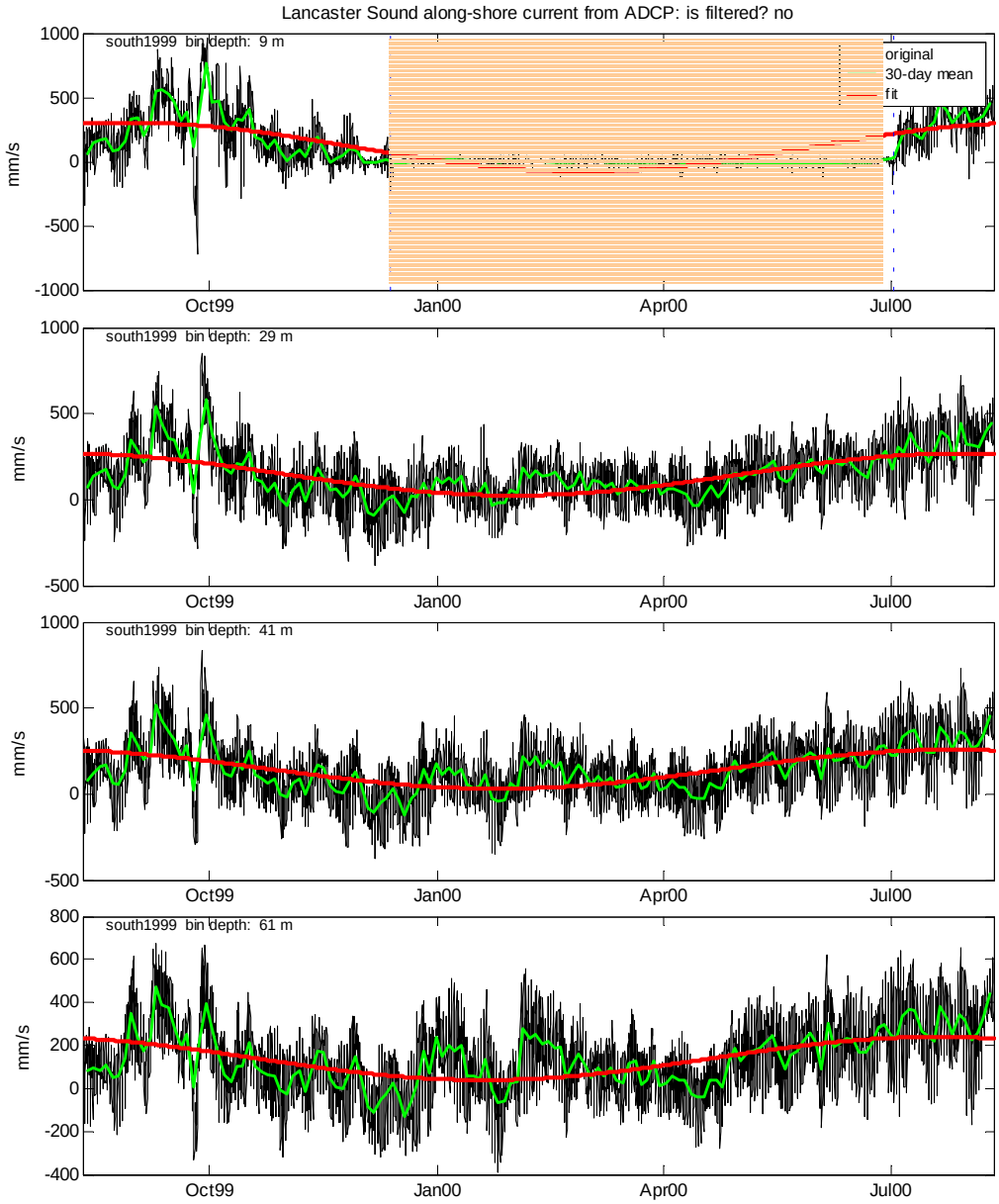

Figure 47 Harmonic fit of 1999 ADCP data from southern mooring measured at 9, 29, 41, and 61 m. The vertical blue lines and the shaded area between the lines in the first plot indicate the start and end of landfast ice cover.

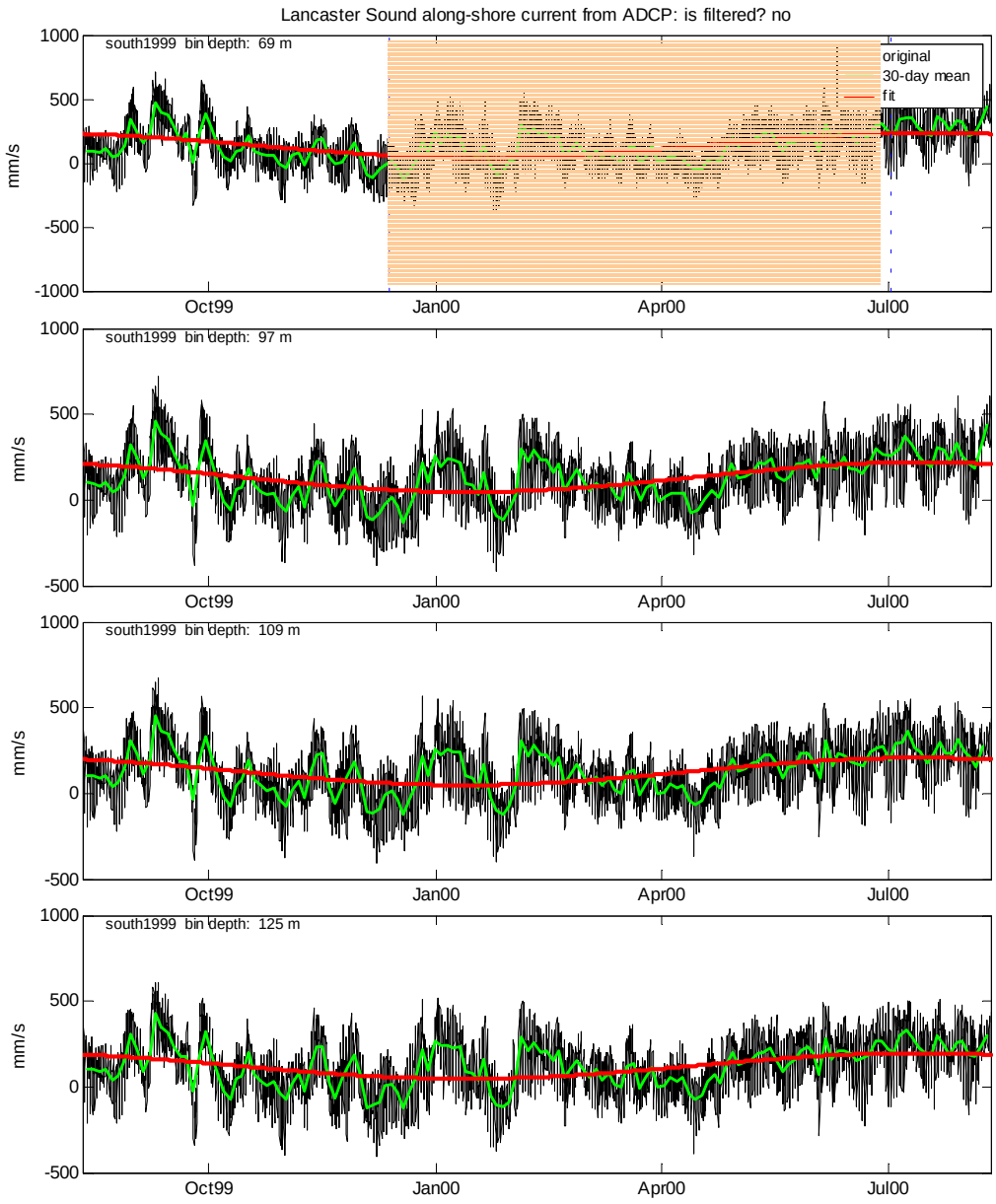

Figure 48 Harmonic fit of 1999 ADCP data from southern mooring measured at 69, 97, 109, and 125 m. The vertical blue lines and the shaded area between the lines in the first plot indicate the start and end of landfast ice cover.

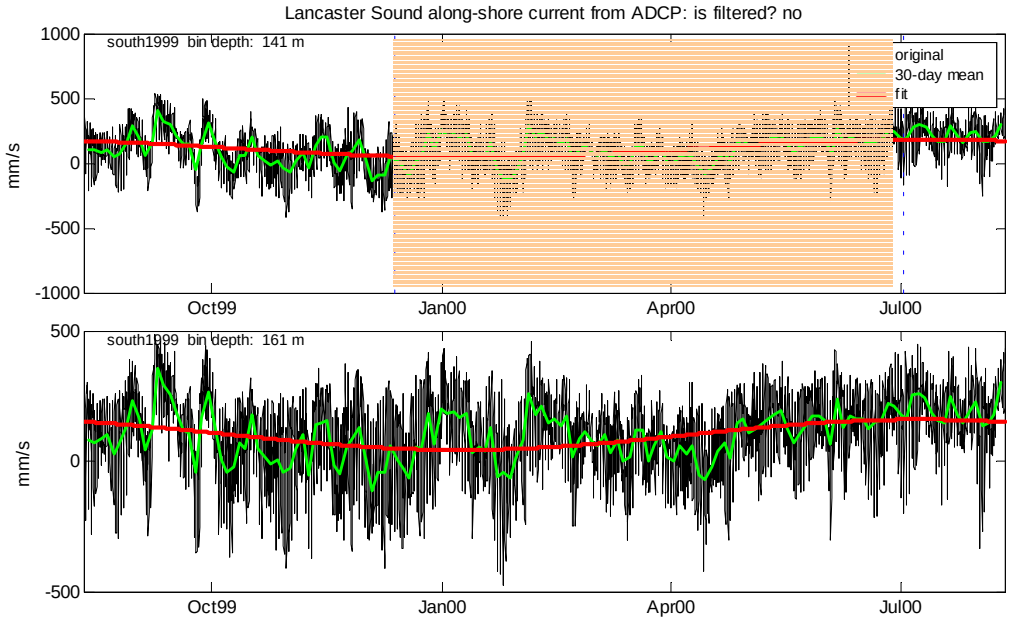

Figure 49 Harmonic fit of 1999 ADCP data from southern mooring measured at 141 and 161 m. The vertical blue lines and the shaded area between the lines in the first plot indicate the start and end of landfast ice cover.

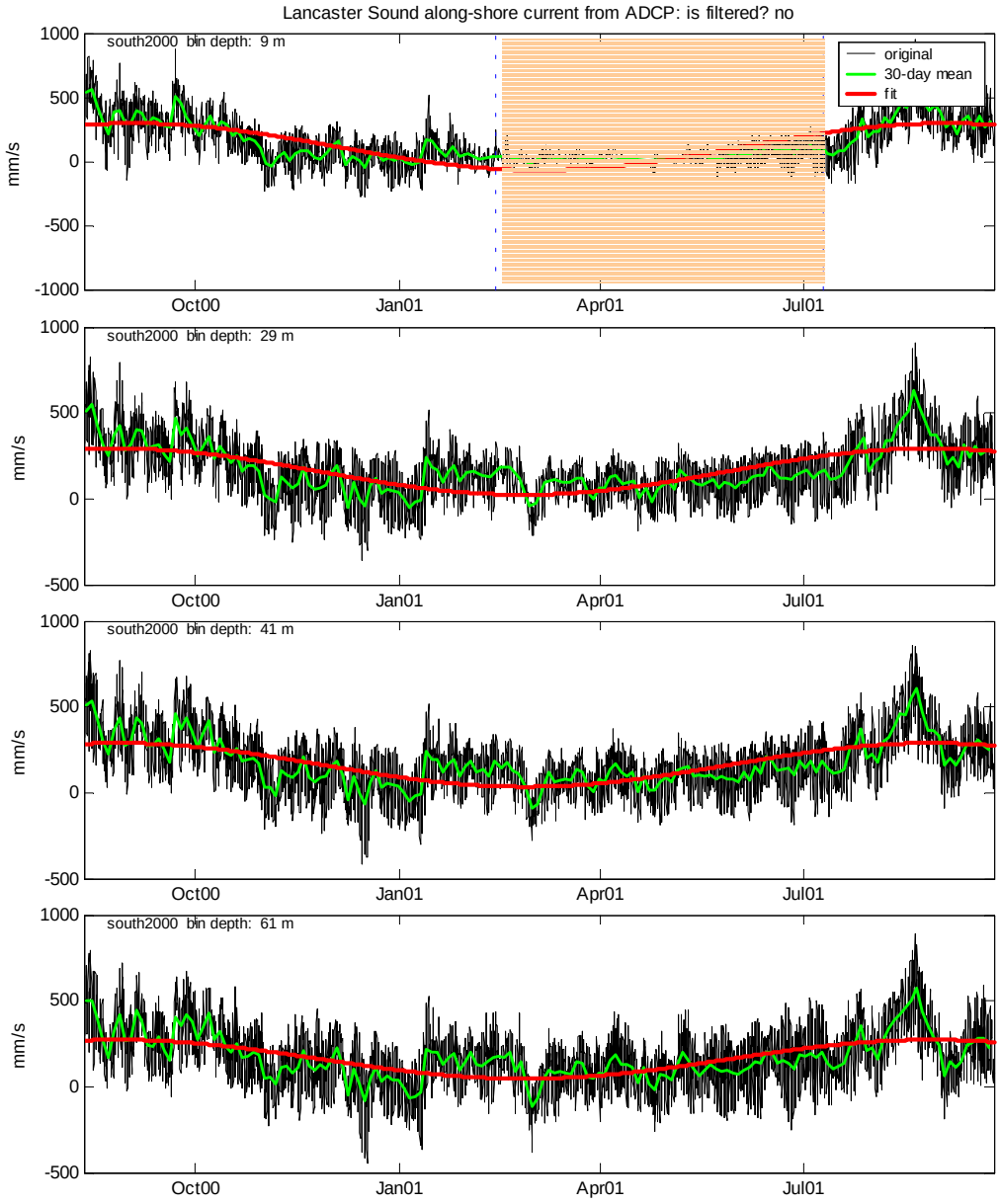

Figure 50 Harmonic fit of 2000 ADCP data from southern mooring measured at 9, 29, 41, and 61 m. The vertical blue lines and the shaded area between the lines in the first plot indicate the start and end of landfast ice cover.

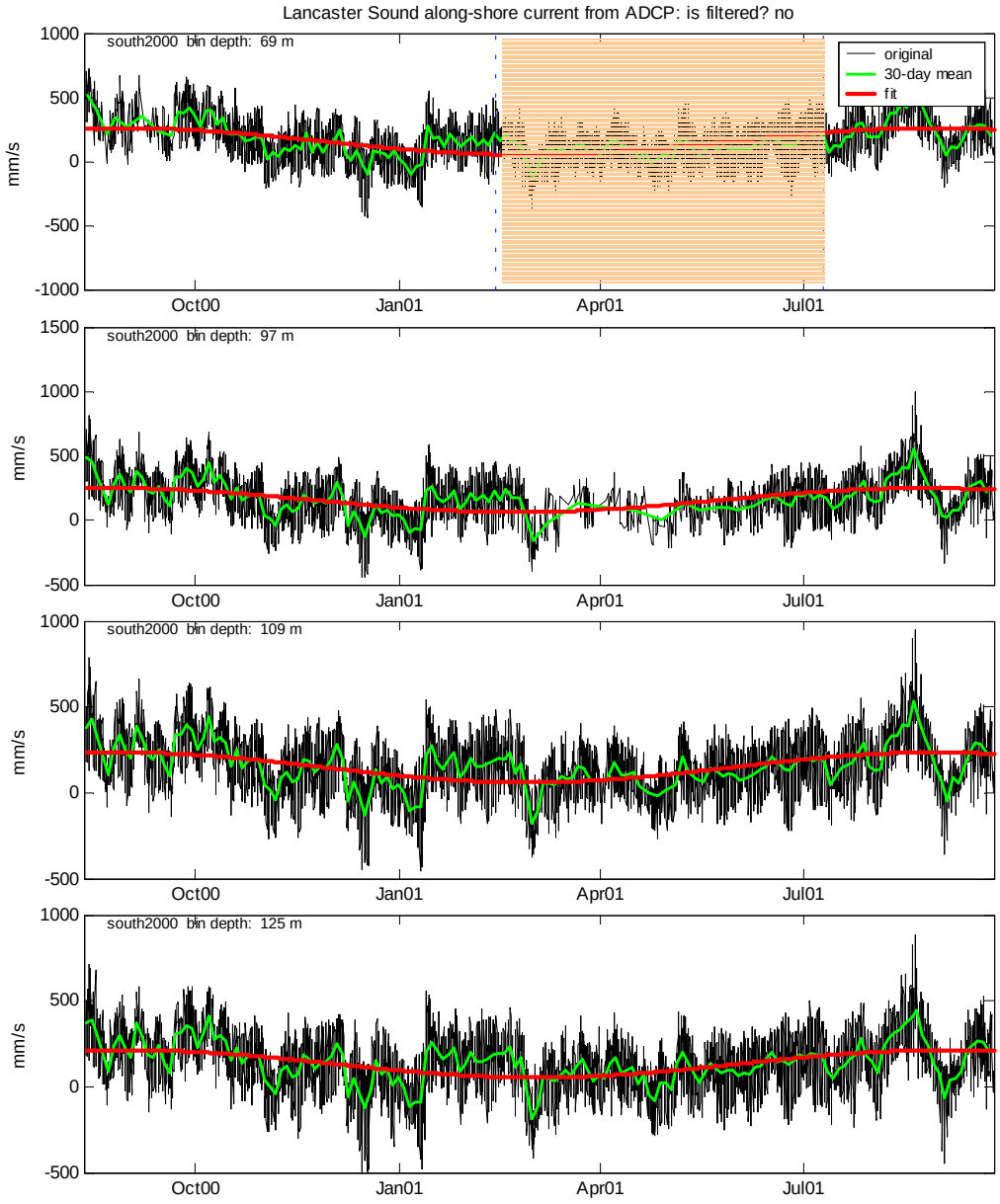

Figure 51 Harmonic fit of 2000 ADCP data from southern mooring measured at 69, 97, 109, and 125 m. The vertical blue lines and the shaded area between the lines in the first plot indicate the start and end of landfast ice cover.

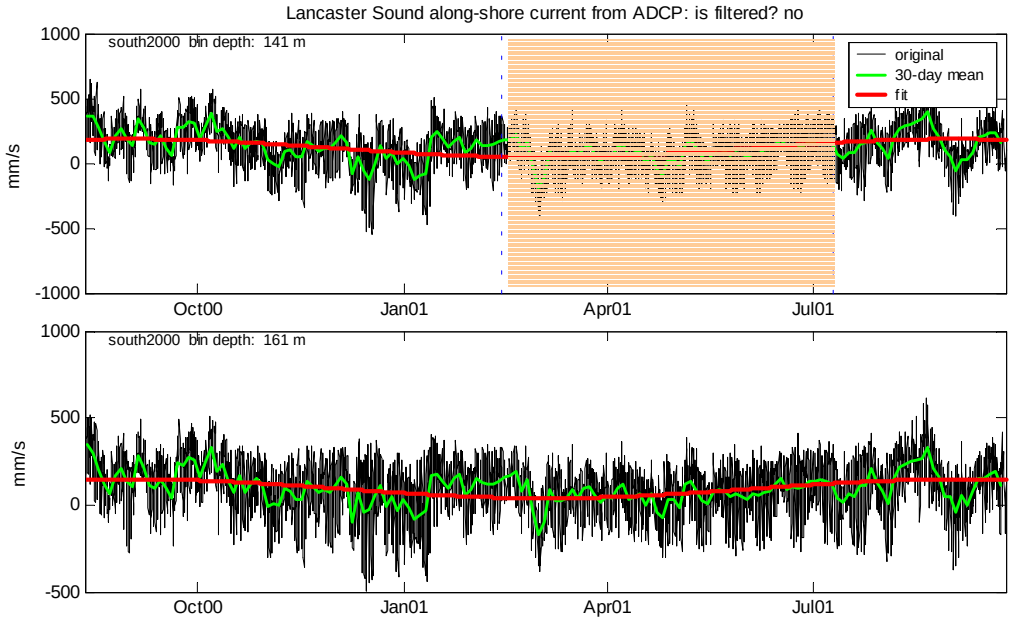

Figure 52 Harmonic fit of 2000 ADCP data from southern mooring measured at 141 and 161 m. The vertical blue lines and the shaded area between the lines in the first plot indicate the start and end of landfast ice cover.

Appendix 2 Spectral Analysis of ADCP Data

Note that a 12 hour period corresponds to a frequency of 2.3×10^{-5} Hz and a 24 hour period corresponds to 1.15×10^{-5} Hz.

North shore

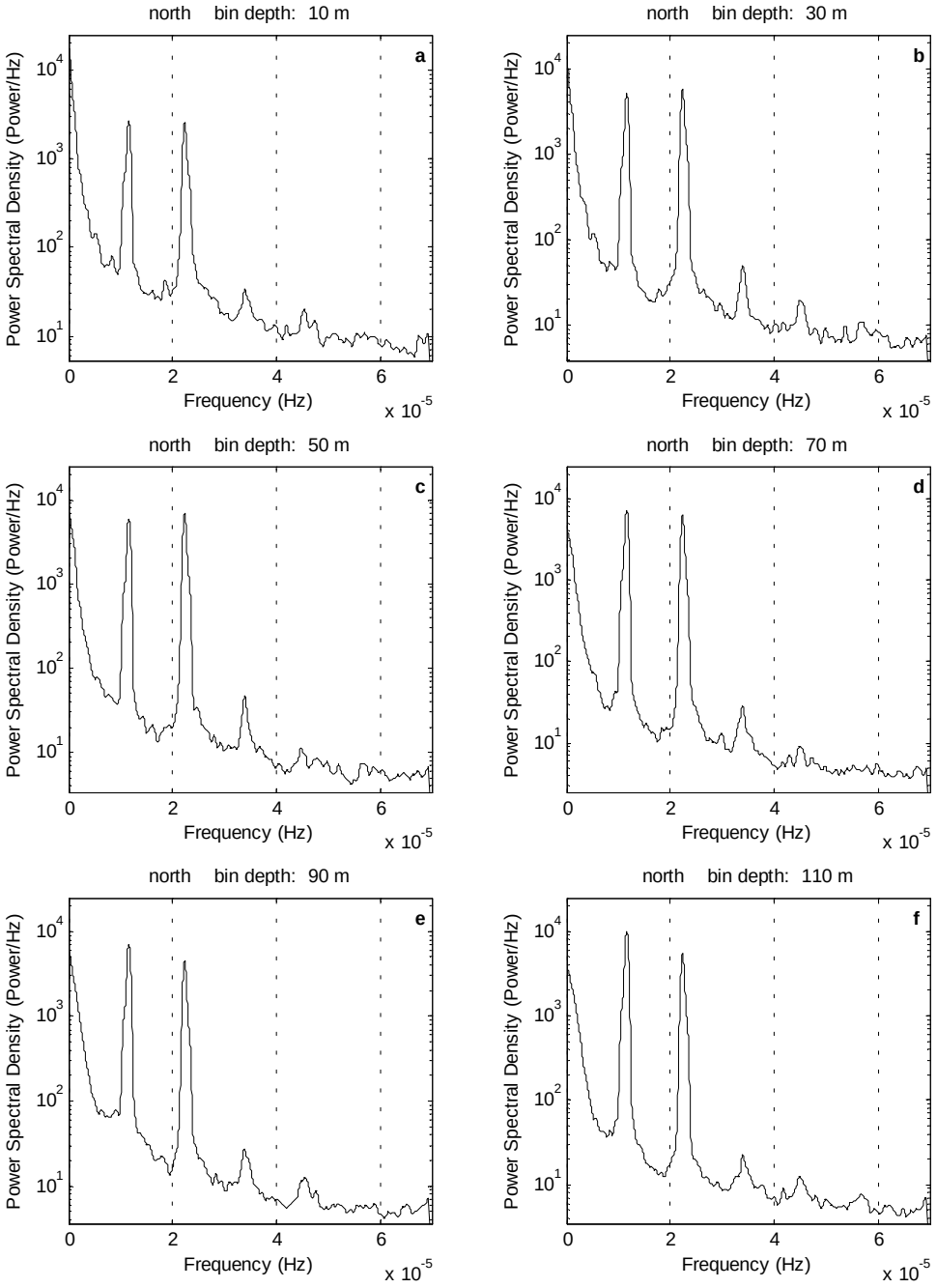

Figure 53 Power spectra for north mooring current at 10, 30, 50, 70, 90, and 110 m

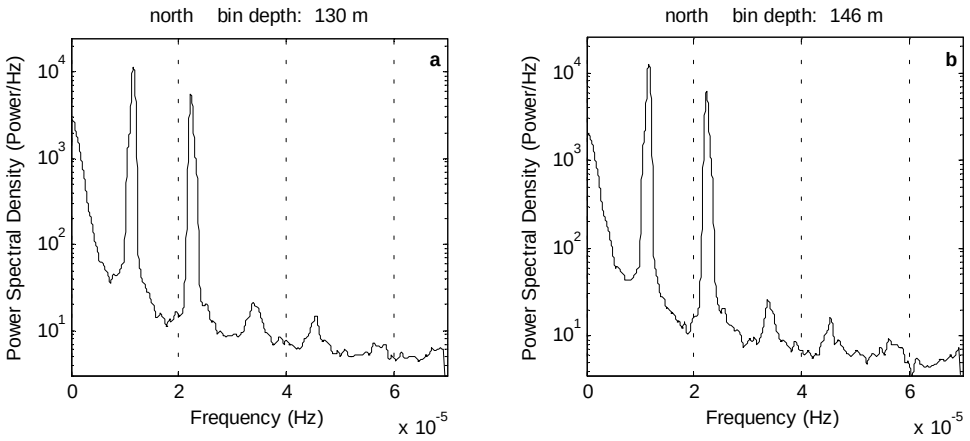

Figure 54 Power spectrum for north mooring current at 130 and 146 m

South shore

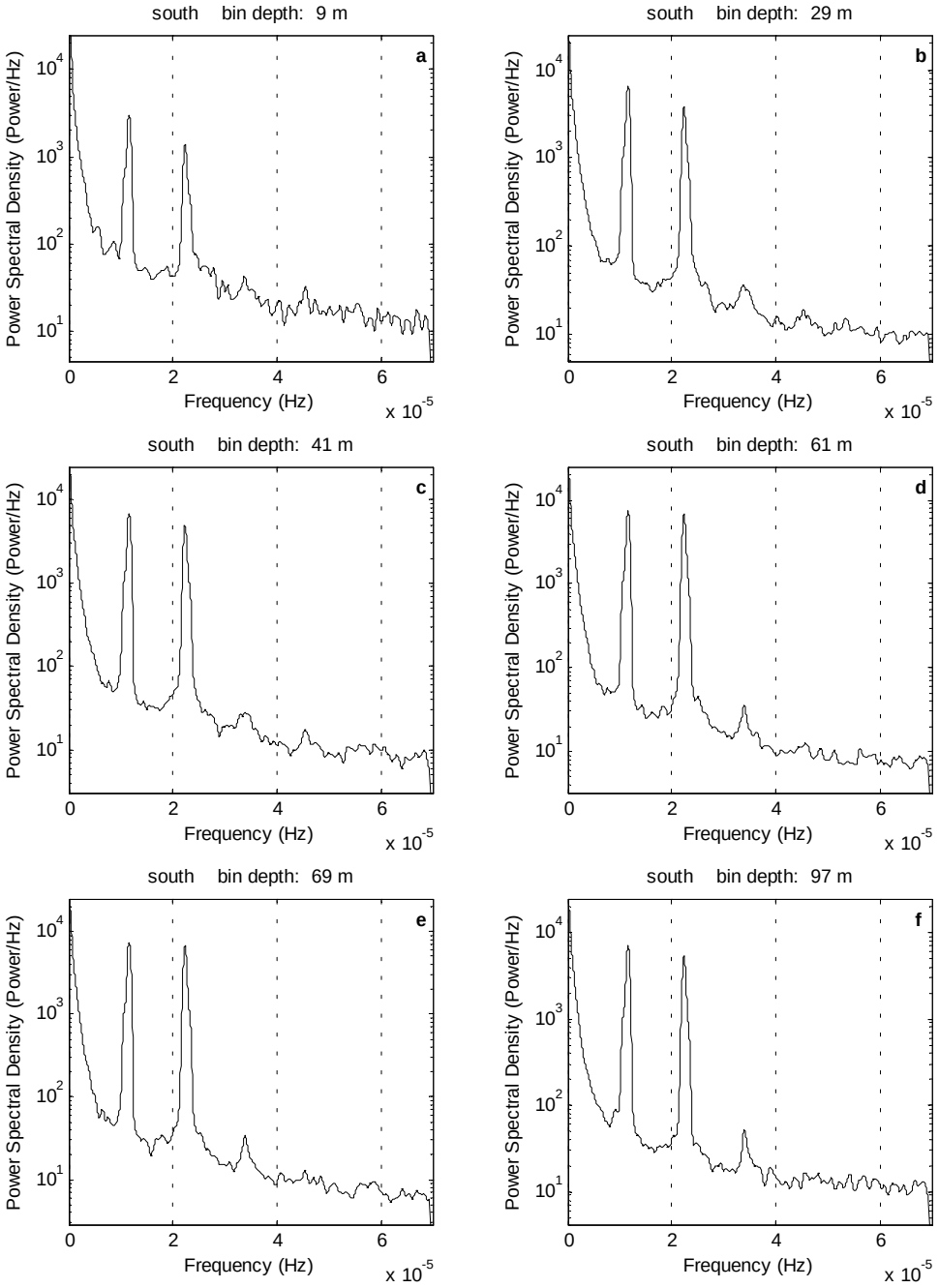

Figure 55 Power spectra for south mooring current at 9, 29, 41, 61, 69, and 97 m.

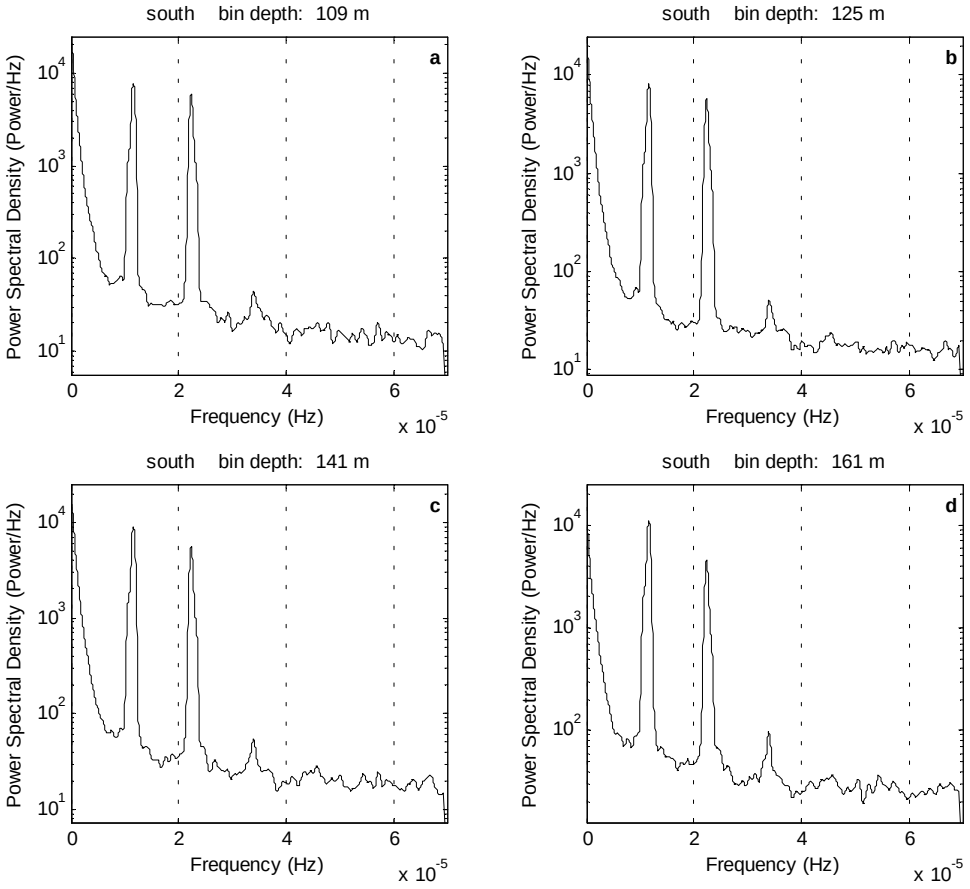

Figure 56 Power spectra for south mooring current at 109, 125, 141, and 161 m

Coherence

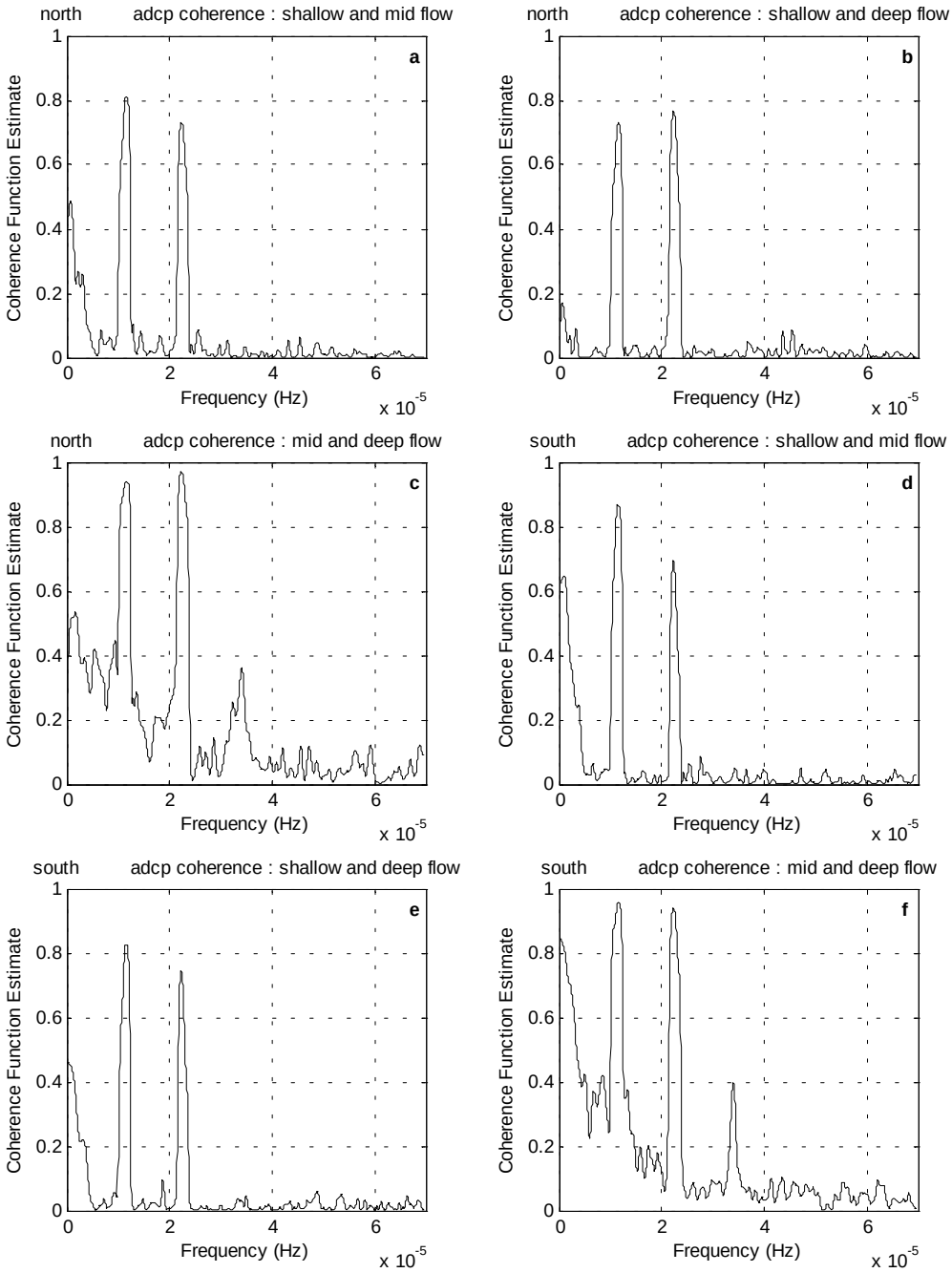

Figure 57 Coherence function for currents: northern shallow and mid-depth (a), shallow and deep (b), mid-depth and deep (c); and southern shallow and mid-depth (d), shallow and deep (e), mid-depth and deep (f)

Appendix 3 CTD (Microcat) Data

3-year record (unfiltered)

North shore

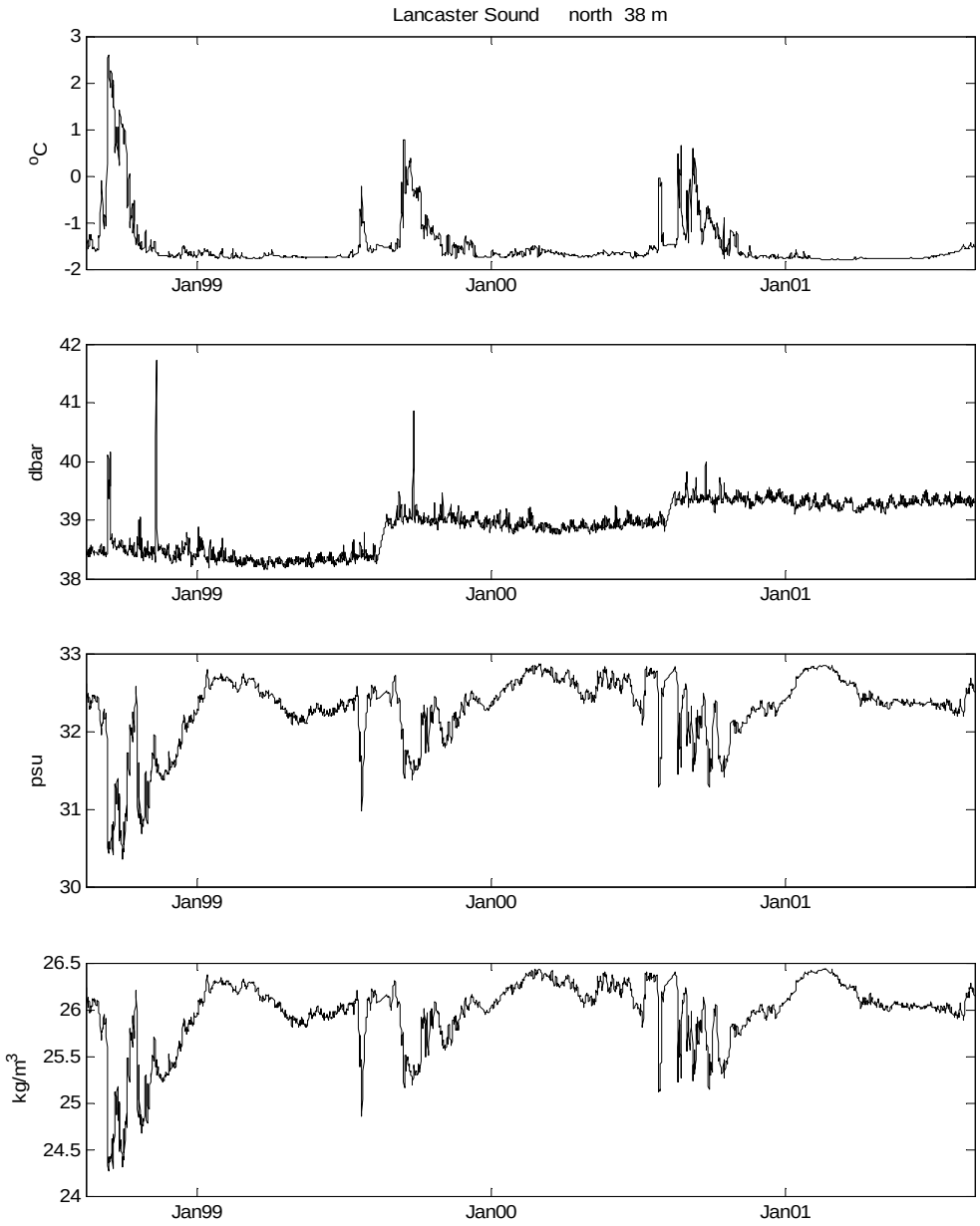

Figure 58 Time series of CTD (T, P, S, ρ) data at 38 m recorded at the northern mooring.

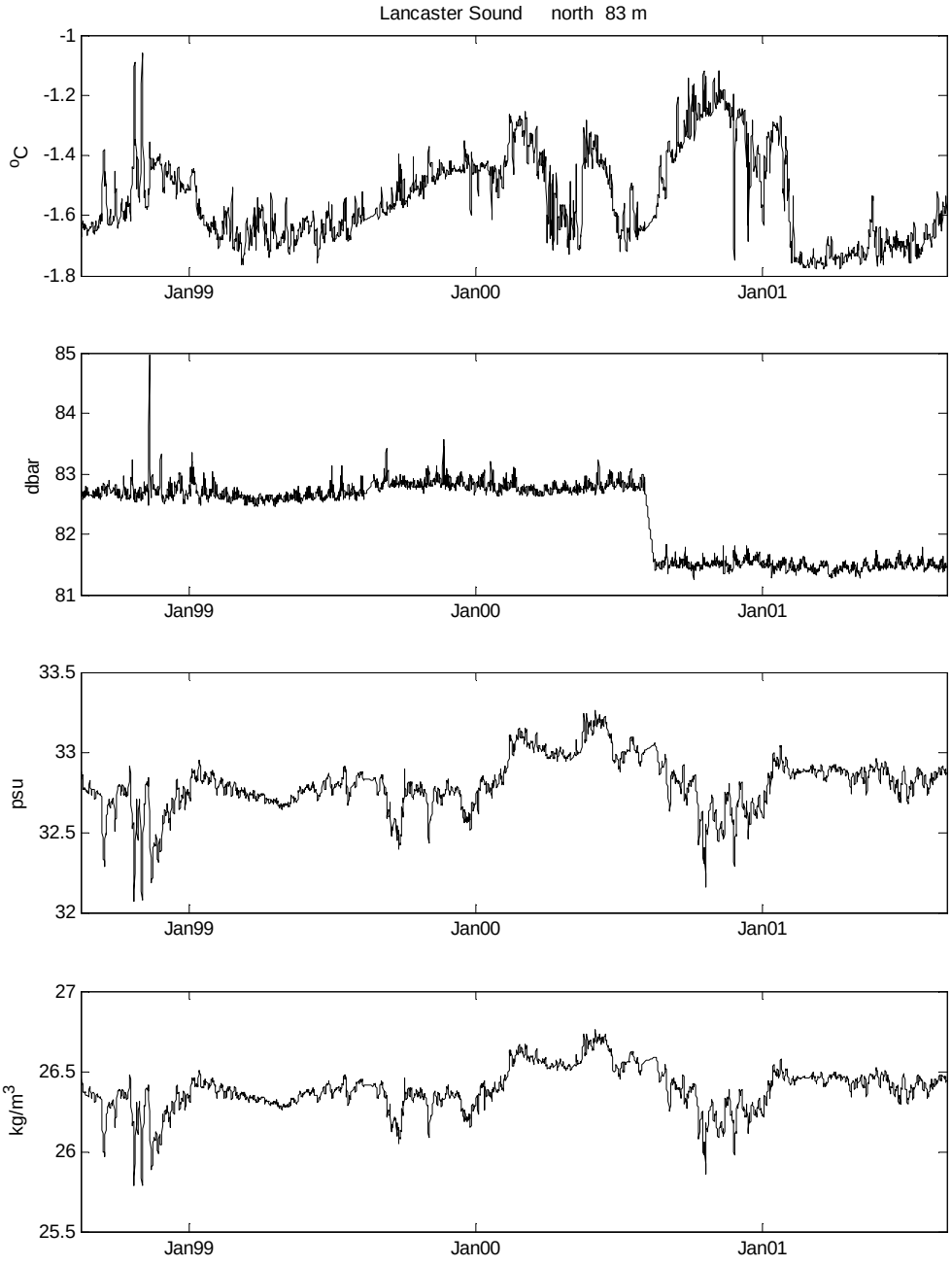

Figure 59 Time series of CTD (T, P, S, ρ) data at 83 m recorded at the northern mooring.

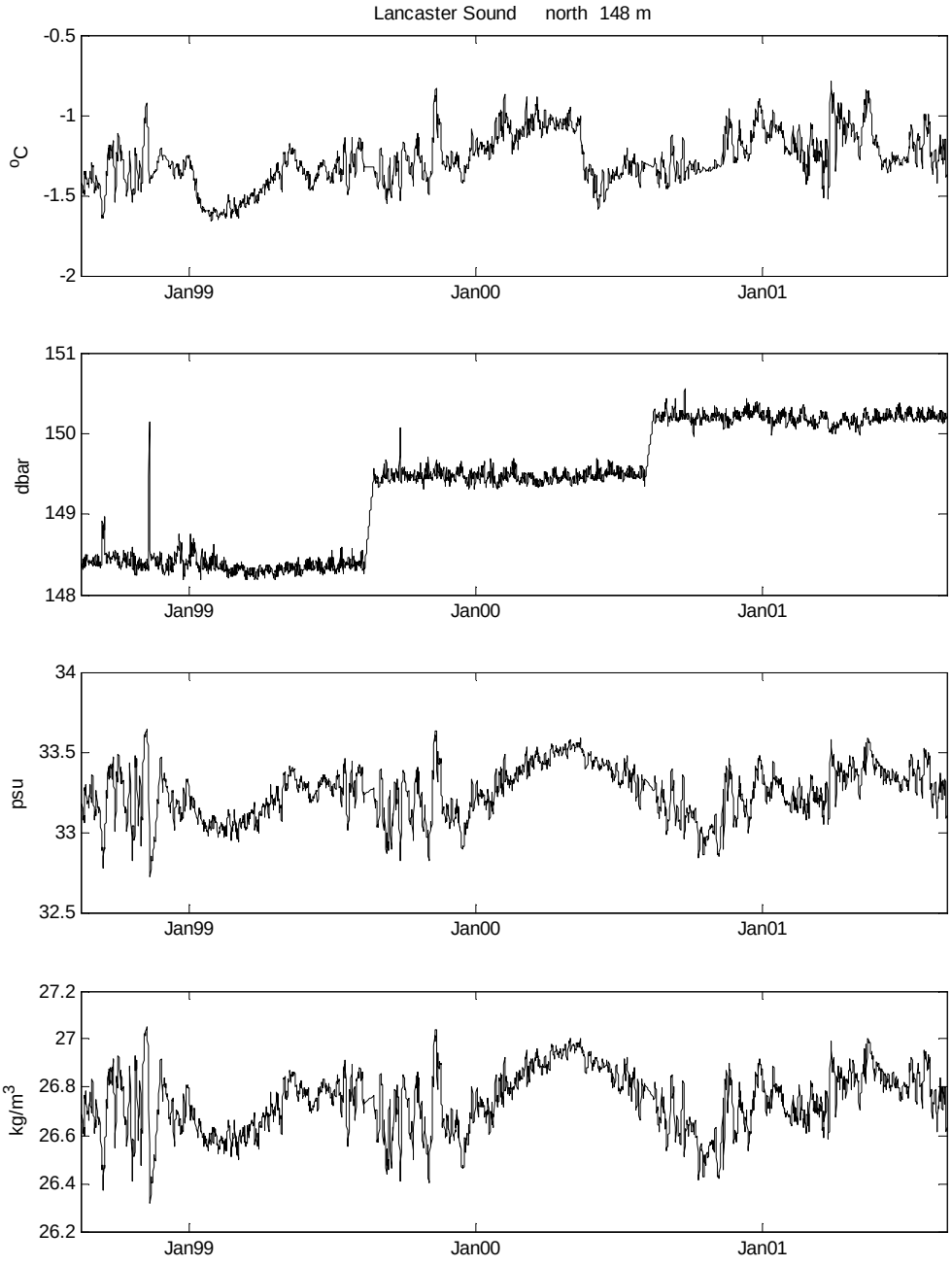

Figure 60 Time series of CTD (T, P, S, ρ) data at 148 m recorded at the northern mooring.

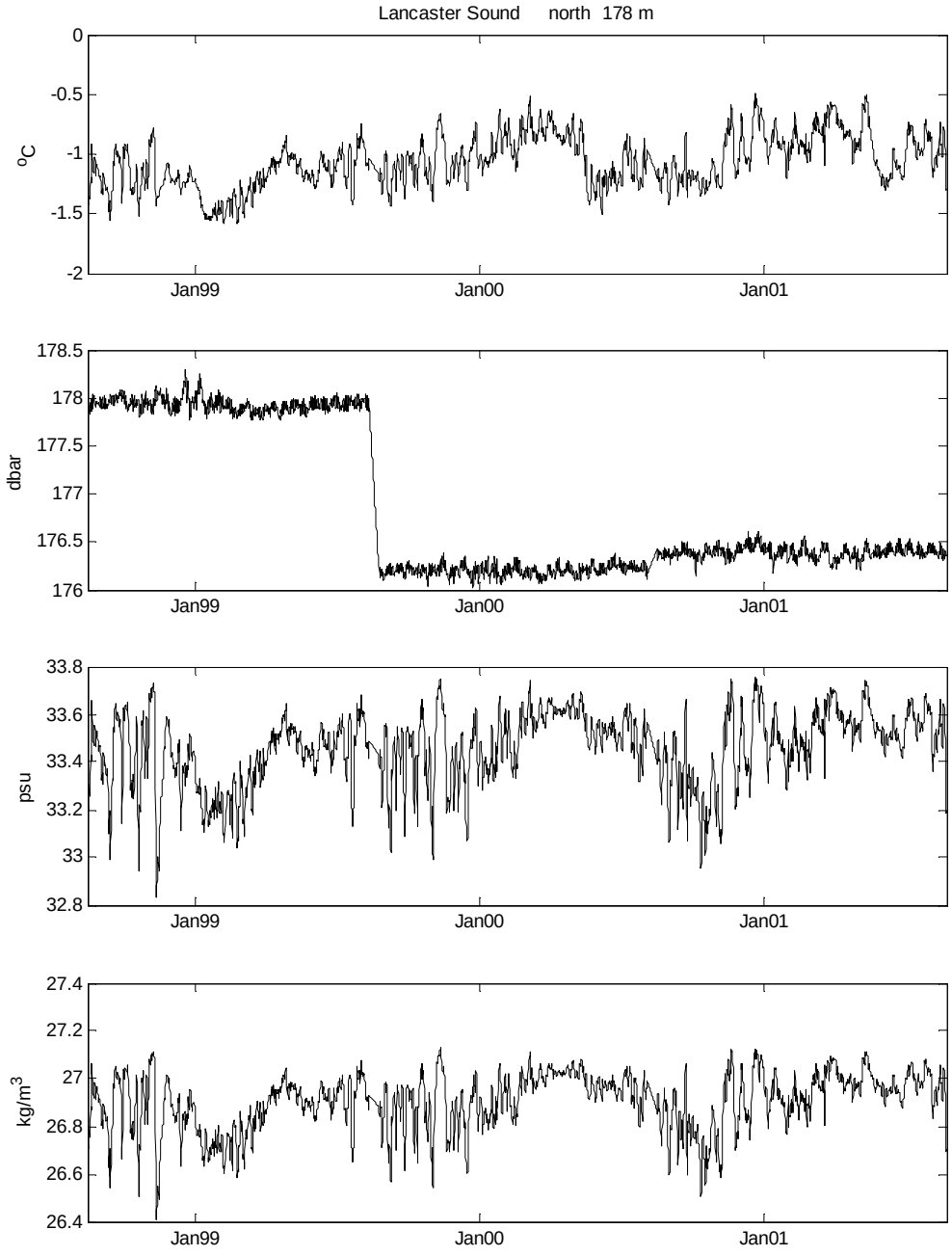

Figure 61 Time series of CTD (T, P, S, ρ) data at 178 m recorded at the northern mooring.

South shore

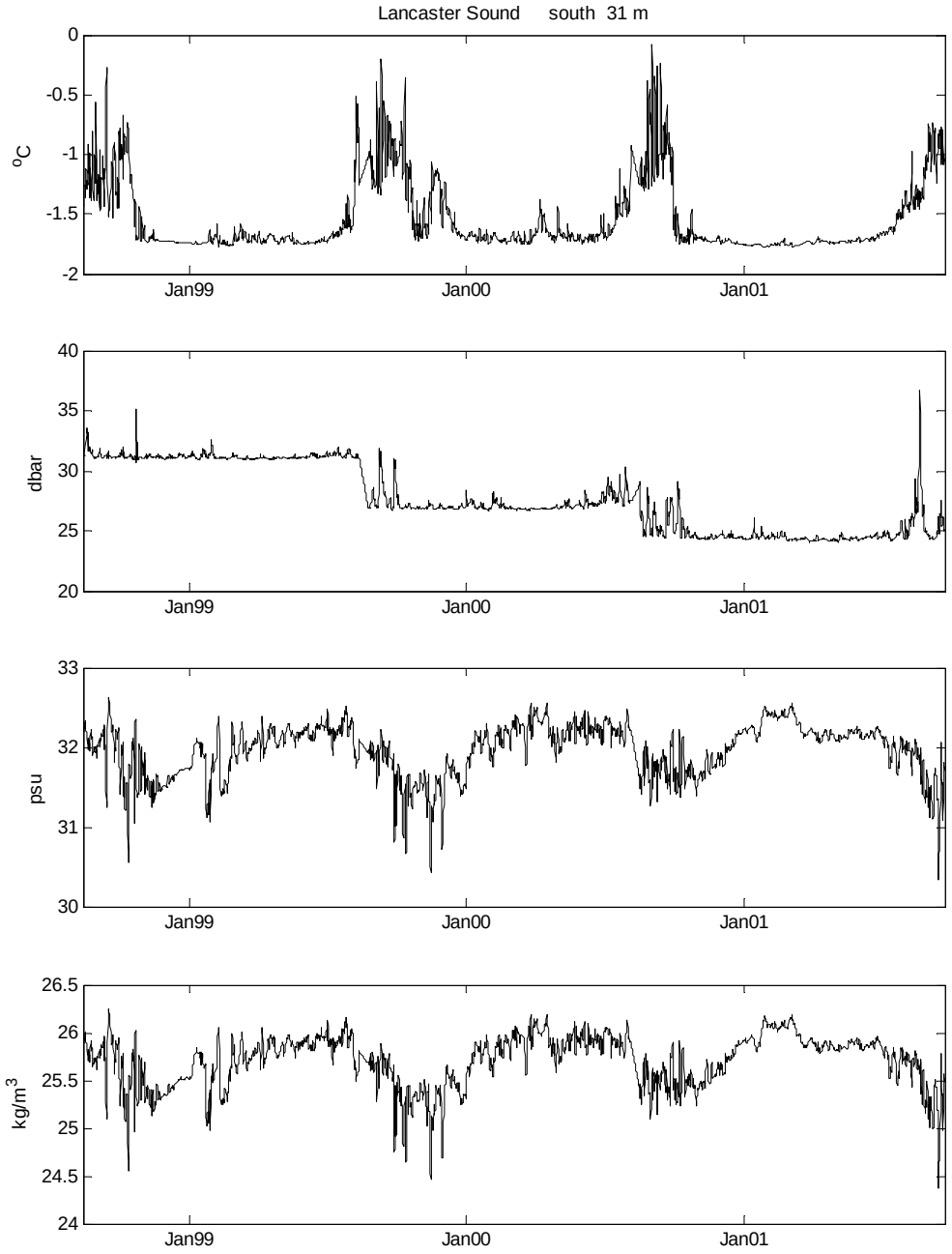

Figure 62 Time series of CTD (T, P, S, ρ) data at 31 m recorded at the southern mooring.

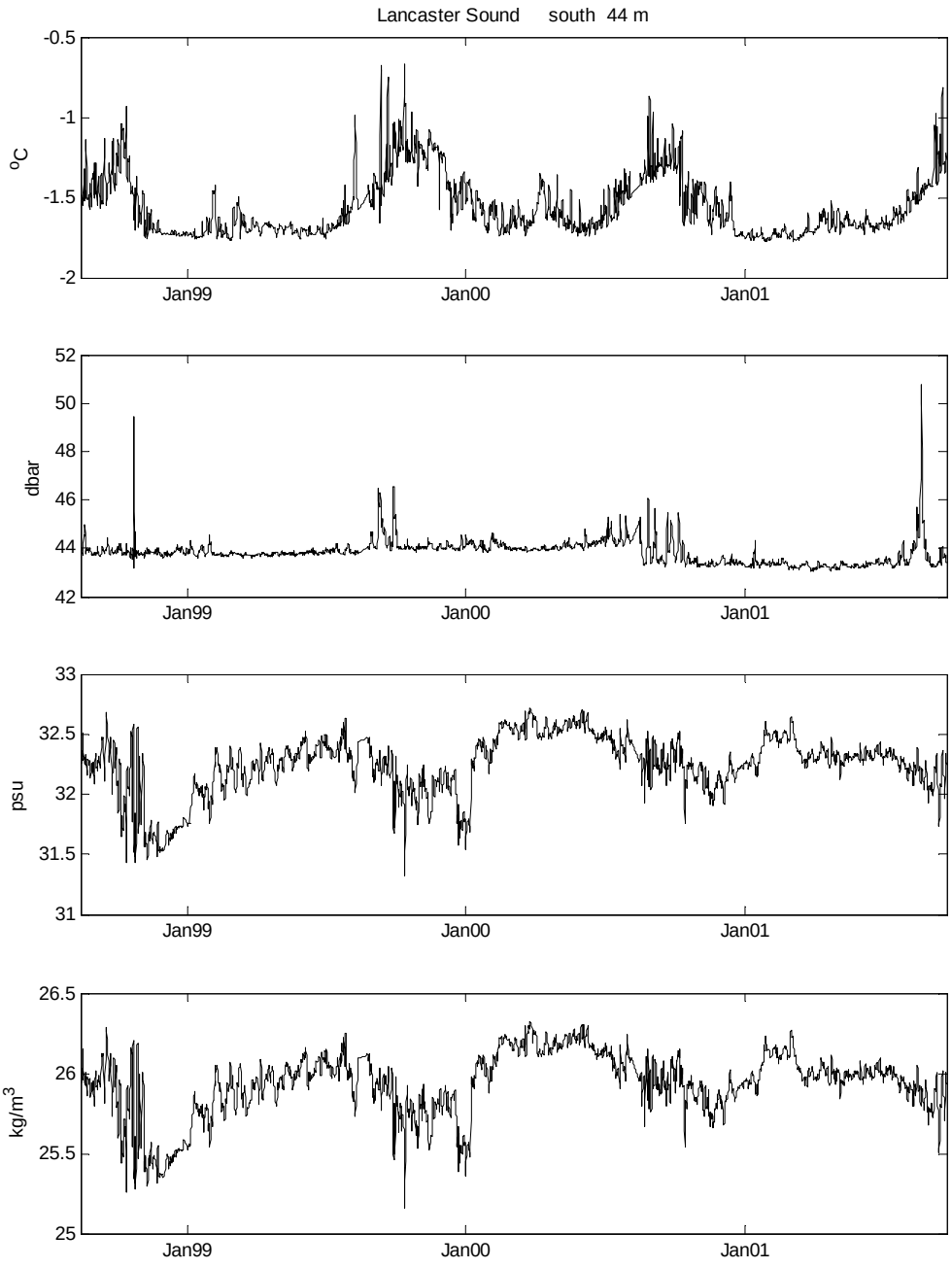

Figure 63 Time series of CTD (T, P, S, ρ) data at 44 m recorded at the southern mooring.

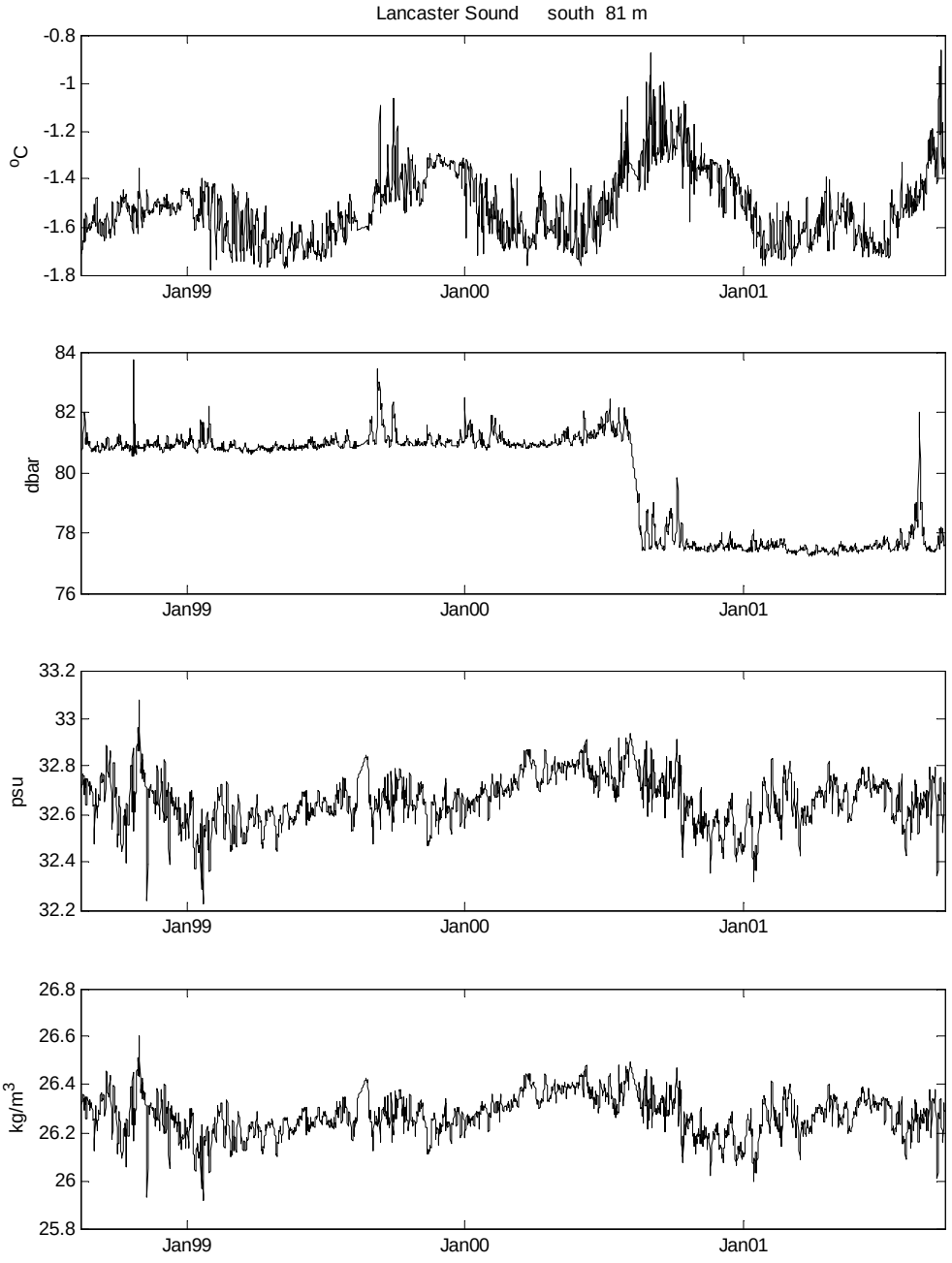

Figure 64 Time series of CTD (T, P, S, ρ) data at 81 m recorded at the southern mooring.

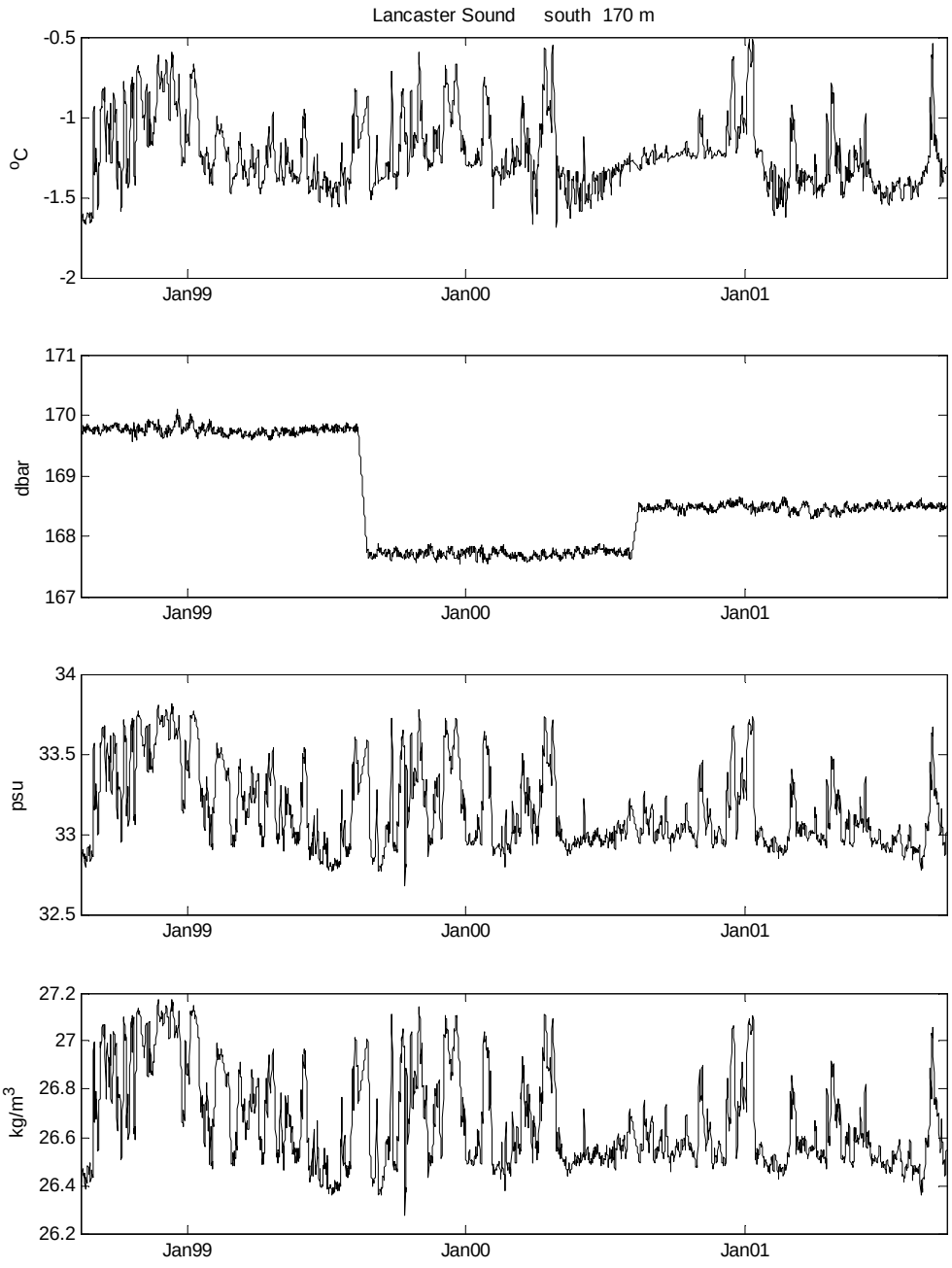

Figure 65 Time series of CTD (T, P, S, ρ) data at 170 m recorded at the southern mooring.

Lowpass-filtered CTD data

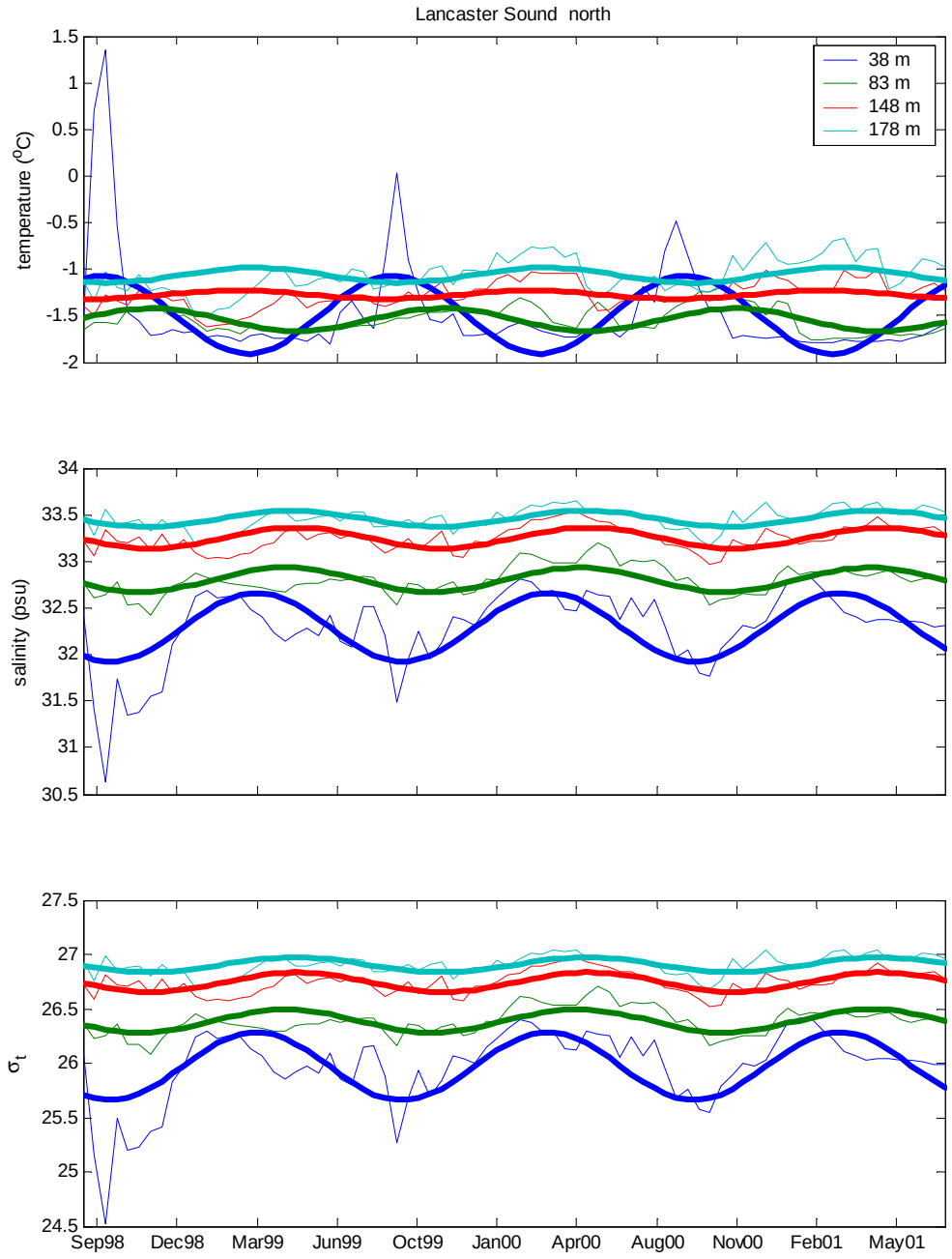

Figure 66 Time series of northern mooring lowpass-filtered CTD data with annual harmonic superimposed.

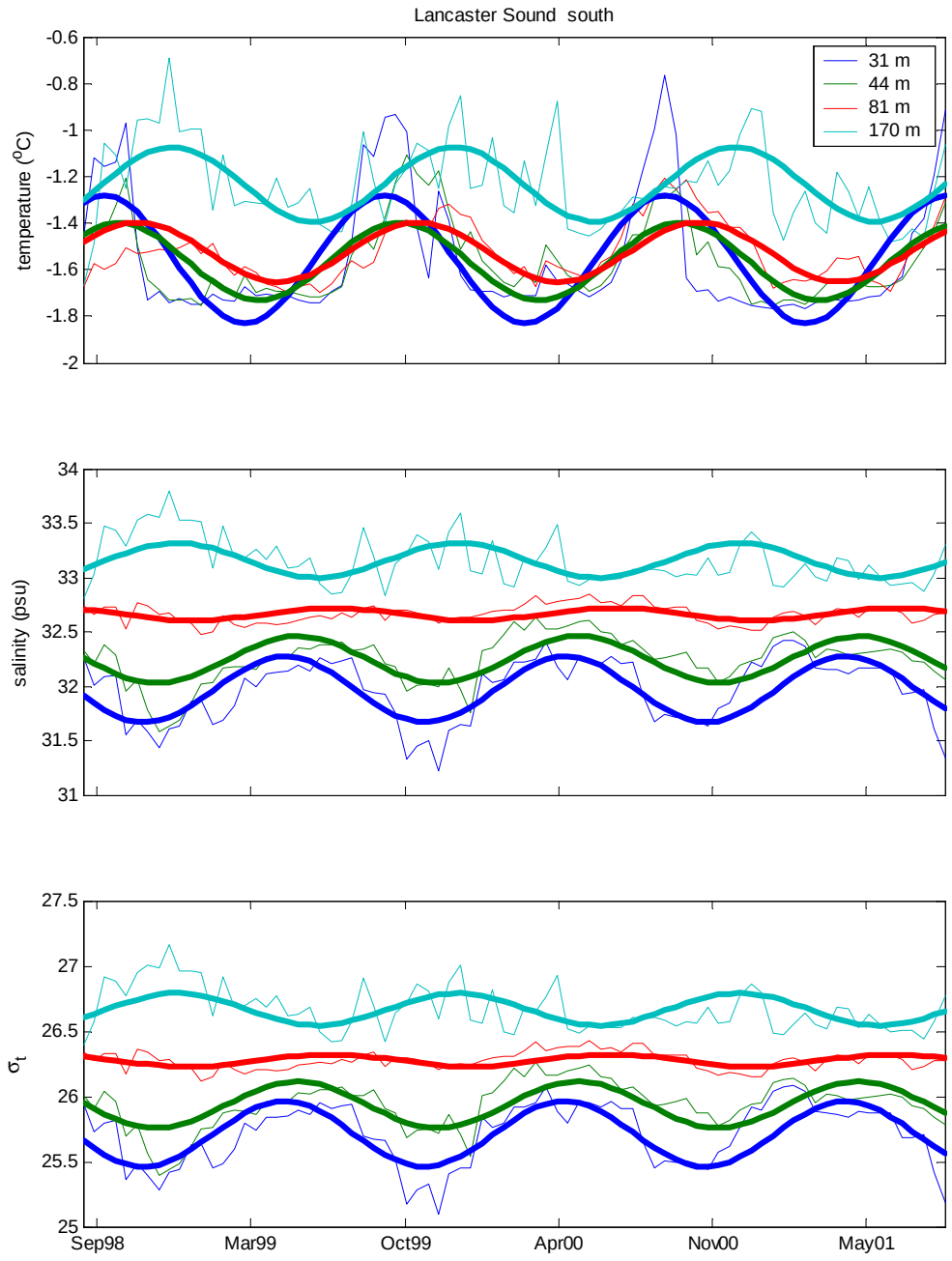

Figure 67 Time series of southern mooring lowpass-filtered CTD data with annual harmonic superimposed.

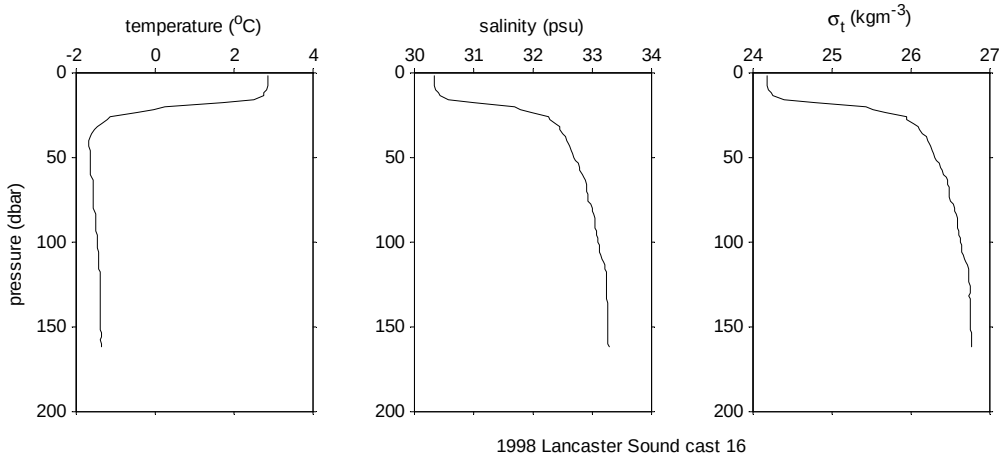

Figure 68 CTD profile from August 1998, north shore

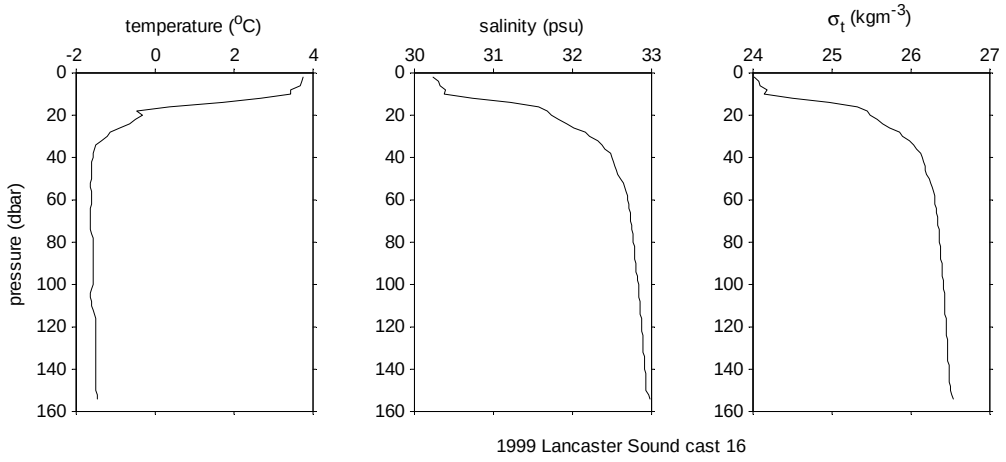

Figure 69 CTD profile from August 1999, north shore

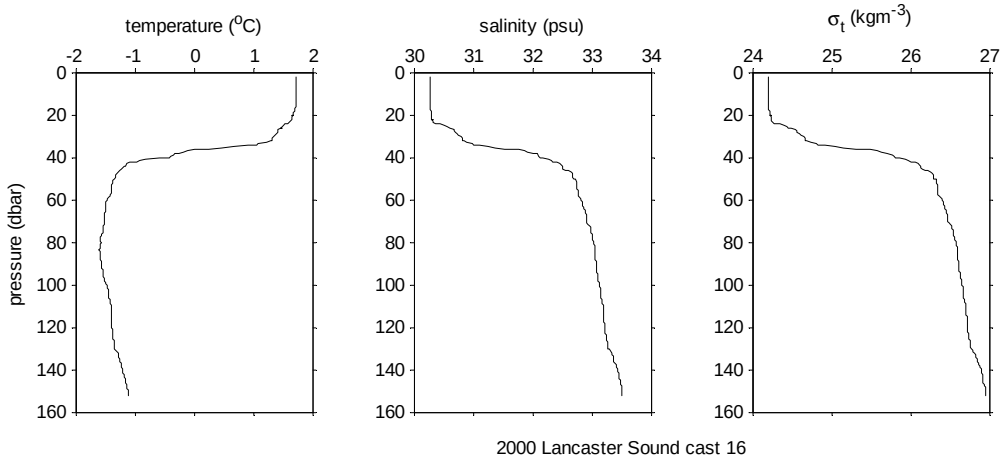

Figure 70 CTD profile from August 2000, north shore

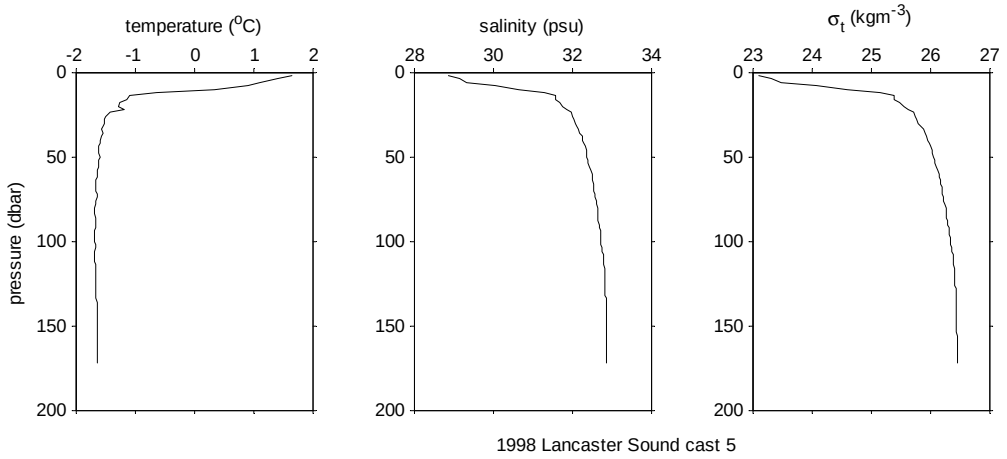

Figure 71 CTD profile from August 1998, south shore

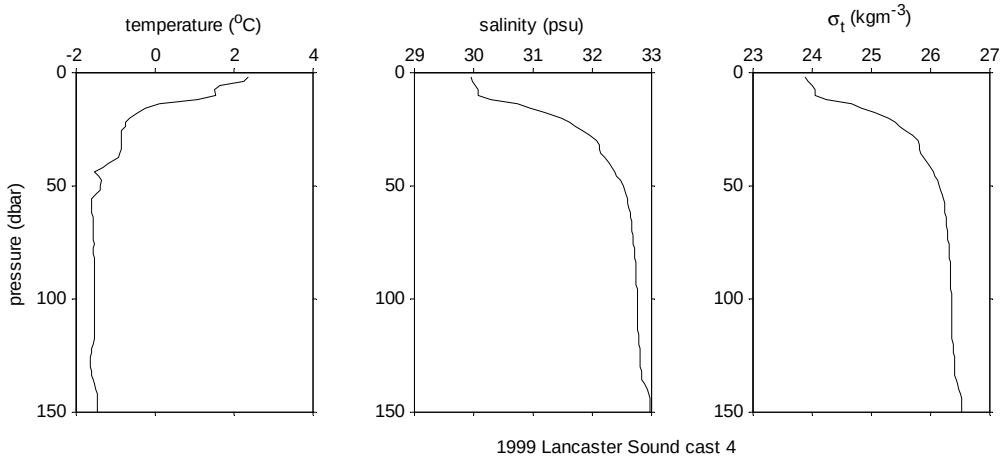

Figure 72 CTD profile from August 1999, south shore

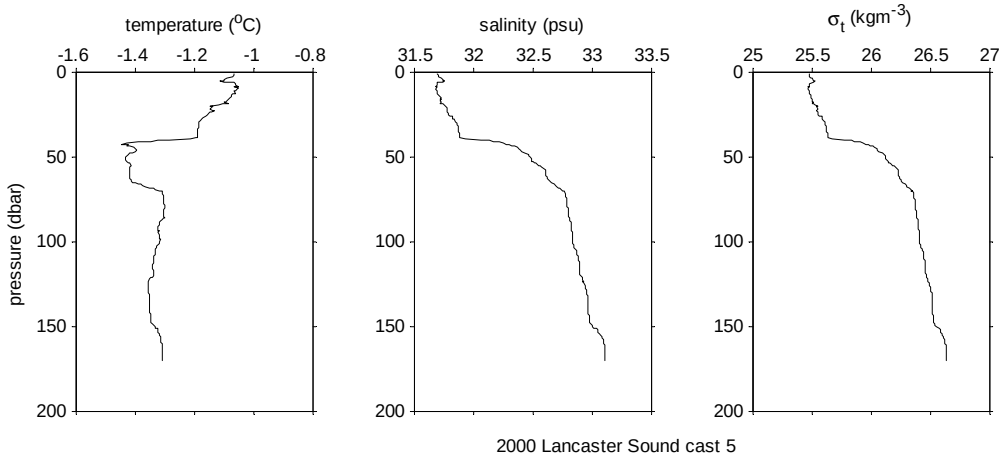

Figure 73 CTD profile from August 2000, south shore

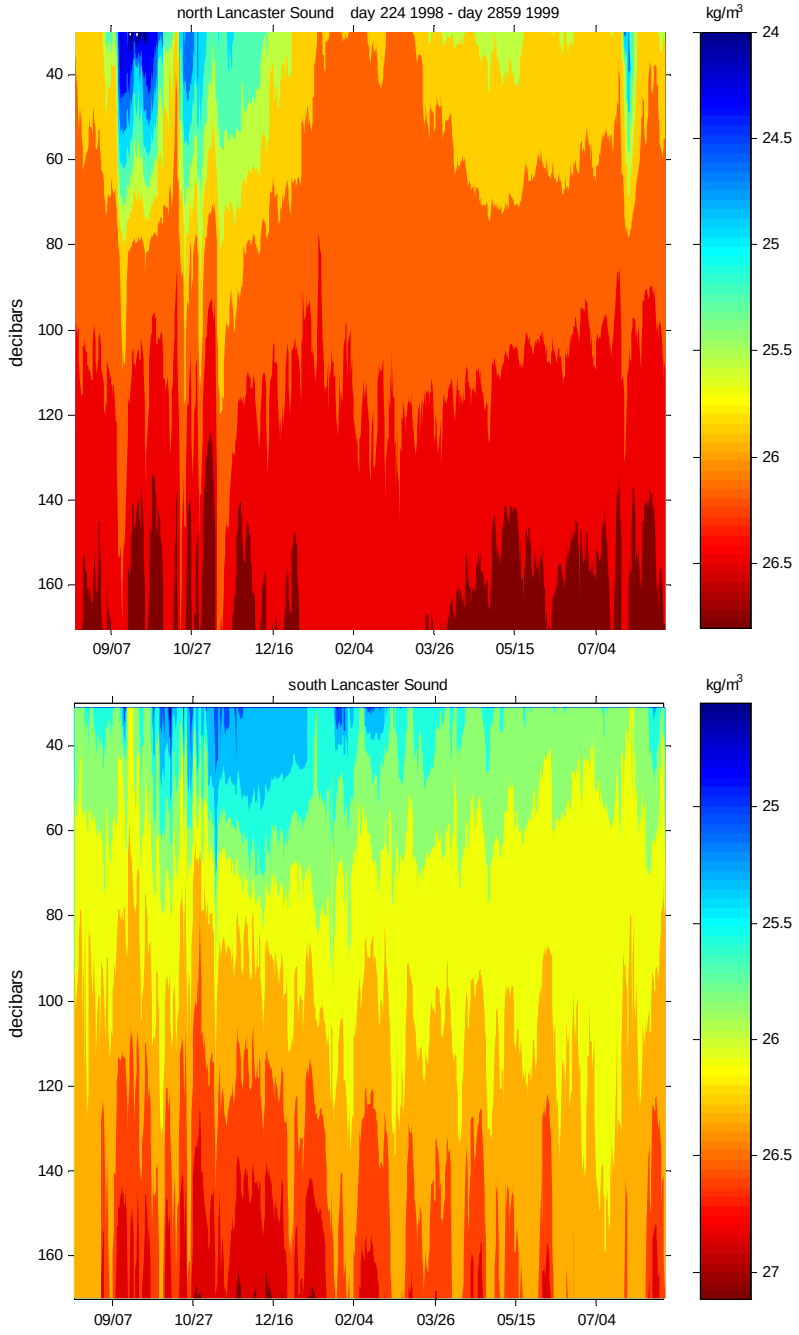

Figure 74 Time series of 1998-1999 density contours.

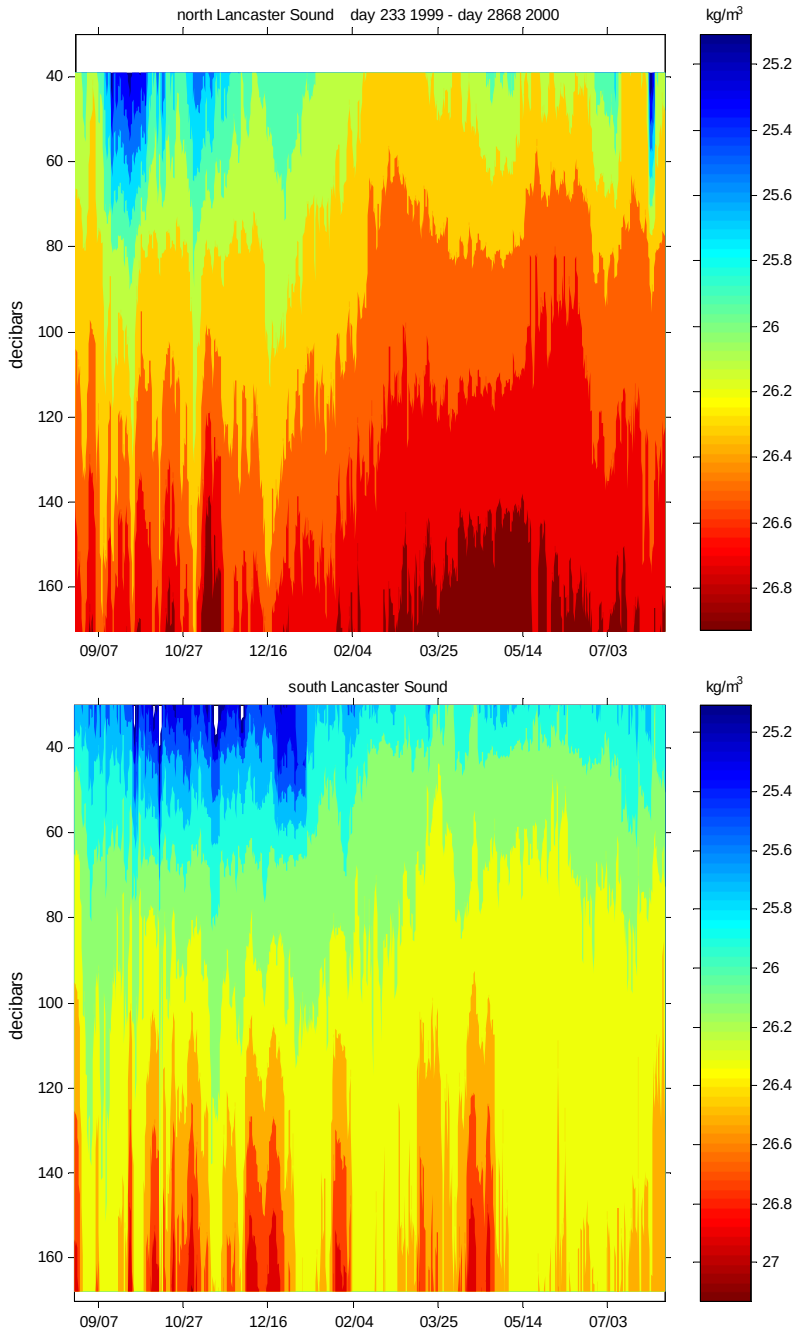

Figure 75 Time series of 1999-2000 density contours.

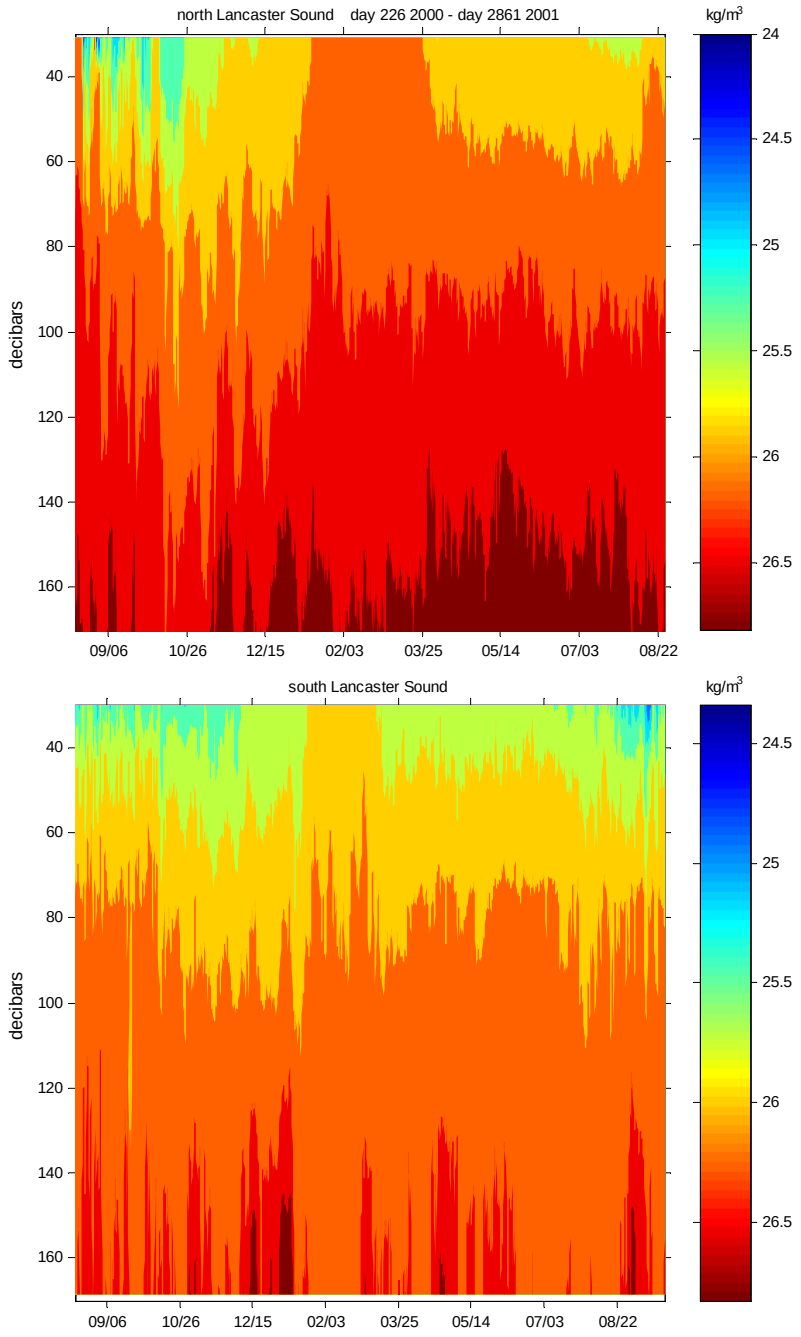

Figure 76 Time series of 2000-2001 density contours.

Appendix 4 Principal Component Analysis

Table 21 Cross-correlation matrix of high frequency ADCP data with tides removed (6-hourly data records).

		38 m	74 m	146 m	29 m	69 m	161 m
north	38 m						
	74 m	0.71					
	146 m	0.26	0.61				
south	29 m	**0.00**	**0.05**	**0.03**			
	69 m	**0.04**	**0.08**	**0.04**	0.93		
	161 m	**0.03**	**0.07**	**0.08**	0.82	0.90	

Table 22 Results of principal component analysis of high frequency (6-hourly with tides removed) ADCP data for comparison of 3 depths (shallow, mid-depth, and deep).

ADCP ALONGSHORE FLOW						
North	Eigenvectors			Eigenvalues		% variance
	Mode 1	Mode 2	Mode 3			
38 m	0.7233	0.5634	0.3993	Mode 1	13618.4952	71.70
74 m	0.6005	-0.2275	-0.7666	Mode 2	4281.9627	22.54
146 m	0.3410	-0.7942	0.5029	Mode 3	1093.8896	5.76
South	Eigenvectors			Eigenvalues		% variance
	Mode 1	Mode 2	Mode 3			
29 m	-0.6449	0.6561	-0.3920	Mode 1	43244.5886	92.53
69 m	-0.6323	-0.1700	0.7559	Mode 2	2641.0153	5.65
161 m	-0.4293	-0.7353	-0.5244	Mode 3	851.2914	1.82

Table 23 Cross-correlation matrix for high frequency (6-hourly with tides removed) moored CTD data with tides removed.

temperature									
north	38 m	83 m	148 m	178 m	south	31 m	44 m	81 m	170 m
38 m					31 m				
83 m	0.11				44 m	0.75			
148 m	-0.18	0.09			81 m	0.45	0.62		
178 m	-0.18	-0.06	0.85		170 m	0.02	0.09	0.24	
salinity									
north	38 m	83 m	148 m	178 m	south	31 m	44 m	81 m	170 m
38 m					31 m				
83 m	0.66				44 m	0.72			
148 m	0.23	0.57			81 m	0.21	0.48		
178 m	0.17	0.39	0.84		170 m	-0.26	-0.39	0.03	
density									
north	38 m	83 m	148 m	178 m	south	31 m	44 m	81 m	170 m
38 m					31 m				
83 m	0.65				44 m	0.73			
148 m	0.23	0.58			81 m	0.23	0.49		
178 m	0.17	0.40	0.84		170 m	-0.26	-0.39	0.02	

Table 24 Results of PCA of high frequency (6-hourly with tides removed) data from moored CTDs; data are from 4 depths (shallow, 2 mid-depths, and deep).

TEMPERATURE							
North	Eigenvectors				Eigenvalues		% variance
	mode 1	mode 2	mode 3	mode 4			
38 m	0.9942	0.1024	0.0319	-0.0070	mode 1	0.3259	78.36
83 m	0.0311	0.0169	-0.9847	0.1704	mode 2	0.0640	15.39
148 m	-0.0611	0.5782	-0.1309	-0.8030	mode 3	0.0217	5.22
178 m	-0.0829	0.8093	0.1101	0.5711	mode 4	0.0043	1.04
South	Eigenvectors				Eigenvalues		% variance
	mode 1	mode 2	mode 3	mode 4			
31 m	-0.8453	0.1424	-0.4611	-0.2294	mode 1	0.1158	61.39
44 m	-0.4683	-0.0311	0.4801	0.7411	mode 2	0.0488	25.87
81 m	-0.2493	-0.1739	0.7159	-0.6286	mode 3	0.0167	8.84
170 m	-0.0641	-0.9739	-0.2106	0.0551	mode 4	0.0074	3.90
SALINITY							
North	Eigenvectors				Eigenvalues		% variance
	mode 1	mode 2	mode 3	mode 4			
38 m	-0.9510	0.2290	-0.1987	-0.0607	mode 1	0.2014	77.11
83 m	-0.2714	-0.2992	0.8540	0.3278	mode 2	0.0461	17.63
148 m	-0.1180	-0.6805	0.0017	-0.7232	mode 3	0.0108	4.12
178 m	-0.0895	-0.6285	-0.4808	0.6049	mode 4	0.0030	1.14
South	Eigenvectors				Eigenvalues		% variance
	mode 1	mode 2	mode 3	mode 4			
31 m	-0.7792	0.3658	-0.4861	-0.1506	mode 1	0.1582	65.19
44 m	-0.5358	0.0027	0.7289	0.4262	mode 2	0.0559	23.03
81 m	-0.0802	0.0729	0.4570	-0.8828	mode 3	0.0225	9.28
170 m	0.3151	0.9278	0.1536	0.1275	mode 4	0.0061	2.50
DENSITY							
North	Eigenvectors				Eigenvalues		% variance
	mode 1	mode 2	mode 3	mode 4			
38 m	-0.9572	0.2171	-0.1848	-0.0503	mode 1	0.1422	79.05
83 m	-0.2578	-0.3411	0.8536	0.2976	mode 2	0.0289	16.05
148 m	-0.1066	-0.6823	-0.0533	-0.7213	mode 3	0.0070	3.88
178 m	-0.0774	-0.6091	-0.4841	0.6234	mode 4	0.0018	1.01
South	Eigenvectors				Eigenvalues		% variance
	mode 1	mode 2	mode 3	mode 4			
31 m	-0.7882	0.3520	-0.4834	-0.1456	mode 1	0.1055	66.28
44 m	-0.5368	-0.0262	0.7282	0.4254	mode 2	0.0350	21.97
81 m	-0.0848	0.0710	0.4560	-0.8831	mode 3	0.0147	9.26
170 m	0.2888	0.9329	0.1681	0.1341	mode 4	0.0040	2.50

Table 25 Results of PCA of low frequency (14-day) data from moored CTDs; data are from 4 depths (shallow, 2 mid-depths, and deep).

TEMPERATURE							
North	Eigenvectors				Eigenvalues		%
	Mode 1	Mode 2	Mode 3	Mode 4			variance
38 m	-0.9931	0.1109	-0.0378	-0.0023	Mode 1	0.2863	79.92
83 m	-0.0333	0.0414	0.9843	0.1685	Mode 2	0.0501	13.99
148 m	0.0644	0.5984	0.1124	-0.7907	Mode 3	0.0197	5.49
178 m	0.0922	0.7924	-0.1309	0.5886	Mode 4	0.0022	0.60
South	Eigenvectors				Eigenvalues		%
	Mode 1	Mode 2	Mode 3	Mode 4			variance
31 m	-0.8379	0.1803	-0.4552	0.2414	Mode 1	0.0997	66.28
44 m	-0.4776	-0.0565	0.4612	-0.7457	Mode 2	0.0357	23.71
81 m	-0.2576	-0.2636	0.6964	0.6157	Mode 3	0.0108	7.20
170 m	-0.0594	-0.9459	-0.3084	-0.0810	Mode 4	0.0042	2.81
SALINITY							
North	Eigenvectors				Eigenvalues		%
	Mode 1	Mode 2	Mode 3	Mode 4			variance
38 m	-0.9501	-0.2344	0.1941	0.0689	Mode 1	0.1734	81.43
83 m	-0.2828	0.3683	-0.8257	-0.3202	Mode 2	0.0306	14.38
148 m	-0.1057	0.6965	0.0731	0.7060	Mode 3	0.0077	3.62
178 m	-0.0789	0.5695	0.5245	-0.6280	Mode 4	0.0012	0.57
South	Eigenvectors				Eigenvalues		%
	Mode 1	Mode 2	Mode 3	Mode 4			variance
31 m	-0.7318	-0.4818	-0.4465	0.1817	Mode 1	0.1366	72.77
44 m	-0.5529	0.0206	0.7006	-0.4506	Mode 2	0.0334	17.80
81 m	-0.0790	-0.0120	0.4946	0.8654	Mode 3	0.0137	7.30
170 m	0.3906	-0.8760	0.2552	-0.1224	Mode 4	0.0040	2.13
DENSITY							
North	Eigenvectors				Eigenvalues		%
	Mode 1	Mode 2	Mode 3	Mode 4			variance
38 m	-0.9558	-0.2264	0.1783	0.0578	Mode 1	0.1224	83.03
83 m	-0.2690	0.4173	-0.8178	-0.2912	Mode 2	0.0194	13.13
148 m	-0.0964	0.6923	0.1348	0.7023	Mode 3	0.0049	3.33
178 m	-0.0689	0.5435	0.5304	-0.6470	Mode 4	0.0007	0.51
South	Eigenvectors				Eigenvalues		%
	Mode 1	Mode 2	Mode 3	Mode 4			variance
31 m	-0.7425	0.4719	-0.4420	0.1751	Mode 1	0.0907	73.45
44 m	-0.5552	-0.0535	0.6973	-0.4503	Mode 2	0.0213	17.23
81 m	-0.0835	0.0094	0.4933	0.8658	Mode 3	0.0089	7.20
170 m	0.3653	0.8800	0.2741	-0.1305	Mode 4	0.0026	2.13

Data presented in the next section are high frequency (6-hourly with tides removed) data and low frequency data (14-day low-pass filtered) records of analysis results not already presented in the main text. The time series plots on the next few pages present not only the time series of the original data but also the analysis results of the modal behaviour as a plot of the individual mode variance at each observation point in time (z-scores). These plots show the data in the coordinate system defined by the linear combination of the eigenvectors.

The first plots of high frequency data (6-hourly data with tides removed) show that the first mode captures the low frequency behaviour exhibited by the original series as well as some of the higher frequency extremes. These plots also give the percentage of explained variance by each mode.

Analysis results of the low frequency (14-day) CTD data at 4 depths are shown with a constructed "synthetic" time series using the first two significant modes and the residual found by subtracting the synthetic series from the original data. Since the data were not normalized but were centred, the synthetic series was constructed by adding the mean of the original series to the product of the modal series ("z-scores") and the eigenvectors.

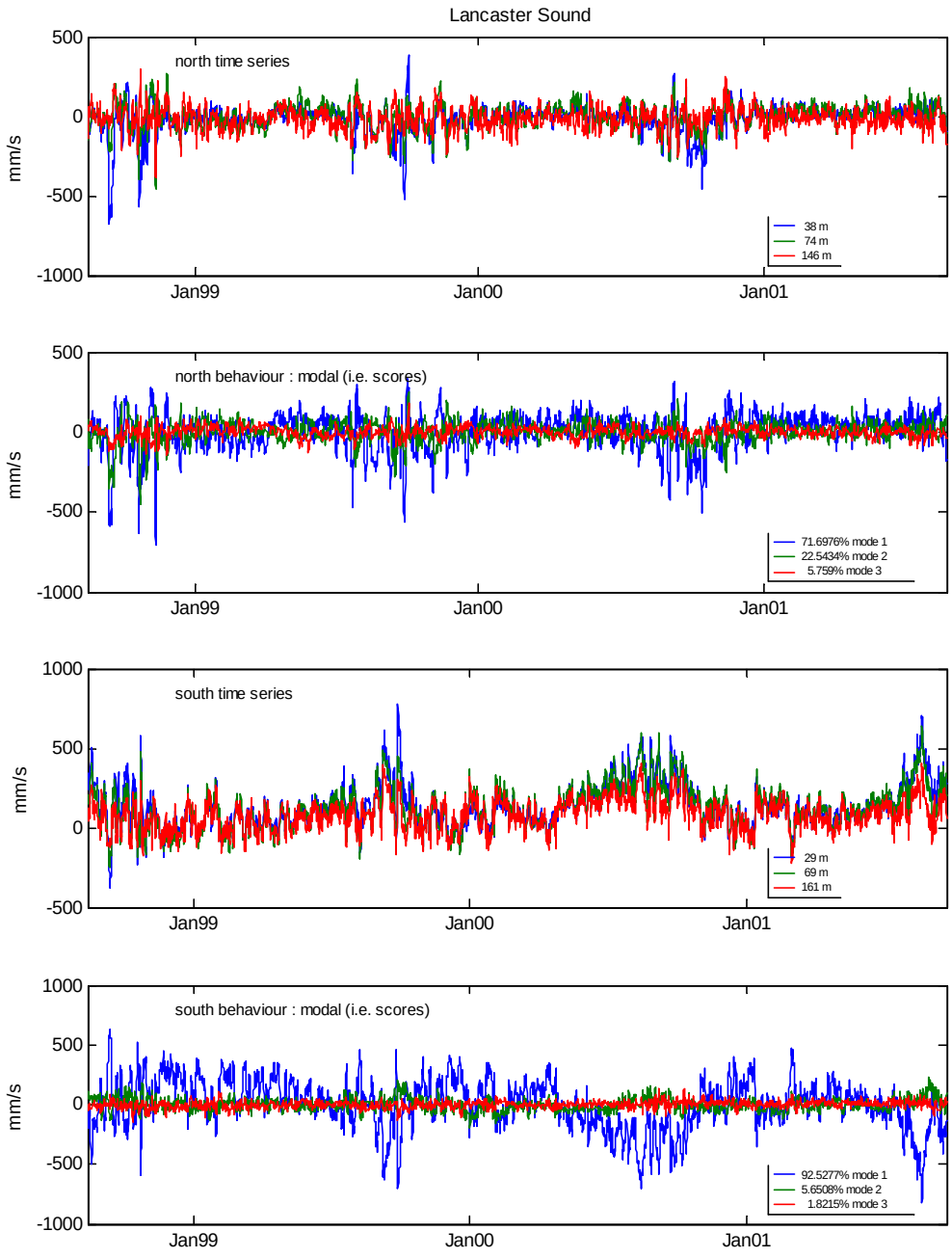

Figure 77 Time series of PCA results for high frequency (6-hourly) alongshore-current data at 3 depths with tides removed.

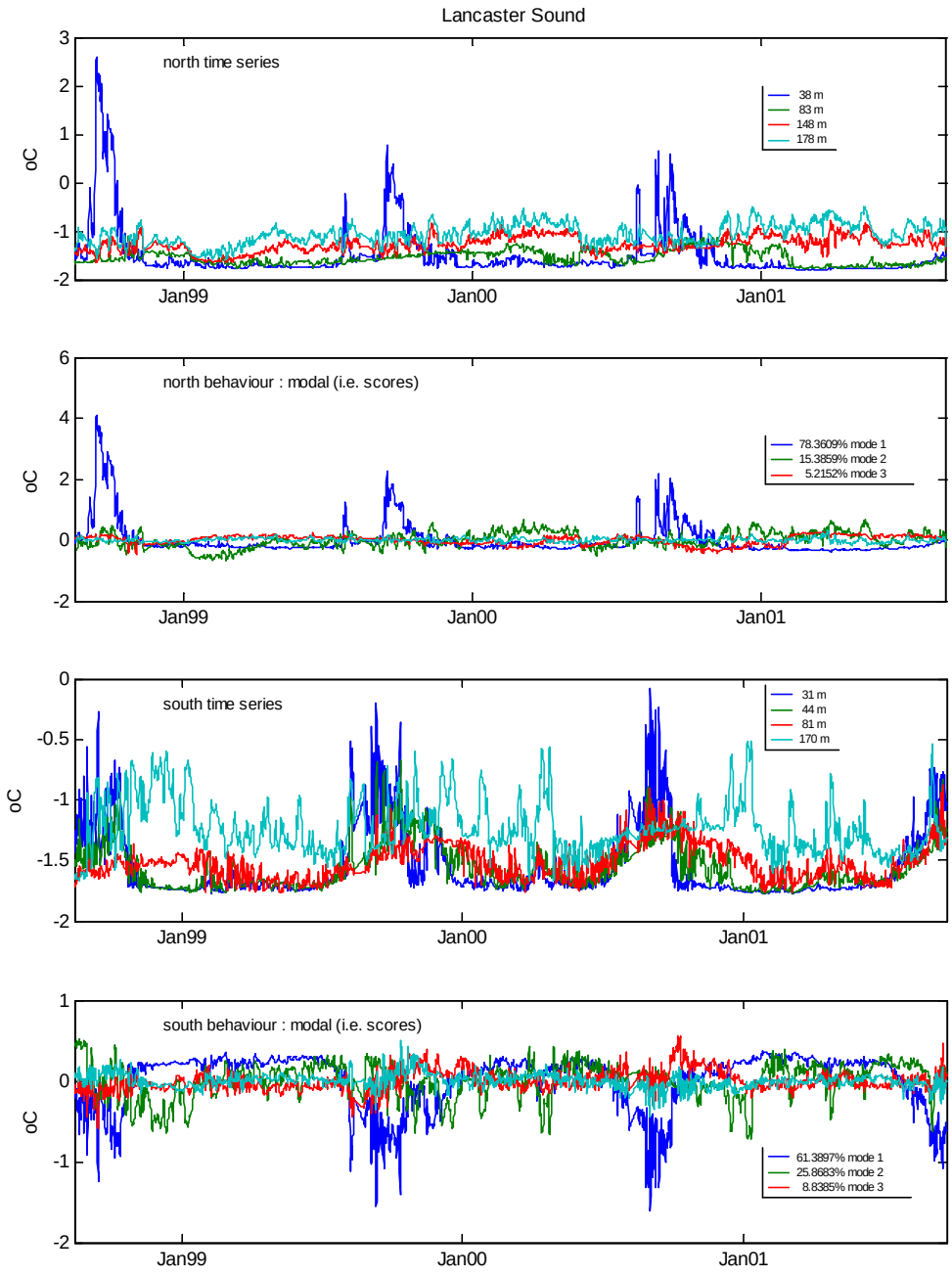

Figure 78 Time series of PCA results for high frequency (6-hourly) temperature data at 4 depths with tides removed.

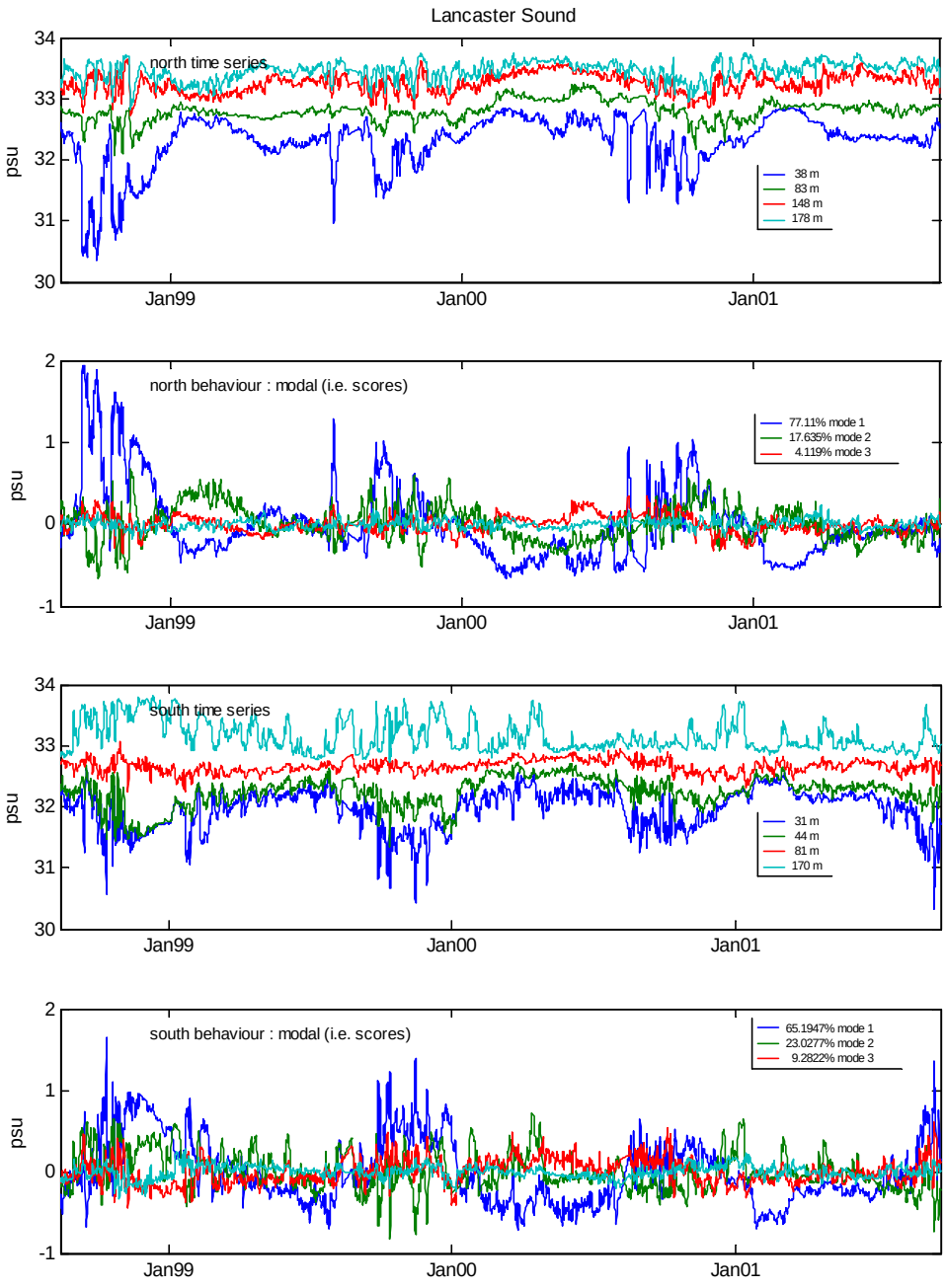

Figure 79 Time series of PCA results for high frequency (6-hourly) salinity data at 4 depths with tides removed.

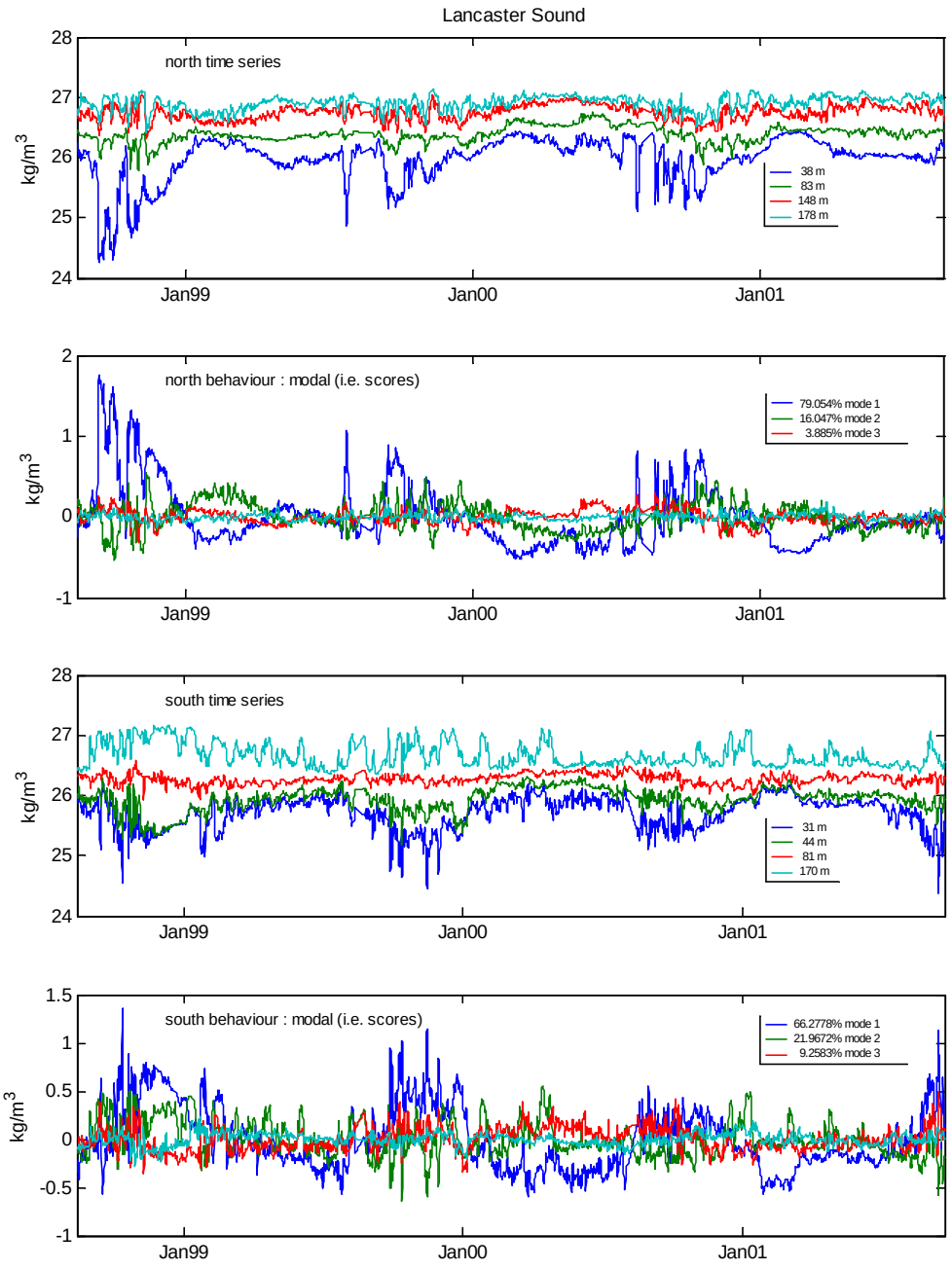

Figure 80 Time series of PCA results for high frequency (6-hourly) density data at 4 depths with tides removed.

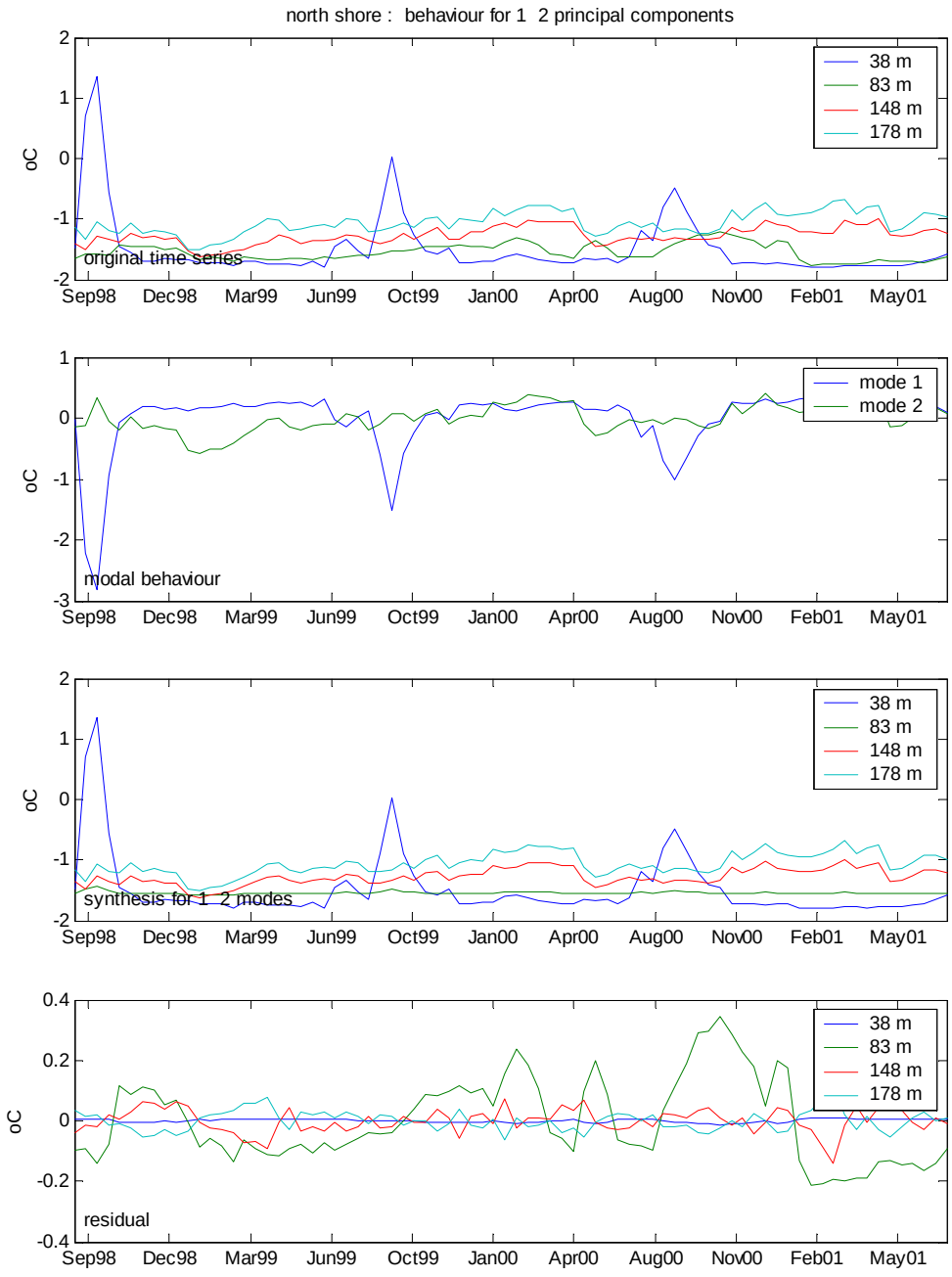

Figure 81 Time series of PCA results for low frequency (14-day) temperature data at northern mooring at 4 depths.

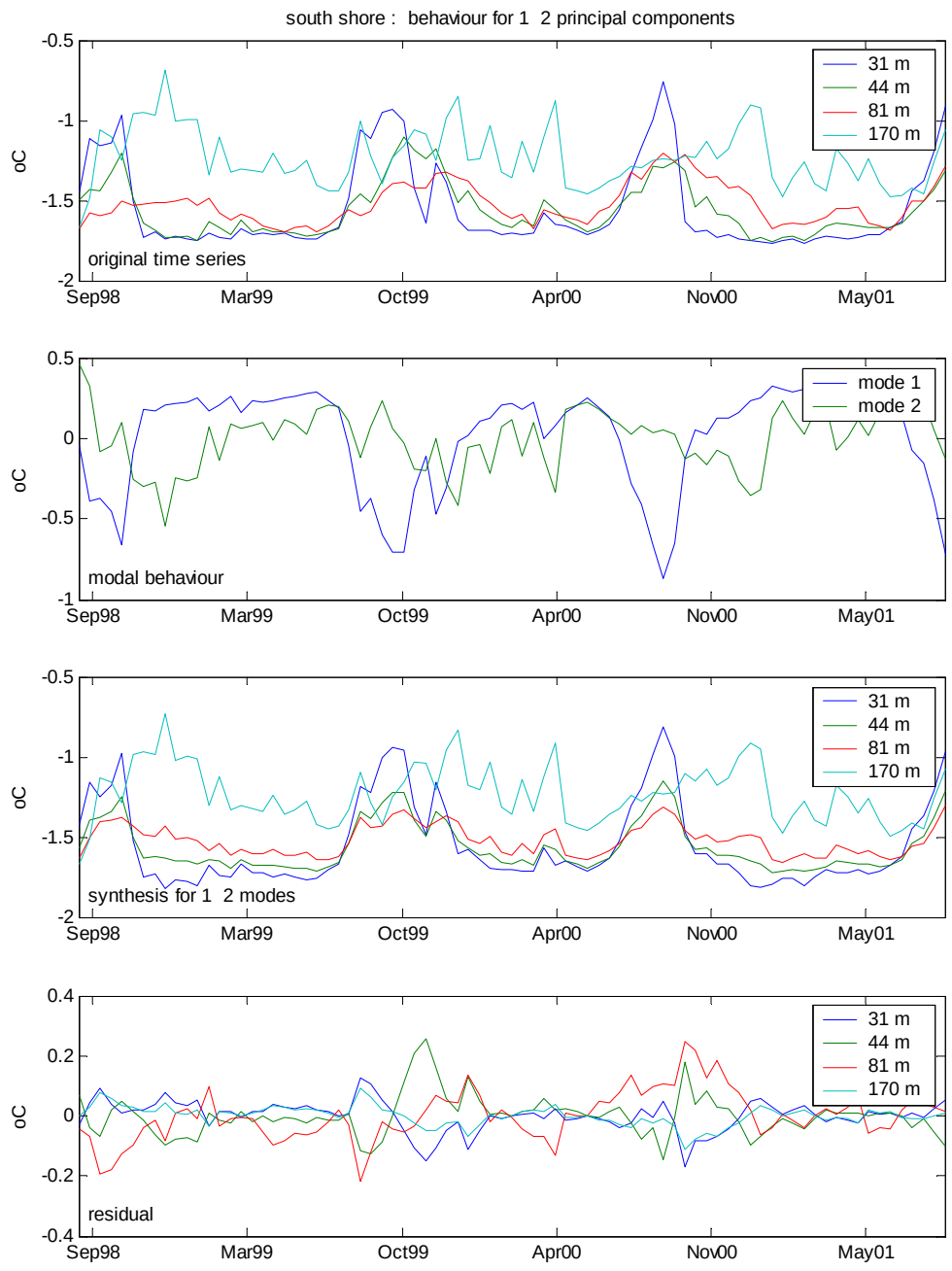

Figure 82 Time series of PCA results for low frequency (14-day) temperature data at southern mooring at 4 depths.

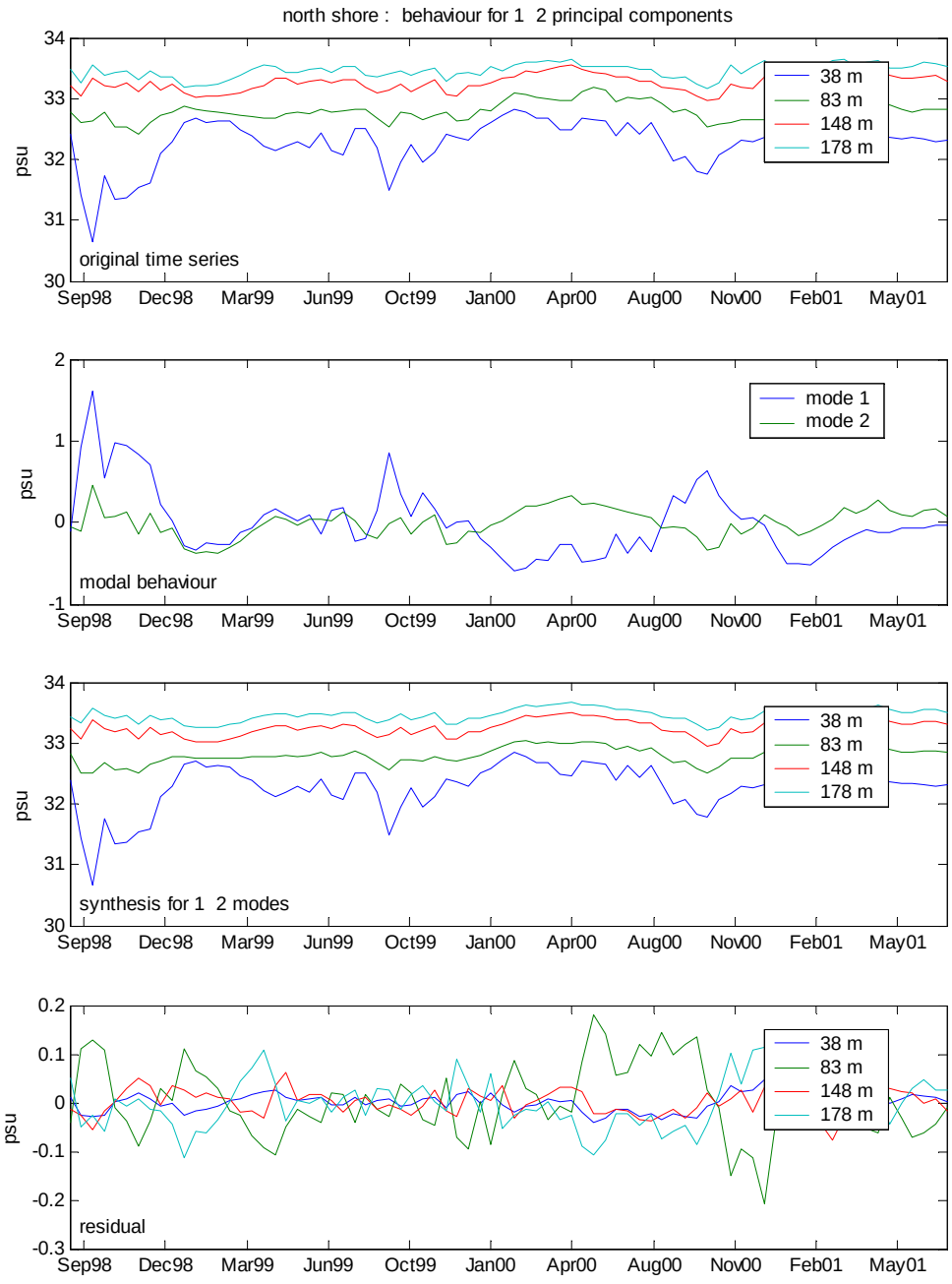

Figure 83 Time series of PCA results for low frequency (14-day) salinity data at northern mooring at 4 depths.

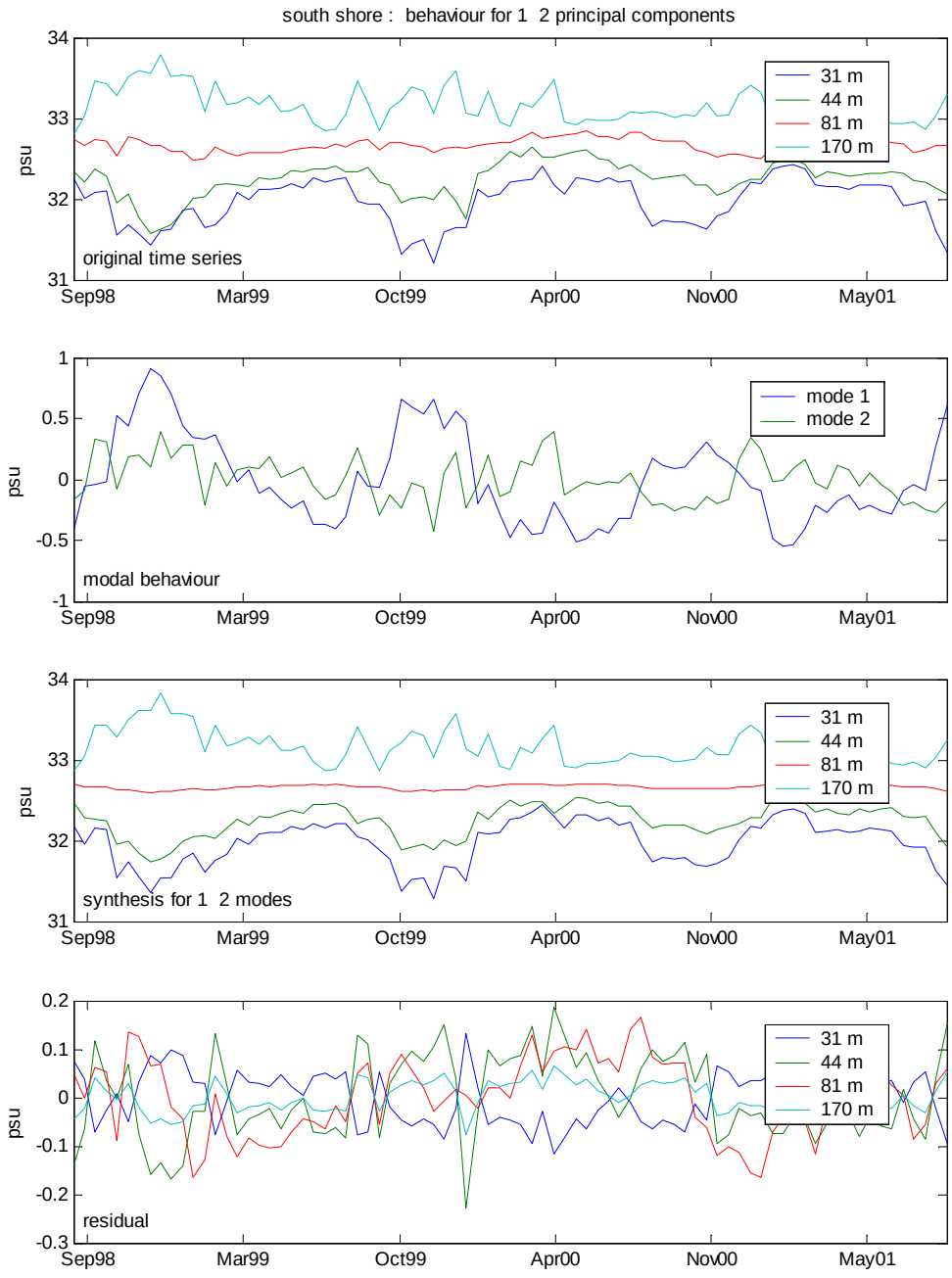

Figure 84 Time series of PCA results for low frequency (14-day) salinity data at southern mooring at 4 depths.

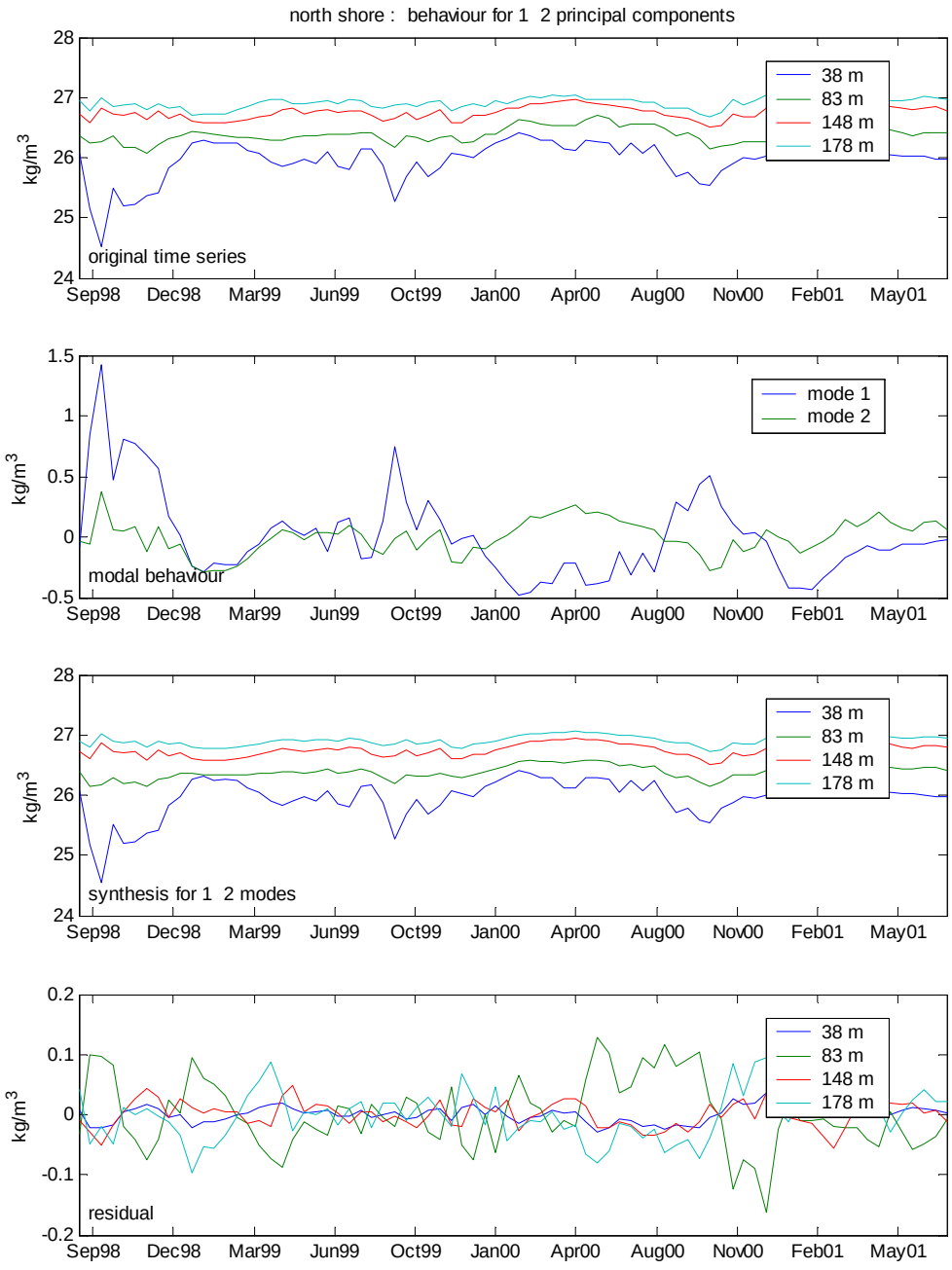

Figure 85 Time series of PCA results for low frequency (14-day) density data at northern mooring at 4 depths.

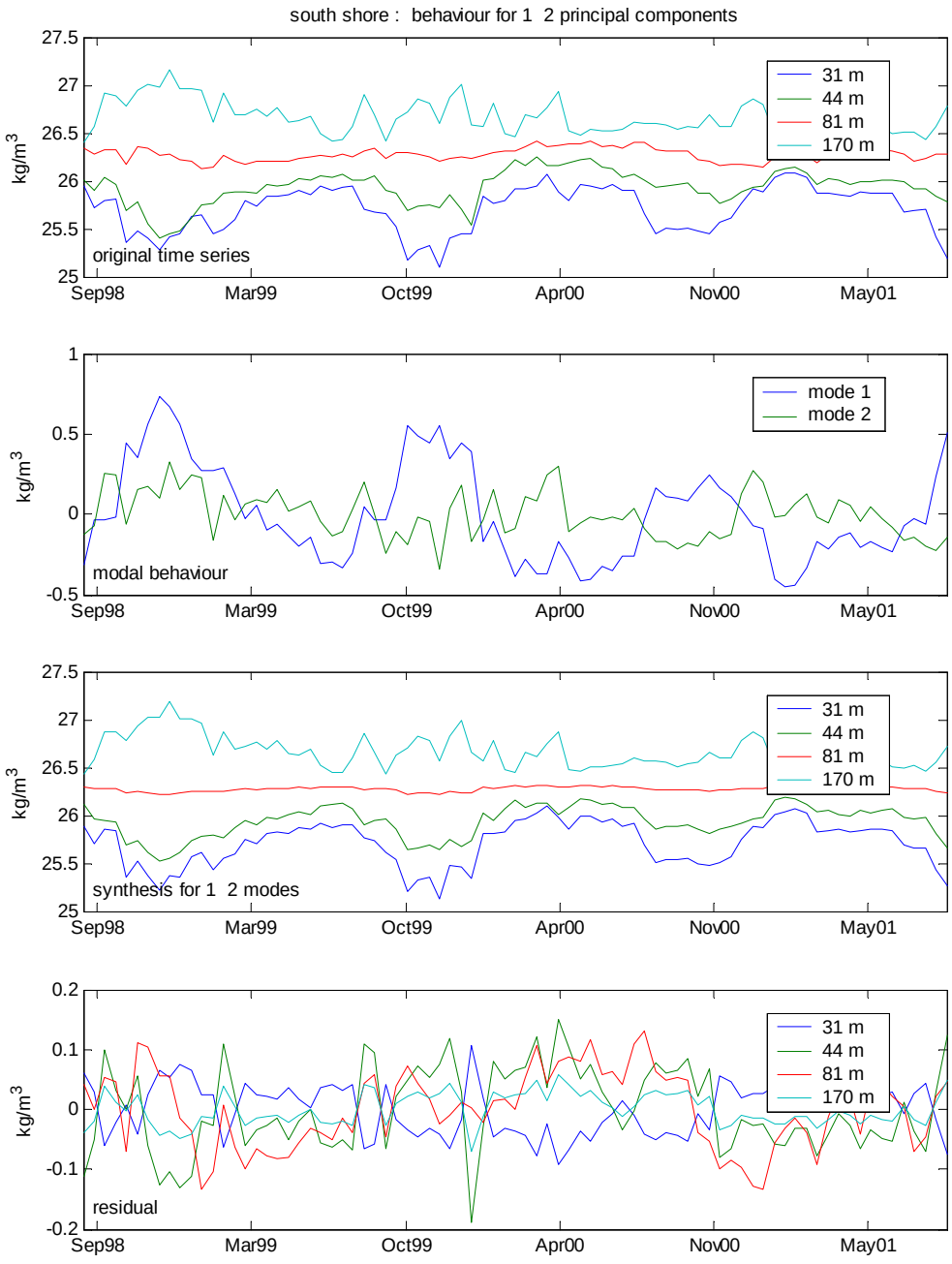

Figure 86 Time series of PCA results for low frequency (14-day) density data at southern mooring at 4 depths.

Appendix 5 Meteorological Data from Resolute

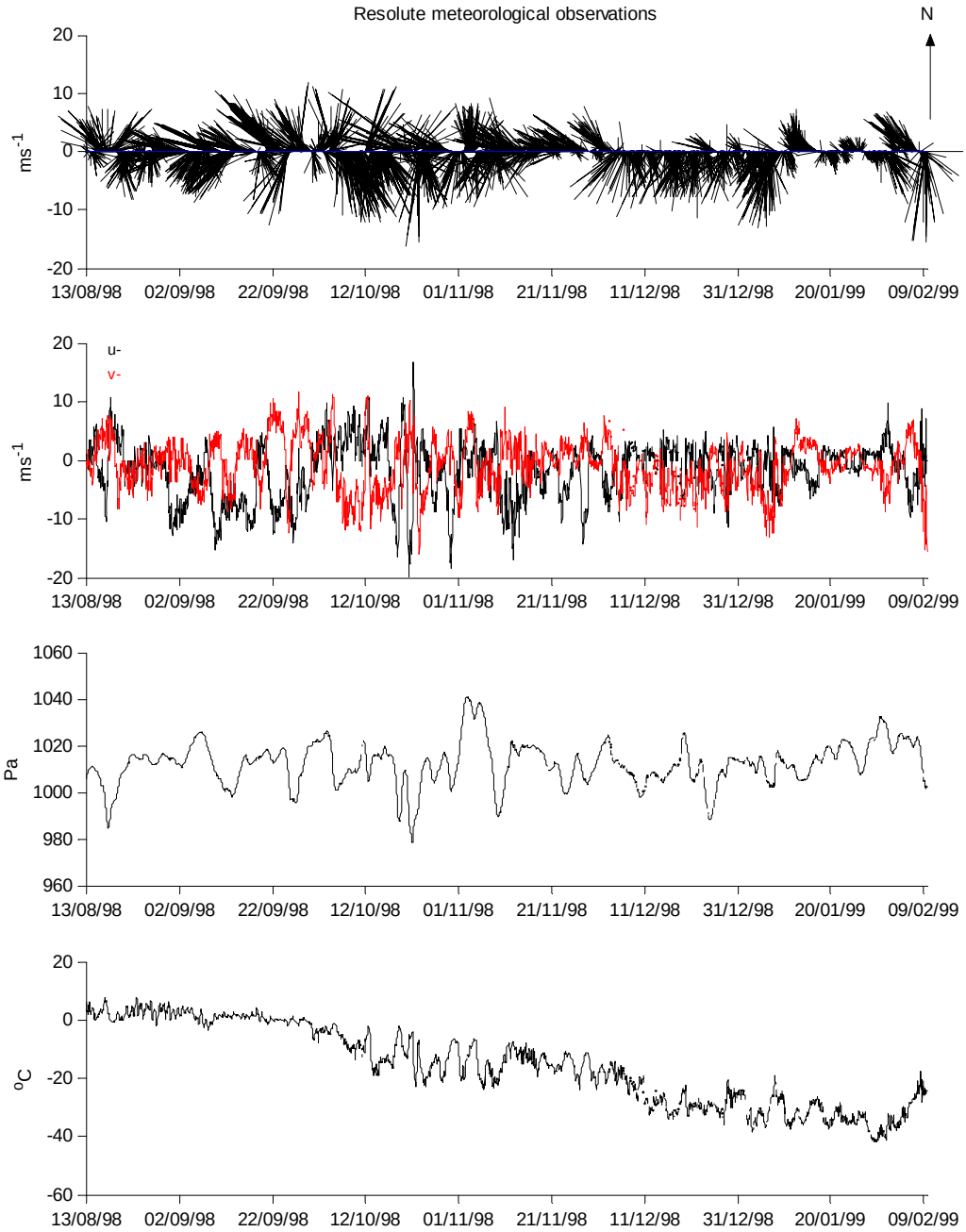

Figure 87 Time series of hourly meteorological data, Aug 1998 – Feb 1999

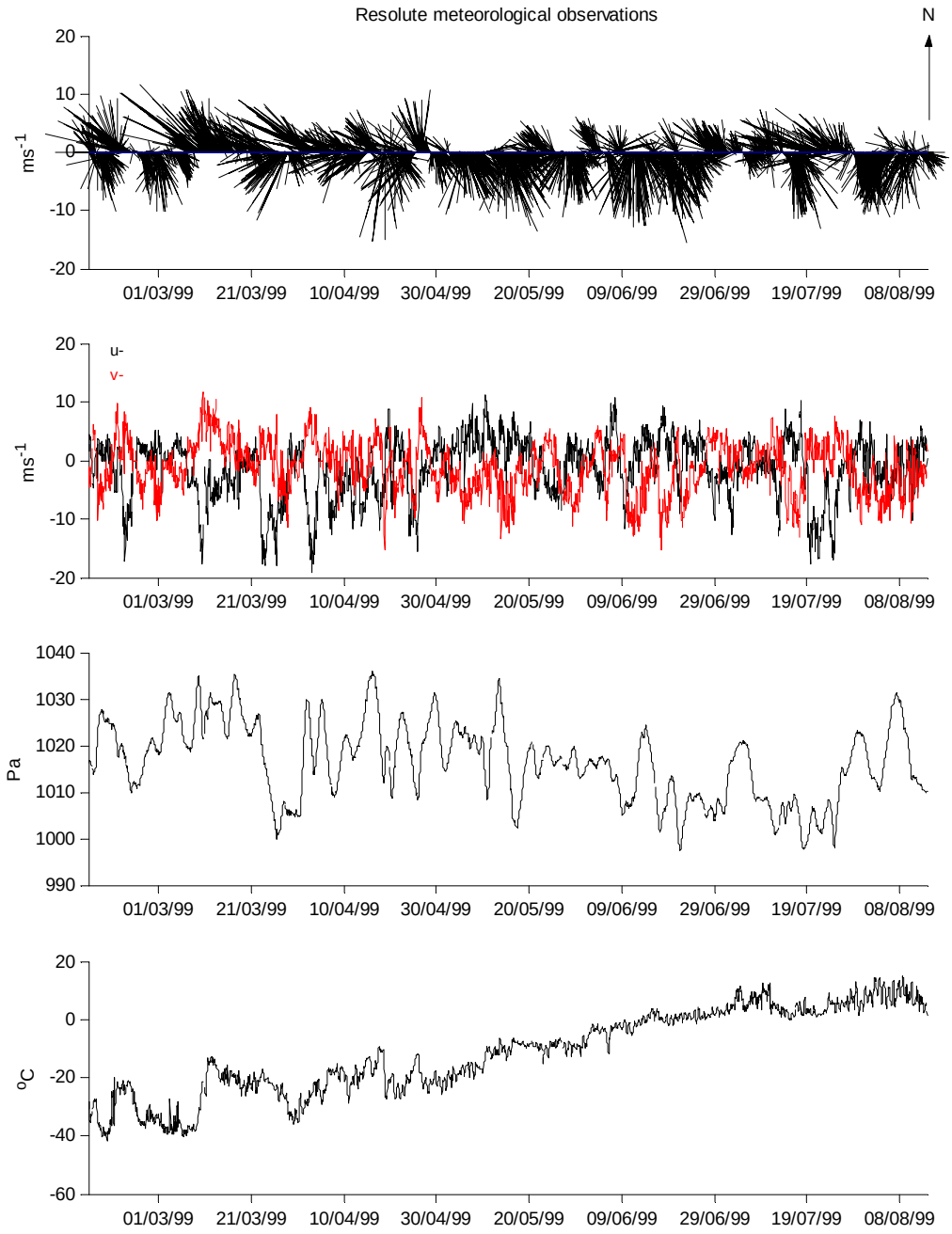

Figure 88 Time series of hourly meteorological data, Feb 1999 – Aug 1999

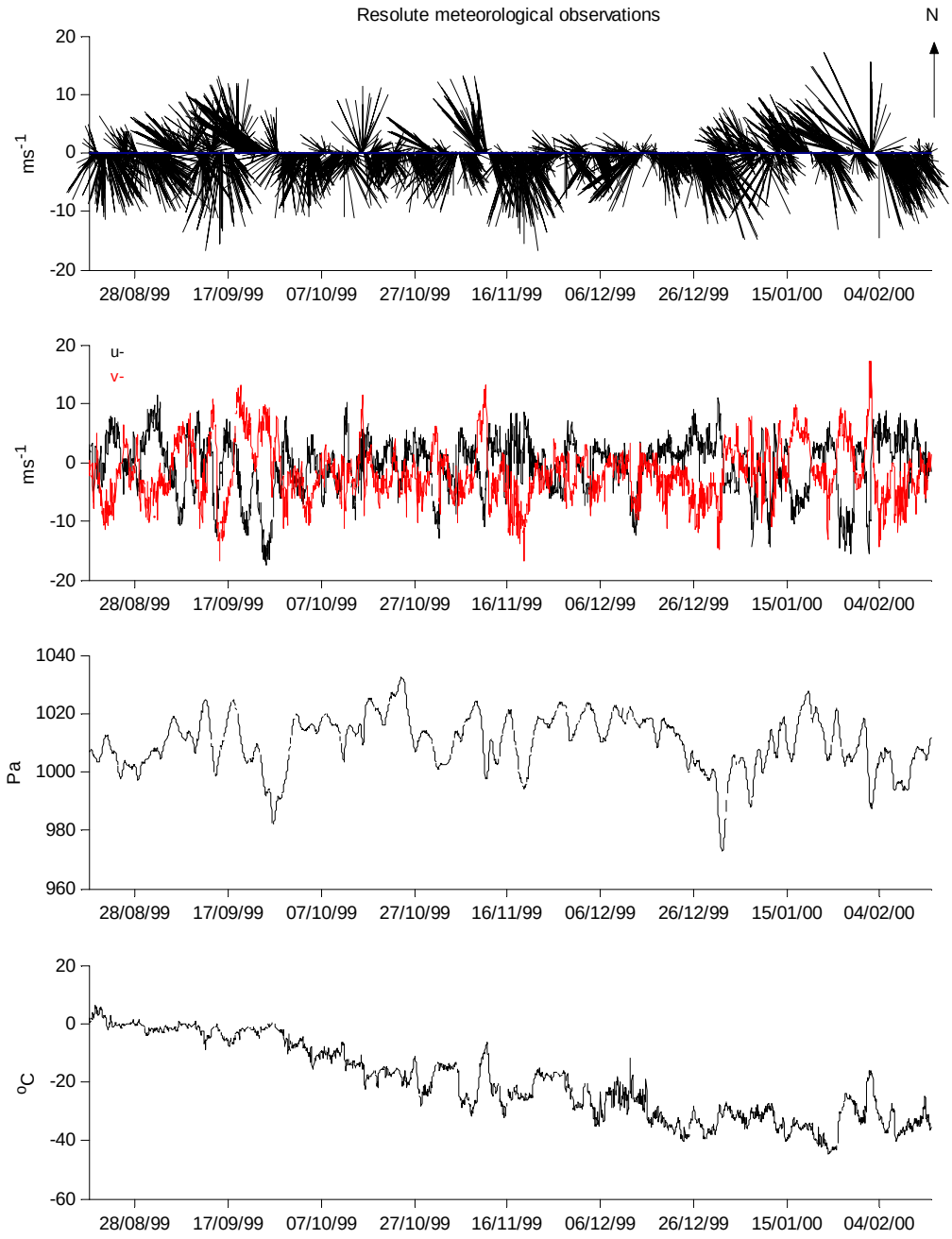

Figure 89 Time series of hourly meteorological data, Aug 1999 – Apr 2000

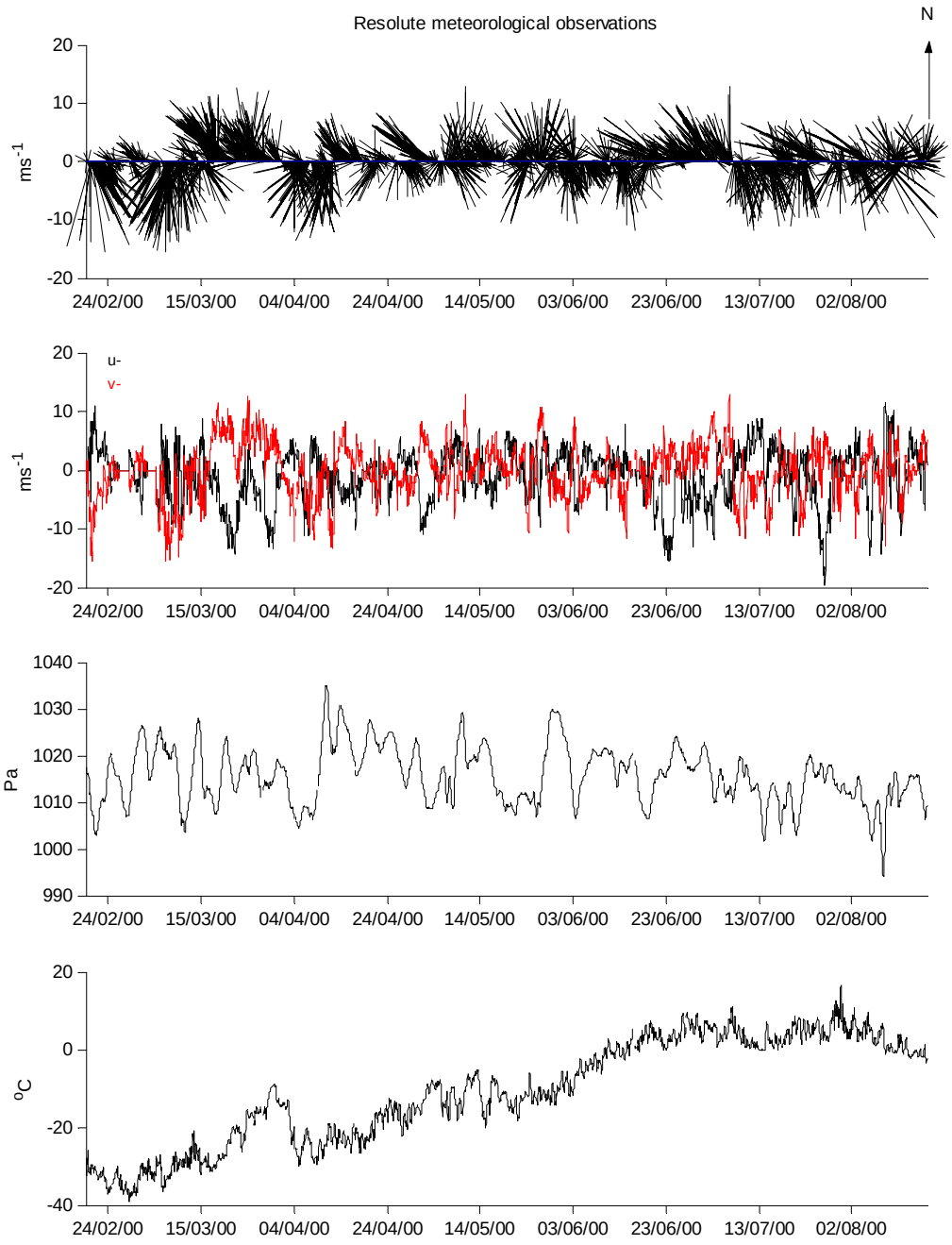

Figure 90 Time series of hourly meteorological data, Feb 2000 – Aug 2000

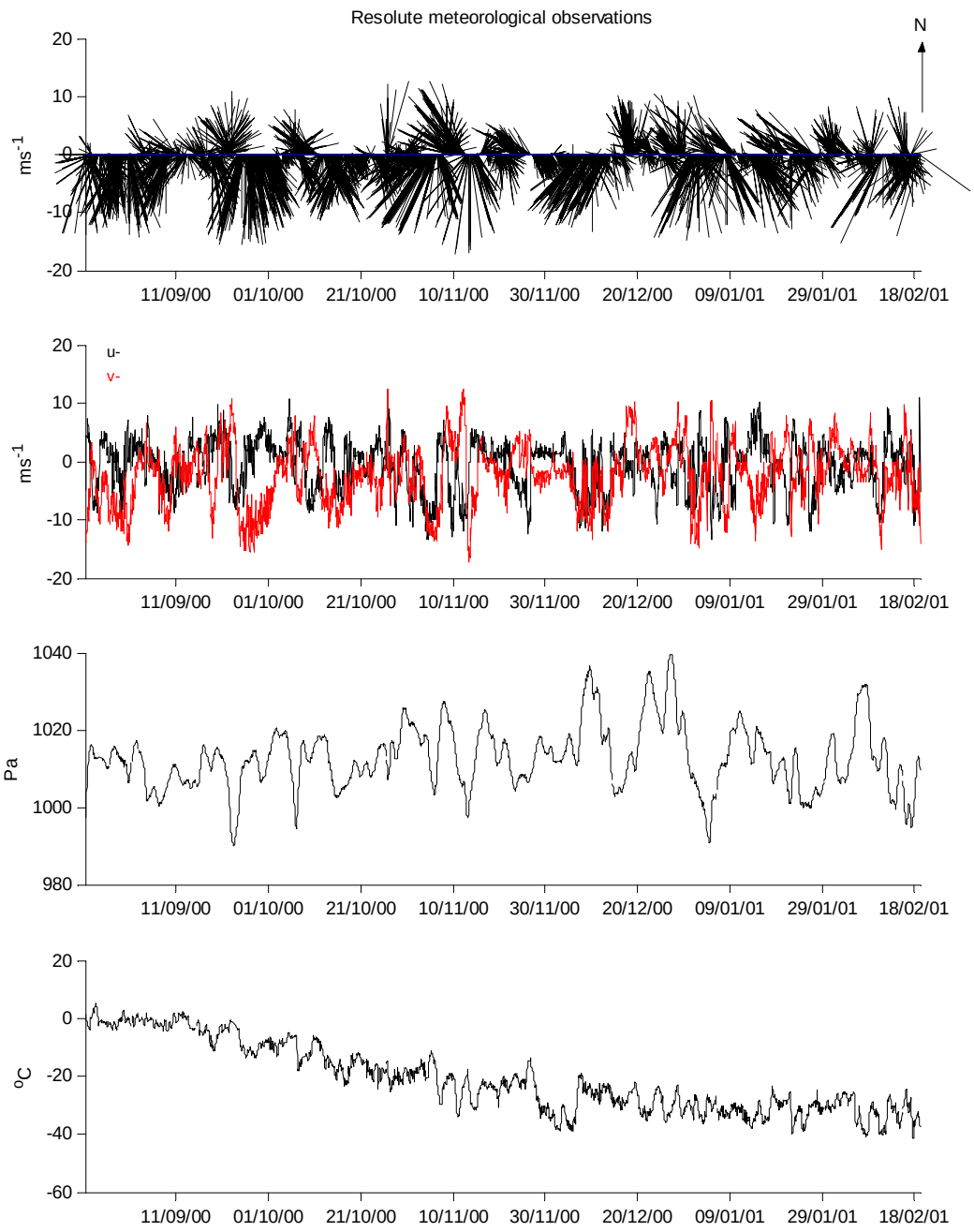

Figure 91 Time series of hourly meteorological data, Sep 2000 – Feb 2001

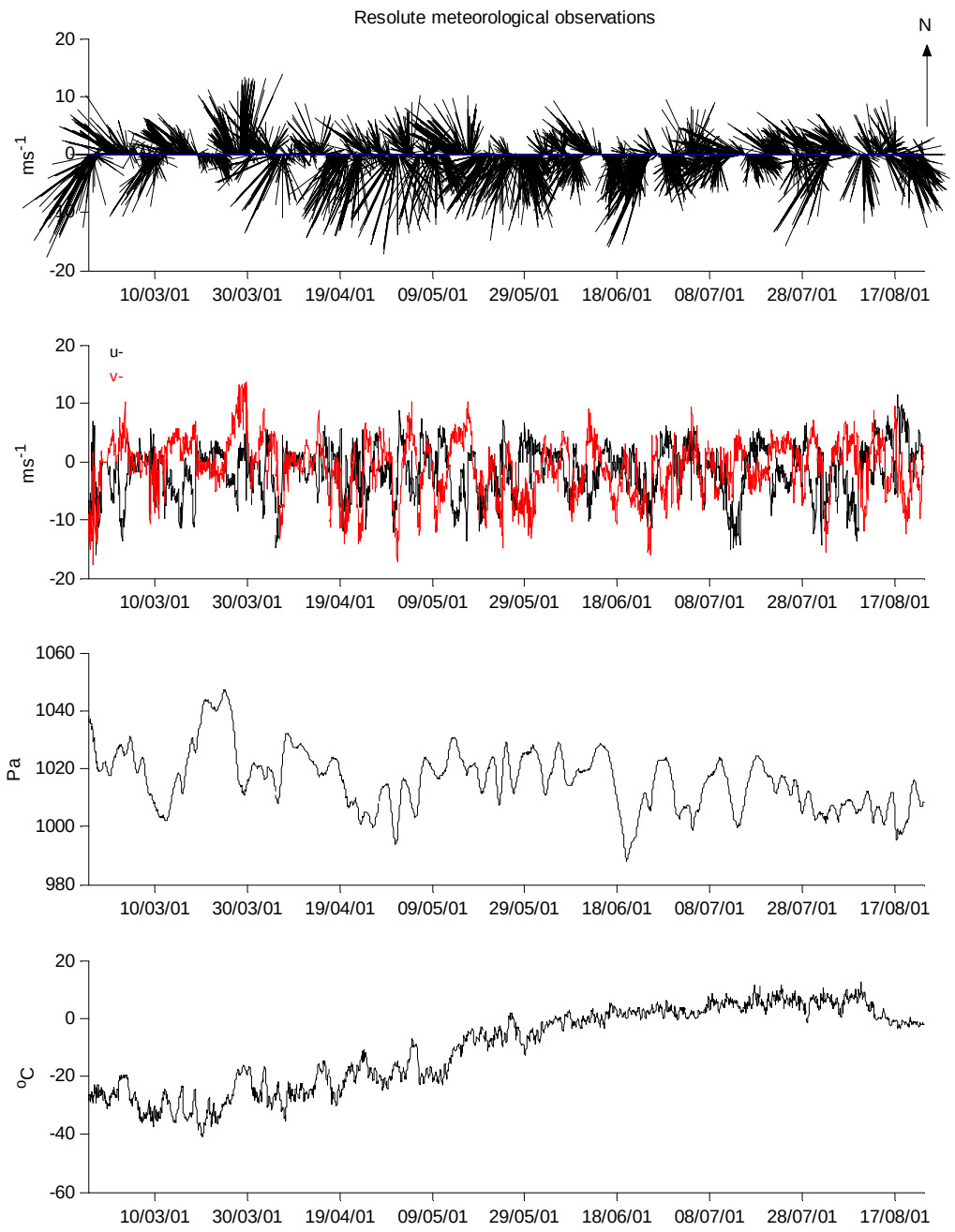

Figure 92 Time series of hourly meteorological data, Mar 2001 – Aug 2001

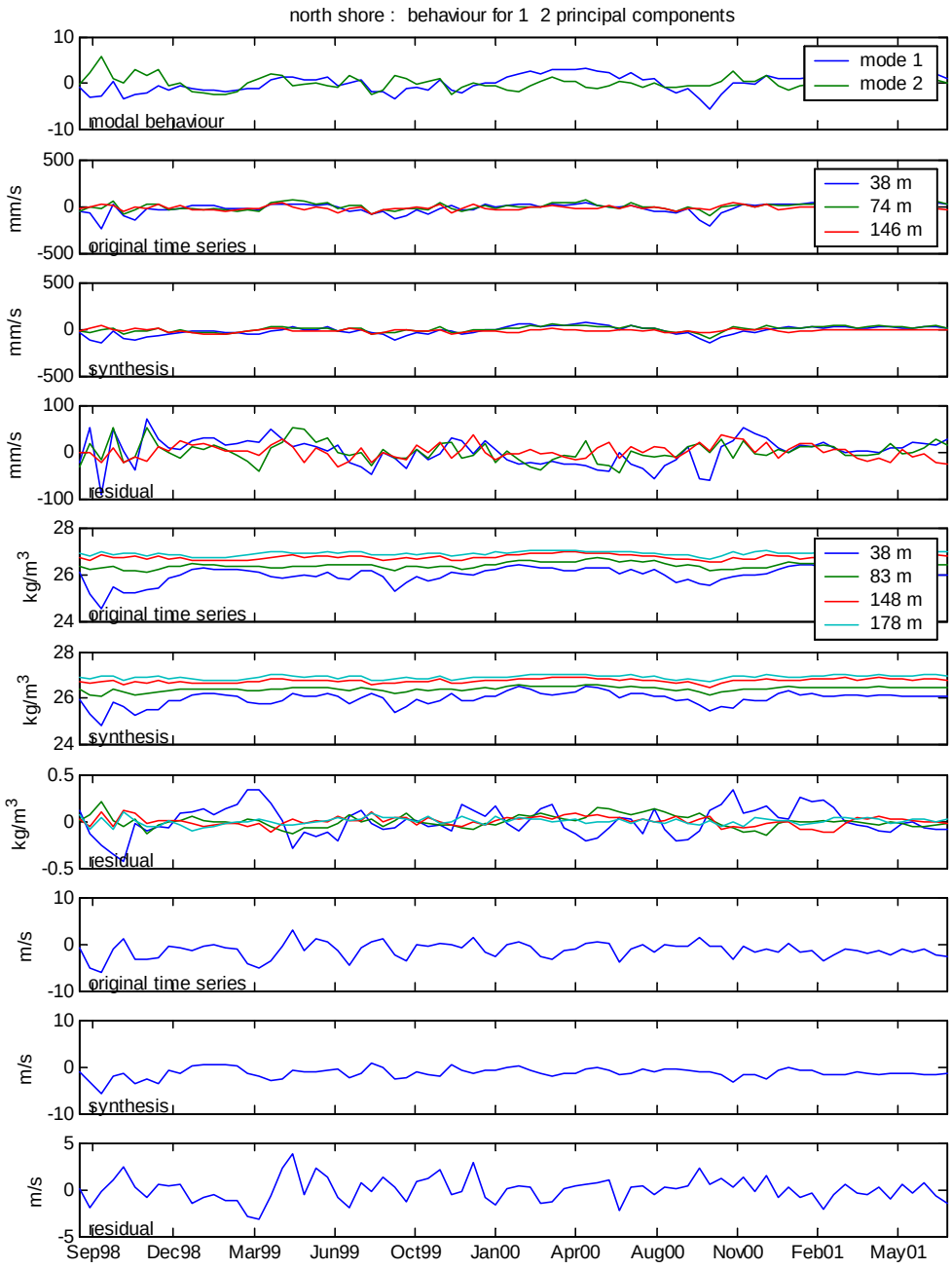

Figure 93 Time series of PCA results for the first two modes for alongshore current, density, and alongshore wind for the northern moorings using 14-day filtered data.

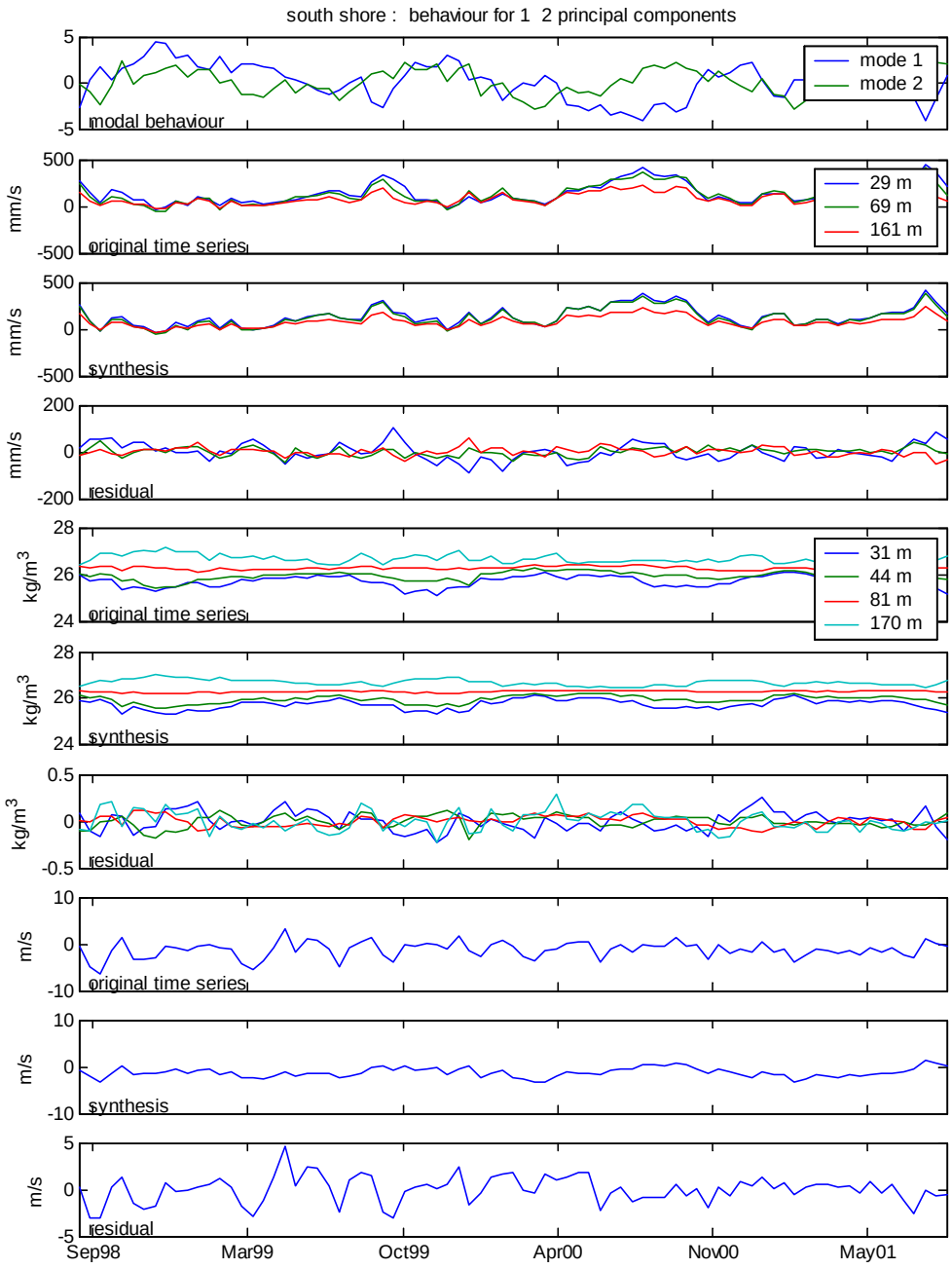

Figure 94 Time series of PCA results for the first two modes for alongshore current, density, and alongshore wind for the southern moorings using 14-day filtered data.

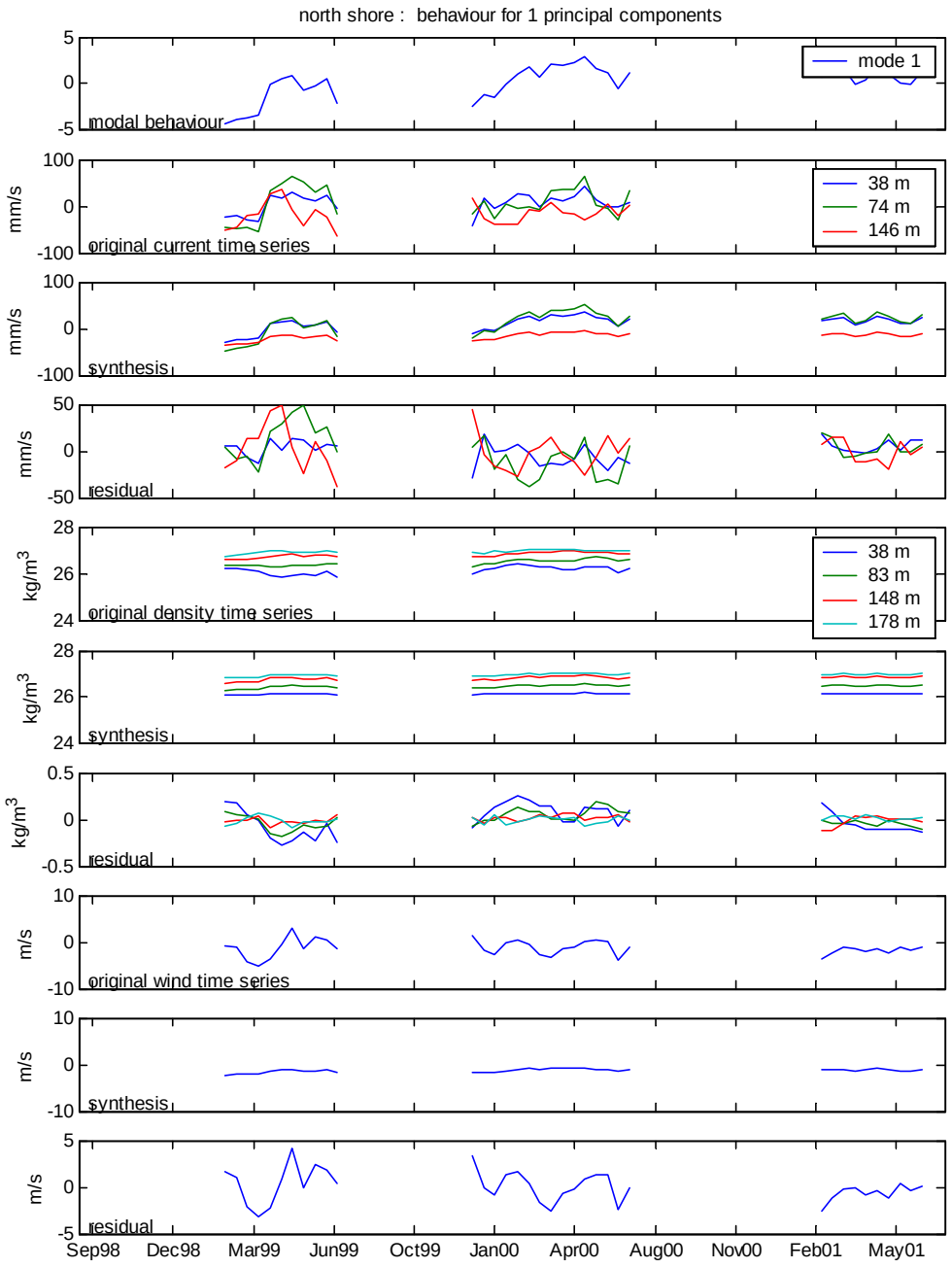

Figure 95 North shore PCA results time series for times of ice cover; synthetic series constructed from first principal component using 14-day filtered data.

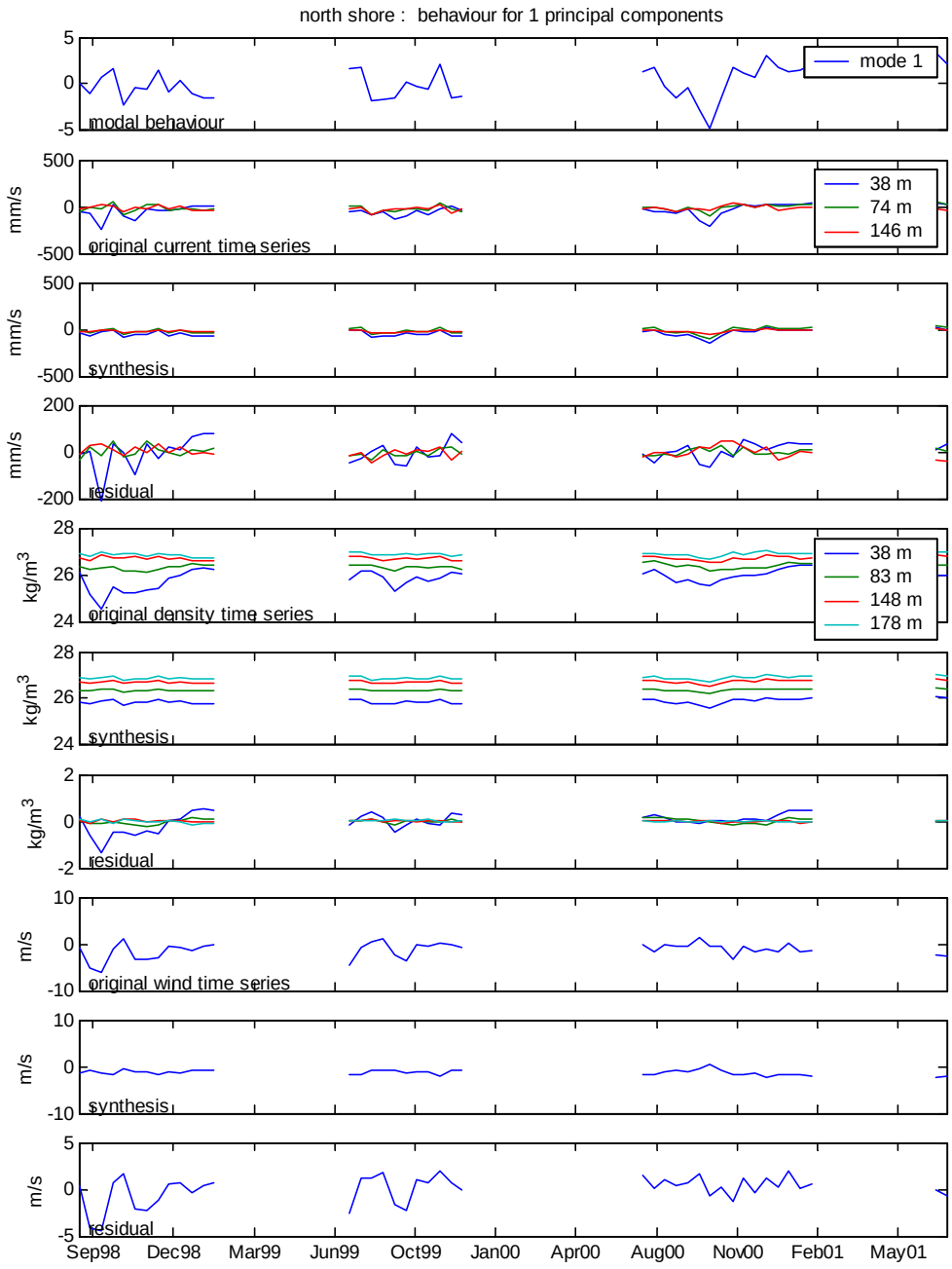

Figure 96 North shore PCA results time series for times of open water; synthetic series constructed from first principal component using 14-day filtered data.

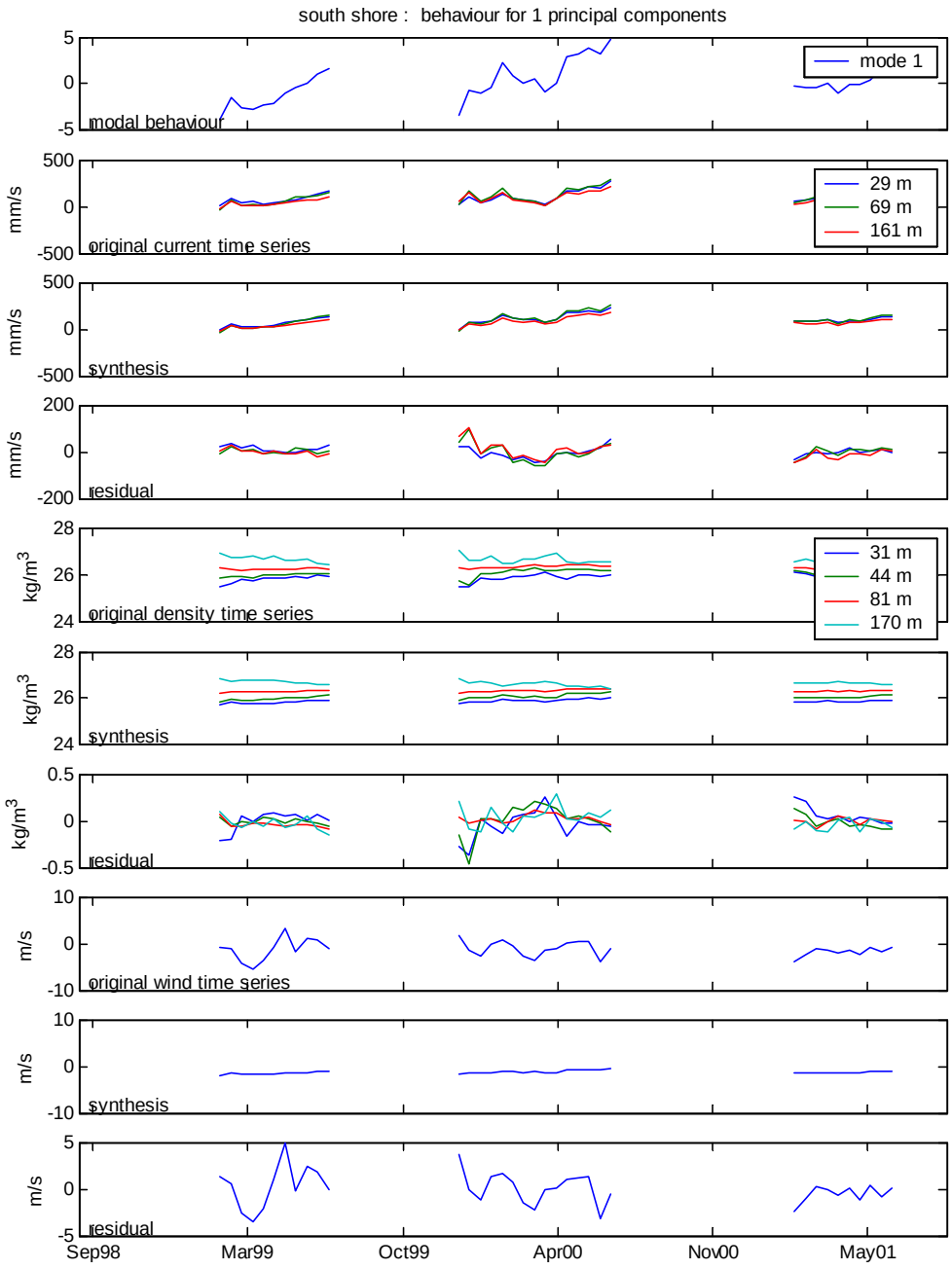

Figure 97 South shore PCA results time series for times of ice cover; synthetic series constructed from first principal component using 14-day filtered data

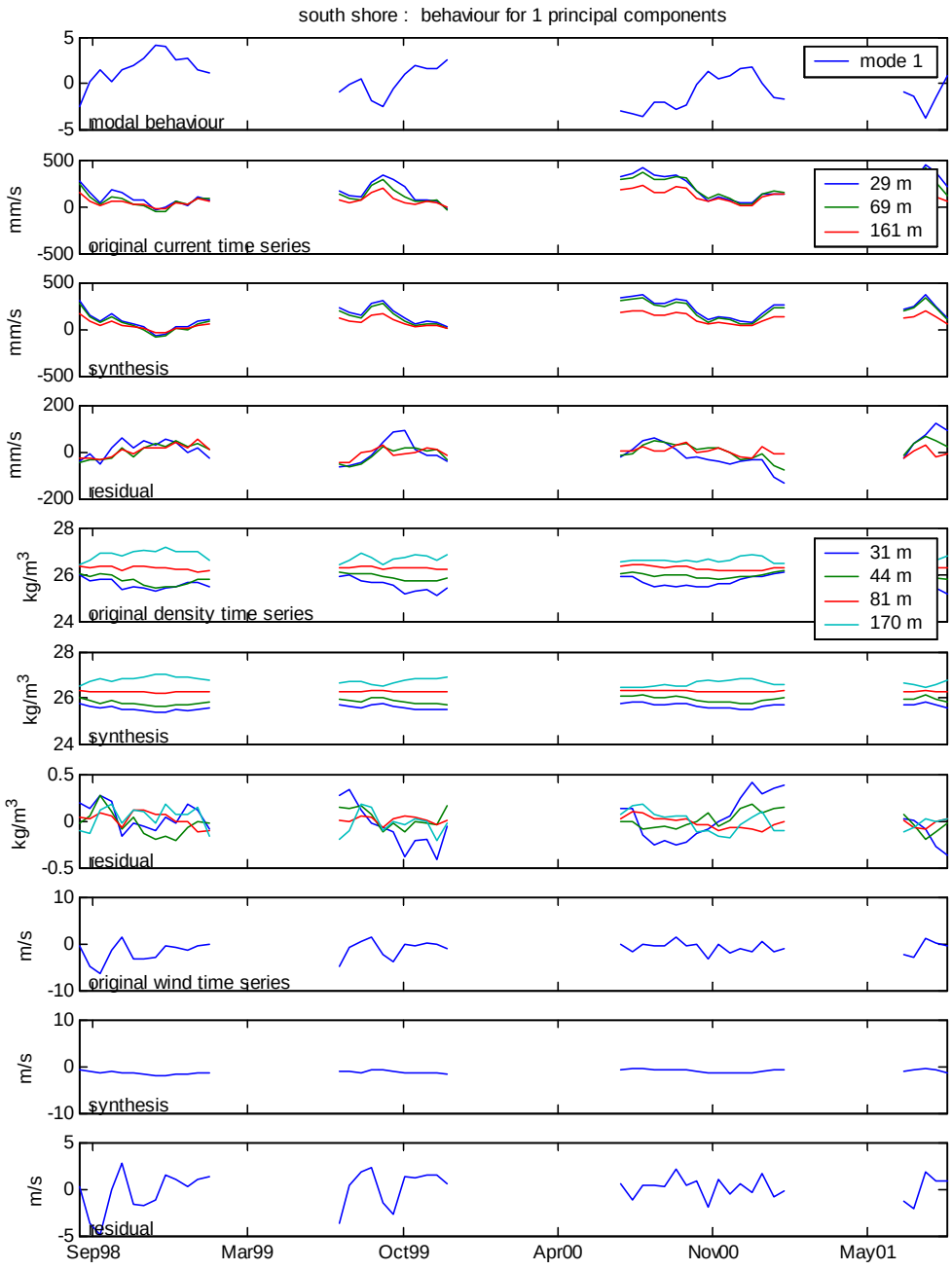

Figure 98 South shore PCA results time series for times of open water; synthetic series constructed from first principal component using 14-day filtered data.

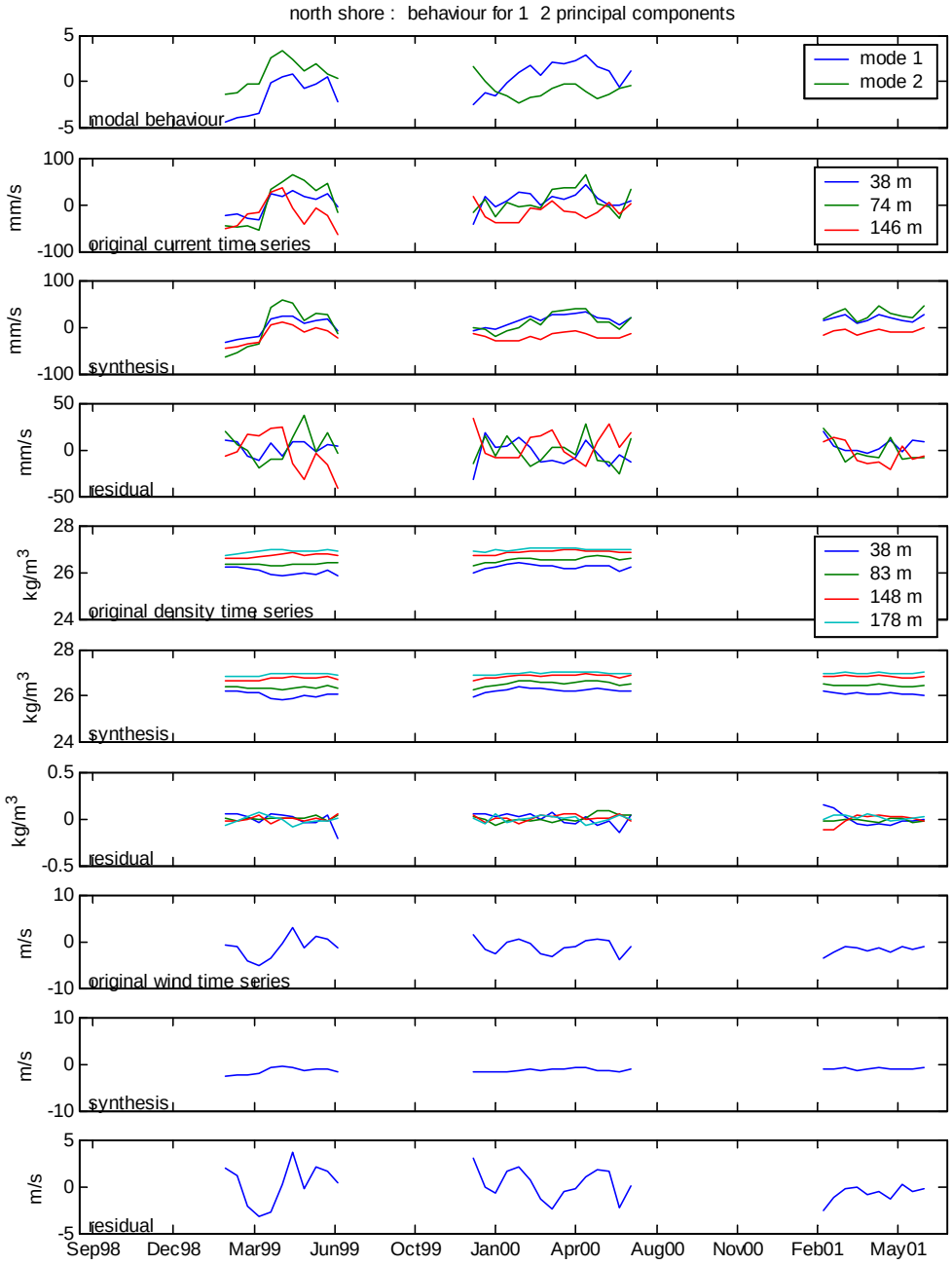

Figure 99 North shore PCA results time series for times of ice cover; synthetic series constructed from first two principal components using 14-day filtered data.

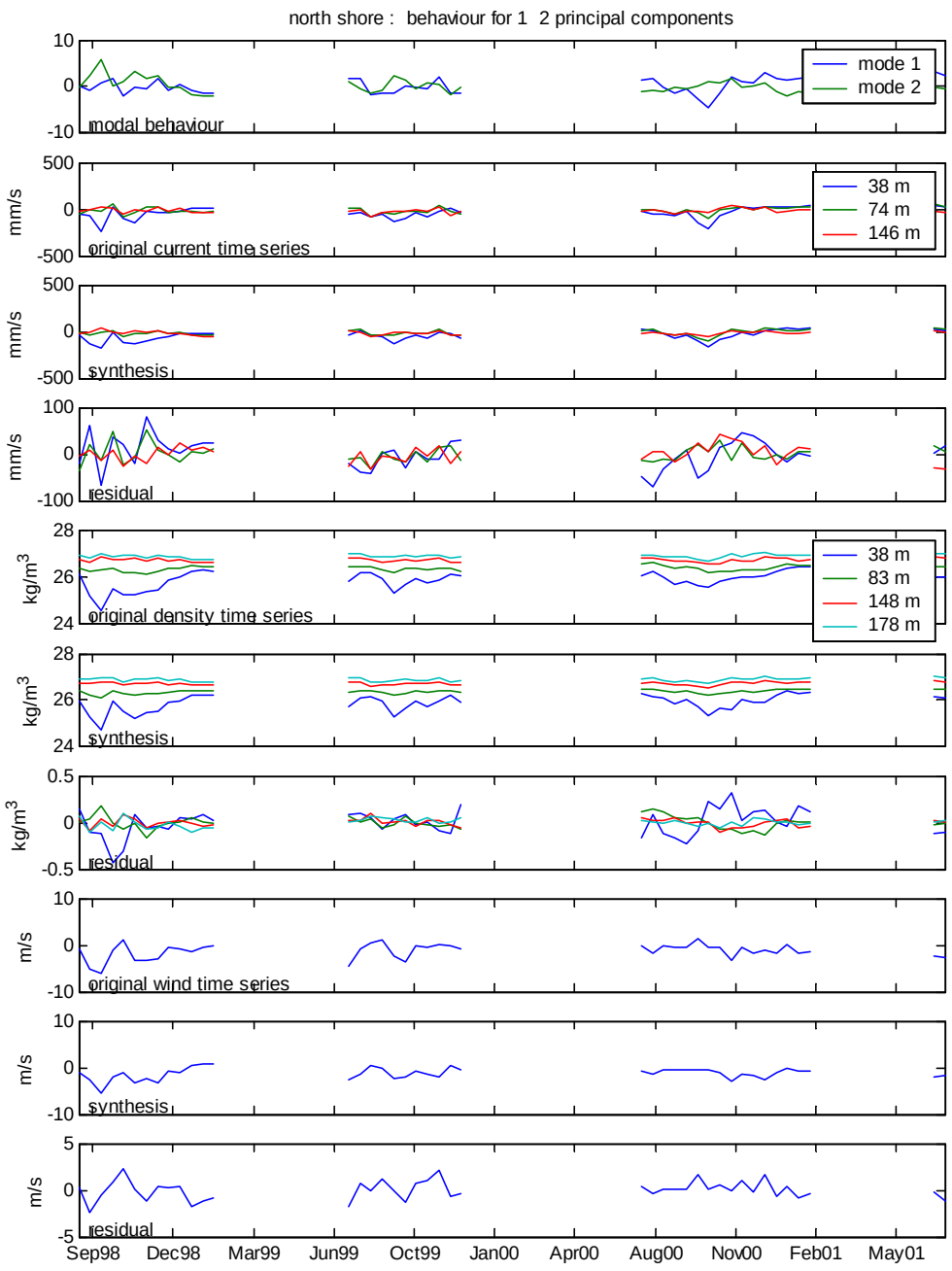

Figure 100 North shore PCA results time series for times of open water; synthetic series constructed from first two principal components using 14-day filtered data.

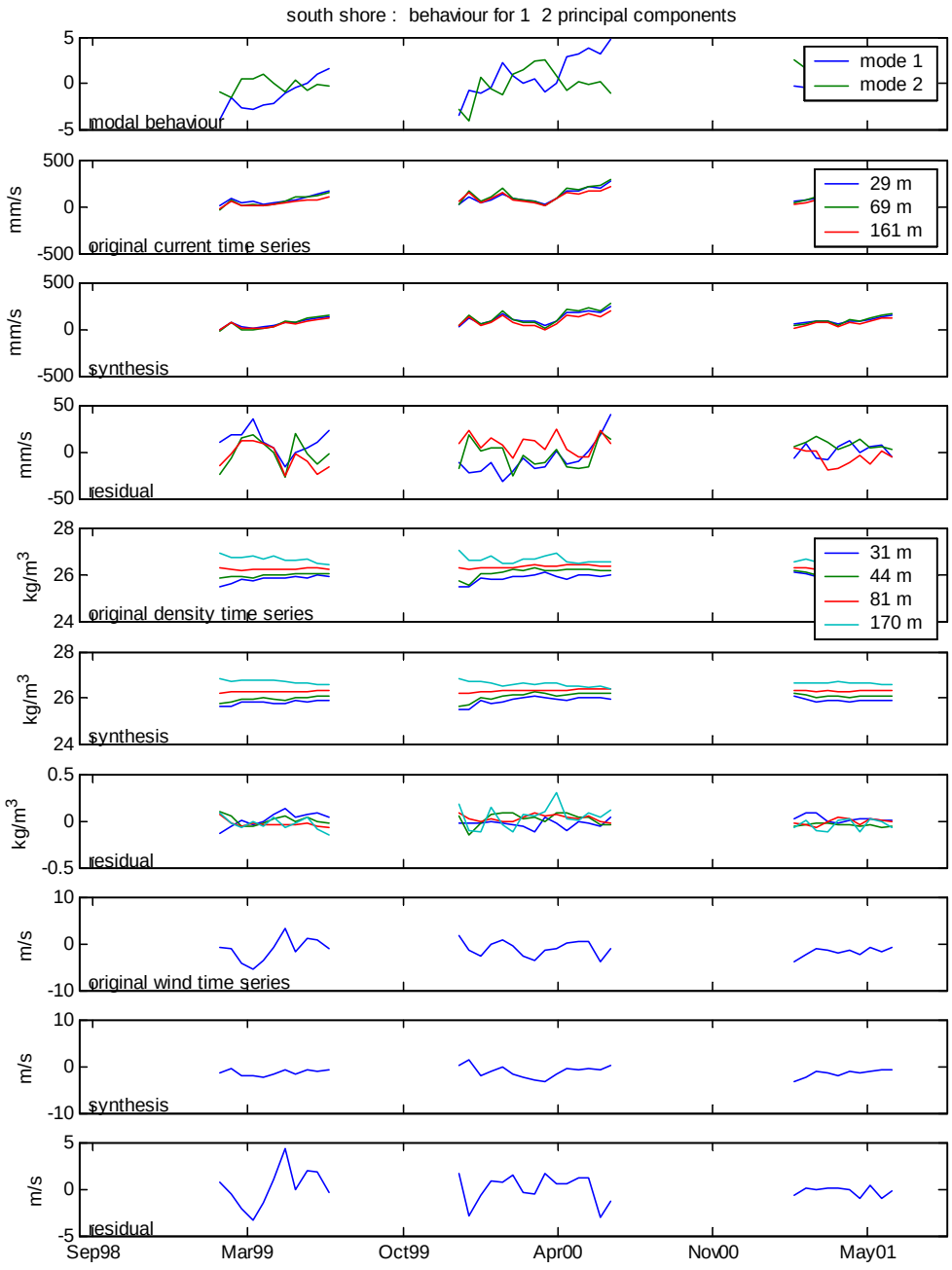

Figure 101 South shore PCA results time series for times of ice cover; synthetic series constructed from first two principal components using 14-day filtered data.

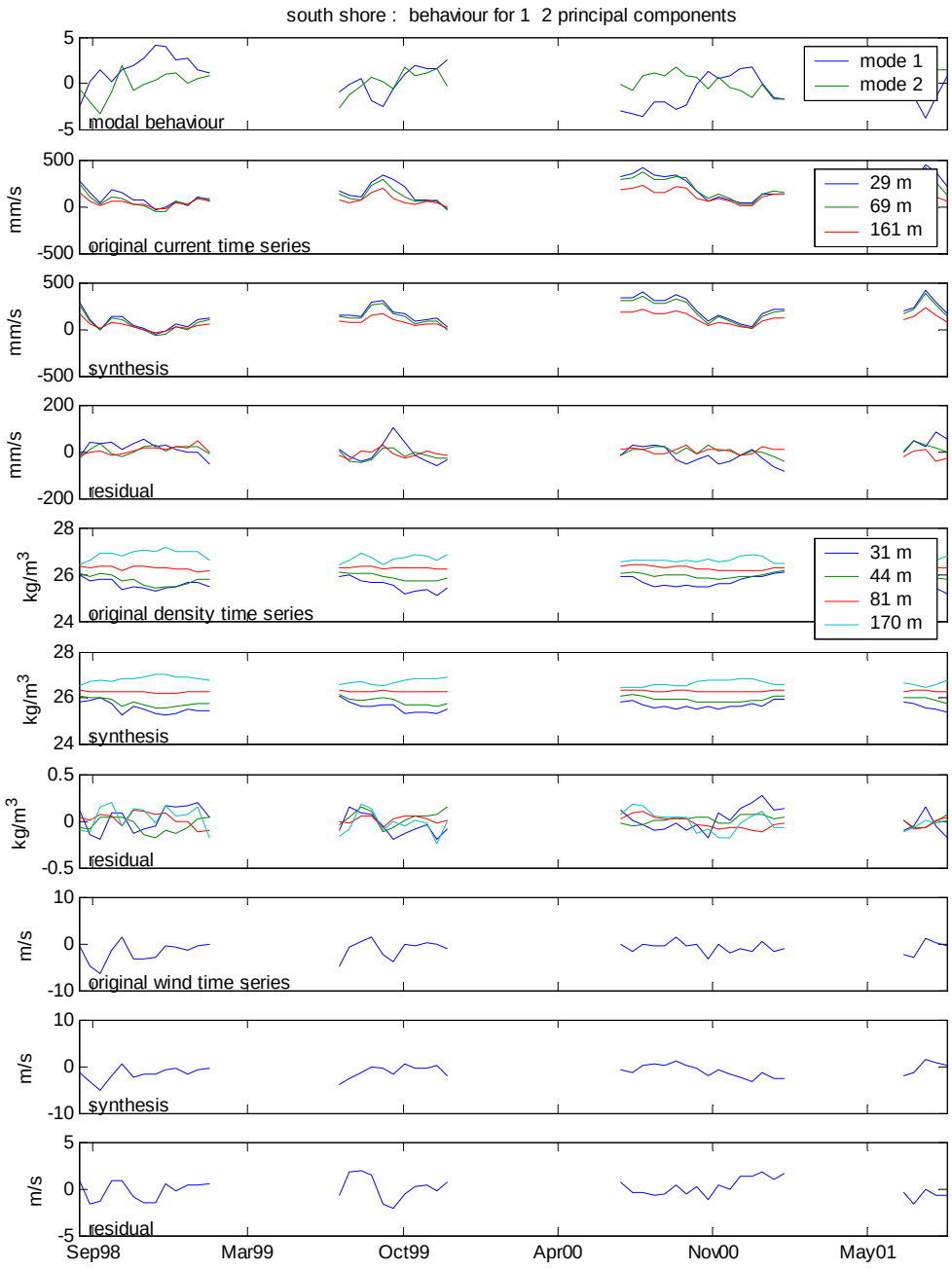

Figure 102 South shore PCA results time series for times of open water; synthetic series constructed from first two principal components using 14-day filtered data.